A graph-based model-free data-driven computing approach for inelasticity : Application to elastoplasticity

Héloïse Dandin

COLLEGE SCIENCES
DOCTORAL DE L'INGENIERIE
PAYS DE LA LOIRE ET DES SYSTEMES

CENTRALE NANTES

MÉMOIRE DE DOCTORAT DE

L'ÉCOLE CENTRALE DE NANTES

ÉCOLE DOCTORALE N° 602
Sciences de l'Ingénierie et des Systèmes
Spécialité : *Mécanique des Solides, des Matériaux, des Structures et des Surfaces*

Par
Héloïse DANDIN

Une approche basée sur les graphes pour le calcul piloté par les données en anélasticité

Application à l'élastoplasticité

Projet de recherche doctoral présenté et soutenu à Nantes, le 26 mars 2024
Unité de recherche : UMR 6183, Institut de Recherche en Génie Civil et Mécanique (GeM)

Rapporteurs avant soutenance :

Ludovic NOELS	Full professor, Université de Liège (Belgique)
Kerstin WEINBERG	Full professor, Universität Siegen (Allemagne)

Composition du Jury :

Président :	David RYCKELYNCK	Professeur des universités, Mines PARISTECH
Examinateurs :	Jean-Marc CADOU	Maître de conférences HDR, Université Bretagne Sud
	Ludovic NOELS	Full professor, Université de Liège (Belgique)
	Auriane PLATZER	Maîtresse de conférences, INSA Lyon
	Kerstin WEINBERG	Full professor, Universität Siegen (Allemagne)
Directeur de recherches doctorales :	Laurent STAINIER	Professeur des universités, Ecole Centrale de Nantes
Co-enc. de recherches doctorales :	Adrien LEYGUE	Chargé de recherche CNRS, Ecole Centrale de Nantes

PHD THESIS

A graph-based model-free data-driven computing approach for inelasticity

Application to elastoplasticity

by

Héloïse Dandin

March 2024

Remerciements

Contrairement à certaines idées reçues, la recherche, et le doctorat en particulier, ne sont pas des expériences solitaires, bien au contraire. Ma première année de thèse, entre télétravail et bureaux désertés, a suffi à m'en convaincre.

Je tiens tout d'abord à remercier Ludovic Noels et Kerstin Weinberg, pour avoir rapporté ce mémoire. Merci à David Ryckelynck pour avoir présidé mon jury de thèse avec beaucoup d'éclat, et à Jean-Marc Cadou et Auriane Platzer, qui ont également accepté d'en faire partie. Vos questions et vos remarques ont véritablement témoigné de votre intérêt scientifique pour ma recherche, ce dont je vous suis très reconnaissante. Les discussions que nous avons eues m'ont poussées à remettre en question mes certitudes et à perfectionner mon travail, et ont fortement contribué à faire de ce jour si particulier pour moi un événement mémorable.

Ce manuscrit est le fruit d'un peu plus de trois années de travail en collaboration avec mes encadrants, Laurent Stainier et Adrien Leygue, et doit beaucoup à leurs exceptionnelles qualités scientifiques. Je vous adresse toute ma reconnaissance pour votre bienveillance et votre écoute, en particulier au début de la thèse, lorsque la pandémie a rendu l'intégration et l'entraide difficiles dans un laboratoire endormi. Votre patience, votre disponibilité et votre confiance ont renforcé la mienne. J'ai énormément appris à vos côtés, à la fois de votre rigueur et de votre éthique de travail, mais surtout grâce à votre générosité scientifique et votre pédagogie. Nos réunions auront été le théâtre de quelques coups de génie, et je retiendrai certainement l'élégance comme maître-mot !

J'ai également beaucoup profité de l'écosystème du laboratoire, et je remercie spécialement les gestionnaires, pour leur efficacité à toute épreuve, les membres des équipes Outlaw et MECNUM, et les enseignant·es avec qui j'ai collaboré et échangé pendant ces trois années.

Plus généralement, toute ma gratitude va aux habitant·es des bâtiments T, O et F, pour la bonne humeur que vous apportez et la solidarité qui permet de venir à bout de tous les obstacles. Merci aux compagnon·es d'open space, aux joueur·ses de badminton et de belote, aux anglophones et aux francophones, aux cinéphiles, aux excellent·es pâtissier·ères, aux buveur·ses de thé et de café, aux nouveau·elles et aux ancien·nes... vous faites de ce coin de campus un endroit où il fait très bon vivre ! Un merci tout particulier

à Léna, ma sœur de thèse, pour tous les bons moments passés ensemble, à un bureau l'une de l'autre.

Je tiens également à remercier mes ami·es et ma famille, pour qui mon travail est parfois un peu obscur mais dont le soutien, proche ou lointain, m'a portée jusqu'à la soutenance et a contribué à en faire une magnifique journée.

Ma dernière pensée s'adresse à mes pierres angulaires : ma sœur et mes parents, sans qui je n'aurais sans doute jamais fait ni mécanique ni doctorat, et dont les encouragements m'ont toujours accompagnée.

Table of Contents

Introduction 1

A State of the Art 7

I Basic principles of solid thermomechanics 9

1 Mechanical principles . . . 10
2 Classes of material behaviours . . . 12
3 Thermomechanical problem . . . 15

II Elastoplasticity and computational elastoplasticity 17

1 Phenomenological aspects of elastoplasticity . . . 19
2 Mathematical theory of elastoplastic constitutive modelling . . . 21
3 Overview of classical constitutive models . . . 25
4 Elastoplastic problem resolution . . . 30
5 Summary . . . 34

III Data and data-driven approaches in computational mechanics 35

1 Model-based methods . . . 36
2 Model-free methods . . . 37
3 Summary . . . 39

IV Model-free data-driven computational mechanics 41

1 Data-Driven Computational Mechanics in elasticity . . . 43
2 Extension to inelasticity . . . 47
3 Overview of related works . . . 50
4 Summary . . . 54

B Towards an incremental problem formulation for model-free data-driven inelasticity 55

V Incremental problem formulation for inelastic data-driven simulation 57
1 Challenges in model-free data-driven inelasticity . . . 59
2 New problem formulation . . . 63
3 Summary . . . 66

VI Graph-based representation of the material database: mathematical framework 67
1 Elements of graph theory . . . 69
2 Digraph associated with the material database . . . 73
3 New definition of local database . . . 76
4 Numerical implementation . . . 78
5 Summary . . . 80

C Application to one-dimensional elastoplasticity 81

VII Numerical implementation and investigation of a single element problem 83
1 Numerical example . . . 85
2 Pre- and post-processing . . . 90
3 Resolution of the elastoplastic problem . . . 95
4 Discussion about the efficiency of the solver . . . 97
5 Summary . . . 98

VIII Numerical experiments on a truss problem 101
1 Numerical problem and preliminary results . . . 103
2 Predictor-corrector algorithm . . . 109
3 Summary . . . 113

IX Material digraph construction: challenges and perspectives 115
1 Material data and challenges toward digraph construction . . . 117
2 Data clustering . . . 119
3 Concluding remarks on digraph construction . . . 122

Conclusion and perspectives **125**

Appendices **129**

A Numerical relaxation for truss problems **131**
1 DDCM algorithm with numerical relaxation 131
2 Sparse material data 131

B Résumé étendu en français **135**
1 Principes fondamentaux de la thermomécanique des solides 135
2 Elastoplasticité et élastoplasticité computationnelle 136
3 Approches data-driven en mécanique numérique 137
4 Mécanique numérique pilotée par les données 137
5 Formulation incrémentale pour la résolution de problèmes anélastiques . . 138
6 Représentation de la base de données matériau avec un graphe : cadre mathématique 138
7 Implémentation numérique et étude d'un problème à un seul élément . . . 139
8 Essais numériques sur un problème de treillis 140
9 Construction du graphe matériau : défis et perspectives 141

References **143**

List of Figures

I.1 A general nonlinear continuum mechanics Boundary Value Problem (BVP), from Platzer (2020 [62]) . . . 10
I.2 Elastic material response, from Lemaitre *et al.* (2009 [51]) . . . 13
I.3 Viscoelastic material response, from Lemaitre *et al.* (2009 [51]) . . . 13
I.4 Plastic material response, from Lemaitre *et al.* (2009 [51]) . . . 14
I.5 Viscoplastic material response, from Lemaitre *et al.* (2009 [51]) . . . 15

II.1 Uniaxial tension experiment. Mathematical model. From De Souza Neto *et al.* (2008 [21]) . . . 20
II.2 Classical Bauschinger effect (from Lubliner (2008 [54])) . . . 21
II.3 Illustration of ratcheting. From Paranjape *et al.* (2018 [60]) . . . 29
II.4 Illustration of return-mapping. From Simo *et al.* (1998 [71]) . . . 32

IV.1 Functional spaces of the data-driven FE formulation. From Platzer (2020 [62]) . . . 45
IV.2 Data-Driven Computational Mechanics (DDCM) algorithm for elastic material response . . . 46
IV.3 Overview of DDCM extensions . . . 53

V.1 Uniaxial loading applied on an elastoplastic material and graphical representation of the material response in strain-stress space with constitutive modelling and DDCM. . . . 60
V.2 Histograms of pairwise-distances between $n = 100$ points sampled uniformly in the hypercube $[0, 1]^p$, from Delon (2017 [22]) . . . 63
V.3 Discrete history of a material loading point. . . . 64
V.4 A graph with 7 vertices and (a) 8 undirected edges, (b) 9 directed edges 65

VI.1 Example of digraph . . . 69
VI.2 Examples of special digraphs . . . 70

VI.3 A digraph with a cost assigned to each arc . . . 71
VI.4 A tree (yellow and dark blue vertices, yellow arcs) obtained by taking the dark blue vertex as root . . . 71
VI.5 (a) A digraph and (b) the corresponding adjacency matrix . . . 72
VI.6 A digraph G for an elastoplastic material response with loading and unloading . . . 73
VI.7 Subgraphs of G (Fig. VI.6): (a) non-dissipative subgraph E, (b) dissipative subgraph P . . . 74
VI.8 Identical states y_k and $y_\varkappa$ in constitutive space $(\boldsymbol{\varepsilon}, \boldsymbol{\sigma})$ but with different histories . . . 75
VI.9 (a) Tree $T(y_{e,k})$ built from G (Fig VI.6) and (b) material database, root $y_{e,k}$ and local database $\mathcal{D}_{e,k+1}$ . . . 76
VI.10 For G from Fig VI.6, reduced local databases with limited: (a) $c_{\mathbb{C}}$ (condition 2, cumulated data-driven distance) (b) c_D (condition 3, dissipation) 78
VI.11 DDCM algorithm for rate-independent elastoplastic material response at loading step $k+1$ . . . 79

VII.1 Spring-bar element system . . . 85
VII.2 Material data sets for the elastic resolution of the spring-bar problem . . . 87
VII.3 Mechanical and material solutions obtained for the elastic spring-bar problem . . . 87
VII.4 Absolute errors between mechanical states and FE reference solution for the elastic spring-bar problem, the black vertical line identifies the slope change . . . 88
VII.5 Material data set from FE simulation with loading and unloading . . . 89
VII.6 Regular material data set under loading, unloading and reloading conditions . . . 91
VII.7 Material database (detail) and effect of reduction criteria on the local database . . . 93
VII.8 Mechanical and material solutions obtained for the elastic spring-bar problem with σ-DB, $C = E$, in comparison with projected mechanical reference states . . . 94
VII.9 Spring-bar element system: applied strain . . . 95
VII.10 Material data set and (left) FE solution, (right) projected reference mechanical states . . . 95

VII.11 DDCM solution for the spring-bar element model under loading, unloading and reloading . . . 96
VII.12 Errors between DDCM and projected reference mechanical states for the spring-bar element model under loading, unloading and reloading 97

VIII.1 (a) Truss geometry and boundary conditions, (b) applied displacement (unloading starts at time step 100) . . . 103
VIII.2 Evolution of DDCM mechanical states and projected reference mechanical states for orange and blue elements during elastic loading 105
VIII.3 Median relative errors between DDCM and projected reference mechanical states and relative errors at time step 33 in elasticity 105
VIII.4 Evolution of resulting force against displacement for the truss problem . 106
VIII.5 Example of local database for the truss problem with $\texttt{TOL2} = 5 \times 10^3 \times C$ and $\texttt{TOL3} = 10^{-5} \times C$ . . . 107
VIII.6 Evolution of DDCM mechanical, material states and projected reference mechanical states for orange and blue elements during loading 107
VIII.7 Median relative errors between DDCM and projected reference mechanical states and relative errors at time step 33 . . . 108
VIII.8 Evolution of resulting force against displacement for the truss problem . 109
VIII.9 Illustration of the predictor-corrector elastoplastic DDCM algorithm . . 110
VIII.10 Evolution of DDCM mechanical, material states and projected reference mechanical states for orange and blue elements with predictor-corrector algorithm . . . 111
VIII.11 Median relative errors between DDCM and projected reference mechanical states and relative errors at time step 33 with predictor-corrector algorithm . . . 112
VIII.12 Evolution of resulting force against displacement for the truss problem with predictor-corrector algorithm . . . 112

IX.1 Material data set for k-means clustering obtained by Finite Element (FE) simulation (elastoplastic constitutive model with isotropic hardening) . . 120
IX.2 Position of clusters in space $(\varepsilon\sqrt{E}, \sigma/\sqrt{E}, D/\sqrt{E})$ for sampling rate $r = 2$ %, with marker size symbolising the number of points in a cluster 120
IX.3 Evaluation and comparison of clustering quality for sampling rates $r = (2\ \%, 5\ \%, 10\ \%)$ in space $(\varepsilon\sqrt{E}, \sigma/\sqrt{E}, D/\sqrt{E})$ . . . 121

A.1 Data-driven fixed-point solver with numerical relaxation 132
A.2 Median relative errors between DDCM and projected reference mechanical states (a) without relaxation, (b) with relaxation 133
A.3 Numerical relaxation and negative dissipation tolerance: (a) median relative errors between DDCM and projected reference mechanical states (b) resulting force against displacement 134

List of Acronyms

ANN Artificial Neural Network . . . 36
BFS Breadth-First Search . . . 98
BVP Boundary Value Problem . . . 10
DDCM Data-Driven Computational Mechanics . . . 3
DFS Depth-First Search . . . 98
DIC Digital Image Correlation . . . 37
DDI Data-Driven Identification . . . 37
FE Finite Element . . . 30
FE^2 multilevel finite element approach . . . 38
FFNN Feedforward Neural Network . . . 36
IBVP Incremental Boundary Value Problem . . . 30
MIQP Mixed-Integer Quadratic Programming . . . 50
ML Machine Learning . . . 36
RNN Recurrent Neural Network . . . 36
UA-DDCM Uncertainty Analysis-based DDCM . . . 51

Introduction

Introduction

Materials, in the most expansive context, demonstrate a wide range of properties that are contingent upon their intrinsic structure. These properties encompass mechanical aspects (elastic limit), chemical attributes (corrosion resistance), thermal characteristics (thermal expansion), electrical qualities (conductivity), etc. Designing and dimensioning engineering components thus require precise material knowledge to ensure:

- the adequacy between material properties and *in-situ* conditions of the mechanical structure,
- sufficient performance of the part in in-service applications,
- extended lifespan of the component.

From a mechanical point of view, knowledge about the material behaviour is gained by experimental means, and then implemented in numerical simulations to predict the mechanical response of a structure under complex loading conditions. Traditionally in computational mechanics, the mechanical response of a material is approximated by a mathematical function, named "constitutive model". The continuous nature of this function simplifies the resolution of mechanical problems and centuries of research led to the development of high-fidelity models for a wide range of materials. Nevertheless, this representation, while straightforward for linear mechanical responses, reaches its limits when dealing with complex behaviours due to nonlinearity and/or dependence on multiple parameters.

Alternatives to constitutive modelling arose during the last decades, brought about by major breakthroughs in computer and data sciences. In particular, Data-Driven Computational Mechanics (DDCM), newly introduced in 2016 by Kirchdoerfer and Ortiz, is a model-free approach that completely bypasses the need for constitutive models. Solely based on observed material data, this method intends to replace models in cases where the latter prove to be inaccurate and challenging to calibrate.

In the data-driven paradigm, materials can be classified into two main categories depending on their behaviour when subjected to external forces:

- elastic materials recover their original size and shape when the force they were subjected to is removed,
- inelastic materials, whose mechanical response is irreversible and path-dependent.

DDCM was initially developed and extensively discussed for the first category, where the material behaviour is encoded by a discrete data set, called material database and composed of experimentally or numerically observed strain-stress pairs.

This description is not sufficient in inelasticity, since in that case loading history has to be taken into account, and an efficient representation has to be developed that, following the philosophy behind DDCM, stays closest to physical principles, and so without any modelling assumption.

The present work therefore addresses the following problem:

How can history be enforced in the discrete representation of the material response?

and the contingent question:

How can we formulate and solve inelastic data-driven problems?

To investigate this topic and answer these questions, we suggest encoding the inelastic material behaviour with directed graphs. Graphs are mathematical structures used to represent pairwise relationships between objects. In DDCM, a graph can thus provide a structured material database which accounts for irreversibility.

This manuscript is divided into three main parts:

- The first one aims to explain in detail the context of this study and takes stock of the state of the art in computational mechanics. We will recall the fundamental principles of continuum thermomechanics for solids in Chapter I. Chapter II considers the special case of elastoplastic materials and how elastoplasticity is treated in constitutive modelling. The computational resolution of the mechanical problem is also addressed, with particular attention paid to the one-dimensional case, which will be studied in the following. Chapter III contextualises and motivates the use of data-driven approaches, then Chapter IV concludes this part with a presentation of DDCM and an overview of related works. The mathematical foundation for the extension to inelastic behaviours is also recalled and will serve as a basis for the next chapters.
- The second part addresses specific challenges arising in data-driven inelasticity, especially regarding the representation of history. Several paradigms are considered and discussed in Chapter V, and the use of graphs is motivated. Chapter VI provides

basic elements of graph theory. Furthermore, the mathematical definitions and principles for the representation of the material data set with a directed graph are given, along with the new procedure for the resolution of the numerical data-driven problem.

- The last part of this manuscript is dedicated to applying the approach in numerical simulations that are performed and analysed for elastoplastic trusses. In Chapter VII, we consider a single element problem and demonstrate the ability of the method to handle history-dependent behaviours. Chapter VIII investigates a truss problem exhibiting combinatorial complexity and provides an enhanced procedure to counteract the numerical effects leading to the failure of the original algorithm. Finally, Chapter IX discusses the construction of the graph when dealing with realistic material data.

Part A

State of the Art

Chapter I

Basic principles of solid thermomechanics

Contents

1 Mechanical principles **10**

2 Classes of material behaviours **12**

2.1 Elasticity 13

2.2 Viscoelasticity 13

2.3 Plasticity 14

2.4 Viscoplasticity 14

3 Thermomechanical problem **15**

1 Mechanical principles

In this section, we define the thermomechanical principles governing a Boundary Value Problem (BVP) in continuum mechanics in the small strains range, to serve as a basis throughout this document. Basic components are kinematics, equilibrium and laws of thermodynamics. The content of this section is taken from the textbooks by De Souza Neto *et al.* (2008 [21]), Lemaitre *et al.* (2009 [51]) and Simo *et al.* (1998 [71]).

Let $\Omega \in \mathbb{R}^d$ be the reference configuration of a body, illustrated in Fig. I.1, where d is the space dimension and let $\partial\Omega$ be the boundary of the domain in the current configuration such that $\Gamma_N \cup \Gamma_D = \partial\Omega$ and $\Gamma_N \cap \Gamma_D = \emptyset$. The body undergoes the action of body forces $\boldsymbol{f}$ per unit deformed volume, traction forces $\boldsymbol{t}$ per unit deformed area of the boundary Γ_N and a displacement field $\boldsymbol{u}_D$ applied on the boundary Γ_D. The latter boundary condition is referred to as Dirichlet boundary condition and reads:

$$\boldsymbol{u}(\boldsymbol{x}) = \boldsymbol{u}_D, \ \forall \boldsymbol{x} \in \Gamma_D. \tag{I.1}$$

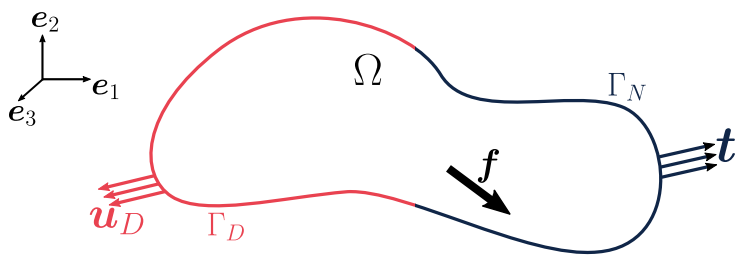

Figure I.1: A general nonlinear continuum mechanics BVP, from Platzer (2020 [62])

In infinitesimal deformation theory, the displacement and its gradient are assumed to be sufficiently small compared to the dimensions of the body, and the current configuration can be assimilated to the reference one. The deformation of the body is then entirely measured by the linearised infinitesimal strain tensor:

$$\boldsymbol{\varepsilon} = \frac{1}{2}\left(\nabla \boldsymbol{u} + \nabla^{\mathsf{T}} \boldsymbol{u}\right). \tag{I.2}$$

The Cauchy stress tensor $\boldsymbol{\sigma}$ linearly relates the surface vector $\boldsymbol{t}$ to the outer normal

vector $\boldsymbol{n}$ of a deformed unit area as:

$$\boldsymbol{t}(\boldsymbol{x}, \boldsymbol{n}) = \boldsymbol{\sigma}(\boldsymbol{x})\boldsymbol{n}(\boldsymbol{x}), \ \forall \boldsymbol{x} \in \Gamma_N. \tag{I.3}$$

This equation, also called Neumann boundary condition, expresses the equilibrium on the boundary of the body. By contrast, the translational equilibrium, derived from the conservation of linear momentum inside the body, reads:

$$\operatorname{div}(\boldsymbol{\sigma}(\boldsymbol{x})) + \boldsymbol{f}(\boldsymbol{x}) = 0, \ \forall \boldsymbol{x} \in \Omega \tag{I.4}$$

in the absence of inertial forces. The conservation of angular momentum yields the symmetry of the Cauchy stress tensor as:

$$\boldsymbol{\sigma} = \boldsymbol{\sigma}^{\mathsf{T}}. \tag{I.5}$$

In order to state the principles of thermodynamics, we introduce the scalar fields θ, e, s and r which represent, respectively, the temperature, specific internal energy, specific entropy and volumetric density of heat production. In addition, we define the vector field $\boldsymbol{q}$ corresponding to heat flux. The density is denoted ρ.

The first principle of thermodynamics governs the conservation of energy during the transformation of the body and is expressed by:

$$\rho \dot{e} = \boldsymbol{\sigma} : \dot{\boldsymbol{\varepsilon}} + r - \operatorname{div}(\boldsymbol{q}), \tag{I.6}$$

under small strains, with $\boldsymbol{\sigma} : \dot{\boldsymbol{\varepsilon}}$ the stress power per unit volume. The second principle defines the irreversibility of entropy production:

$$\rho \dot{s} + \operatorname{div}\left(\frac{\boldsymbol{q}}{\theta}\right) - \frac{r}{\theta} \geqslant 0 \ . \tag{I.7}$$

The combination of Eqs. I.6 and I.7 leads to:

$$\rho \dot{s} + \operatorname{div}\left(\frac{\boldsymbol{q}}{\theta}\right) - \frac{1}{\theta}\left(\rho \dot{e} - \boldsymbol{\sigma} : \dot{\boldsymbol{\varepsilon}} + \operatorname{div}(\boldsymbol{q})\right) \geqslant 0 \ . \tag{I.8}$$

Introducing the specific free energy ψ, or Helmholtz free energy per unit mass as:

$$\psi = e - \theta s \ , \tag{I.9}$$

into the above inequality, we obtain the fundamental Clausius-Duhem inequality that must be satisfied at each step of the process:

$$\boldsymbol{\sigma} : \dot{\boldsymbol{\varepsilon}} - \rho\left(\dot{\psi} + s\dot{\theta}\right) - \frac{1}{\theta}\boldsymbol{q} \cdot \nabla\theta \geqslant 0 \ , \tag{I.10}$$

where the left term corresponds to the total dissipation per unit deformed volume. In the case where the transformation is isothermal ($\dot{\theta} = 0, \nabla\theta = 0$) and adiabatic ($r = 0, \boldsymbol{q} = \boldsymbol{0}$), the expression of dissipation reduces to:

$$D = \boldsymbol{\sigma} : \dot{\boldsymbol{\varepsilon}} - \rho\dot{\psi} \ . \tag{I.11}$$

A non-dissipative transformation is said reversible, and irreversible if the dissipation is strictly positive. The Clausius-Duhem inequality (Eq. I.10) ensures that negative dissipation is not allowed.

2 Classes of material behaviours

The response of solid materials to characteristic experimental tests allows them to be classified as elastic, viscous, plastic and perfectly plastic according to the dependence of stress on strain and/or time (Lemaitre *et al.*, 2009 [51]).

The most common characterisation tests are the uniaxial tension, creep and relaxation tests. These are homogeneous tests, in which strain and stress states are (quasi-)uniform in the region of interest of the sample.

- A uniaxial tension test is performed with prescribed strain, at a constant strain rate. The material response shows the stress variation depending on strain and highlights the work-hardening phenomenon, *i.e.* permanent deformation of the material subjected to sufficiently high strains.
- During a creep test, the sample is subjected to a prescribed stress at a constant stress rate and the evolution of strain over time characterises work-hardening and viscosity.
- The relaxation test is dual to the previous one: the prescribed constant strain allows to characterise the work-hardening and viscous response.

The mechanical response to the three tests is used in the following figures to define the

different classes of material behaviours.

2.1 Elasticity

For elastic solids (Fig. I.2), deformation is reversible and instantaneous. The state of stress and strain does not depend on the loading path followed.

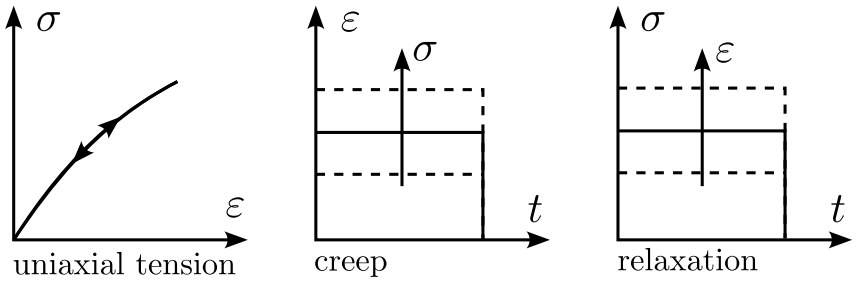

Figure I.2: Elastic material response, from Lemaitre *et al.* (2009 [51])

2.2 Viscoelasticity

Viscoelasticity (Fig. I.3) refers to behaviours that exhibit both elastic and viscous properties under loading. The creep response under stress is time-dependent and the reversibility of deformation only occurs after an infinite time.

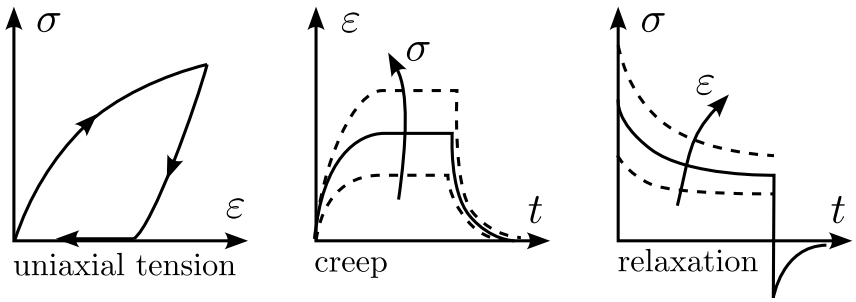

Figure I.3: Viscoelastic material response, from Lemaitre *et al.* (2009 [51])

2.3 Plasticity

Plastic solids (Fig. I.4) are inelastic solids which, once the load has been removed, exhibit instantaneously stable permanent deformations and which are in equilibrium under load. Their behaviour does not explicitly depend on time. They can be perfectly elastic-plastic, *i.e.* with linear elastic strain below an arbitrary stress threshold σ_0 and independent of the strain rate for this stress value (Saint Venant model, [68]). They can also be work-hardening elastoplastic, in which case the total strain is the sum of a linear elastic deformation and a permanent strain, equal to zero below the σ_0 threshold.

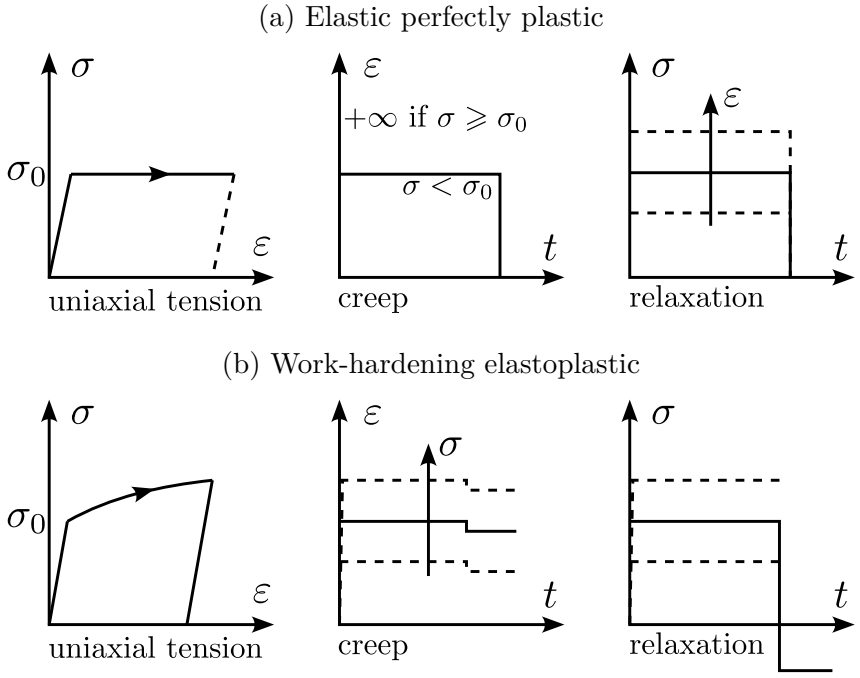

Figure I.4: Plastic material response, from Lemaitre *et al.* (2009 [51])

2.4 Viscoplasticity

Finally, viscoplastic solids (Fig. I.5) are those which, like plastic solids, exhibit permanent deformation after stress has ceased, but which undergo a time-dependent creep flow under stress. As with plastic solids, a distinction is made between perfectly viscoplastic solids, which exhibit a permanent deformation rate as a function of stress, elastic perfectly viscoplastic solids, which are similar but for which elasticity is no longer considered negligible,

and finally work-hardening elasto-viscoplastic solids, which are more complex to model since stress depends on the plastic strain rate and on the plastic strain itself or on another work-hardening variable.

(a) Perfectly viscoplastic

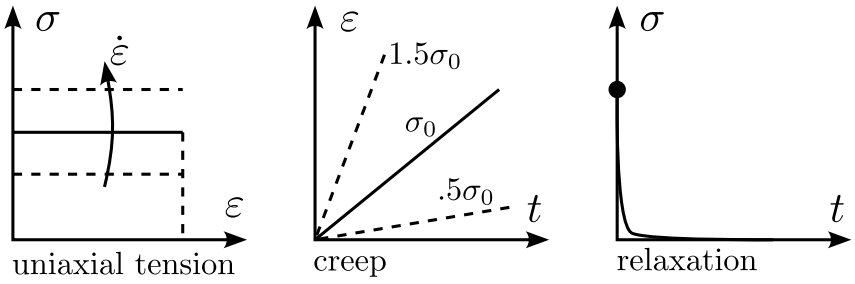

(b) Elastic perfectly viscoplastic

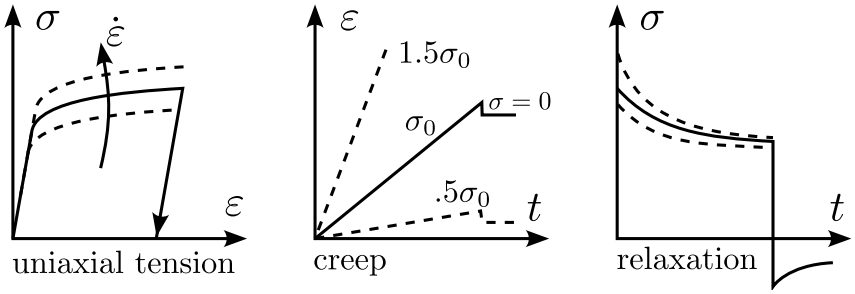

(c) Work-hardening elasto-viscoplastic

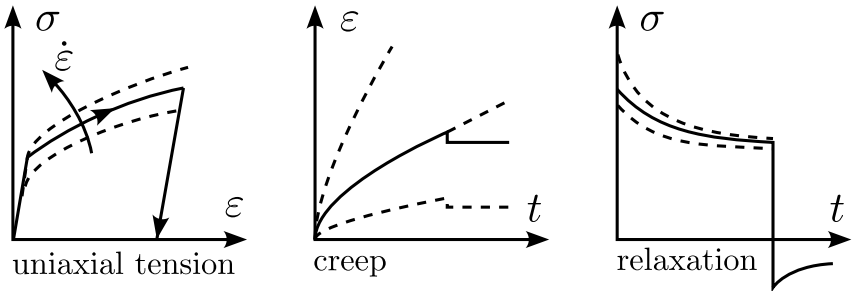

Figure I.5: Viscoplastic material response, from Lemaitre *et al.* (2009 [51])

3 Thermomechanical problem

The BVP defined in Section 1 is a problem composed of linear equations that requires additional information about the material behaviour to be solved. A common method,

known as constitutive modelling, consists in postulating a mathematical relation between strains and stresses based on the characteristics of the material response as described in Section 2 to close the problem.

In plain linear elasticity, the material behaviour is easily approximated with a linear function and the solution is straightforward. For nonlinear behaviours however, constitutive models rely on additional variables and multiple parameters while the problem is solved with complex algorithms.

Chapter II

Elastoplasticity and computational elastoplasticity

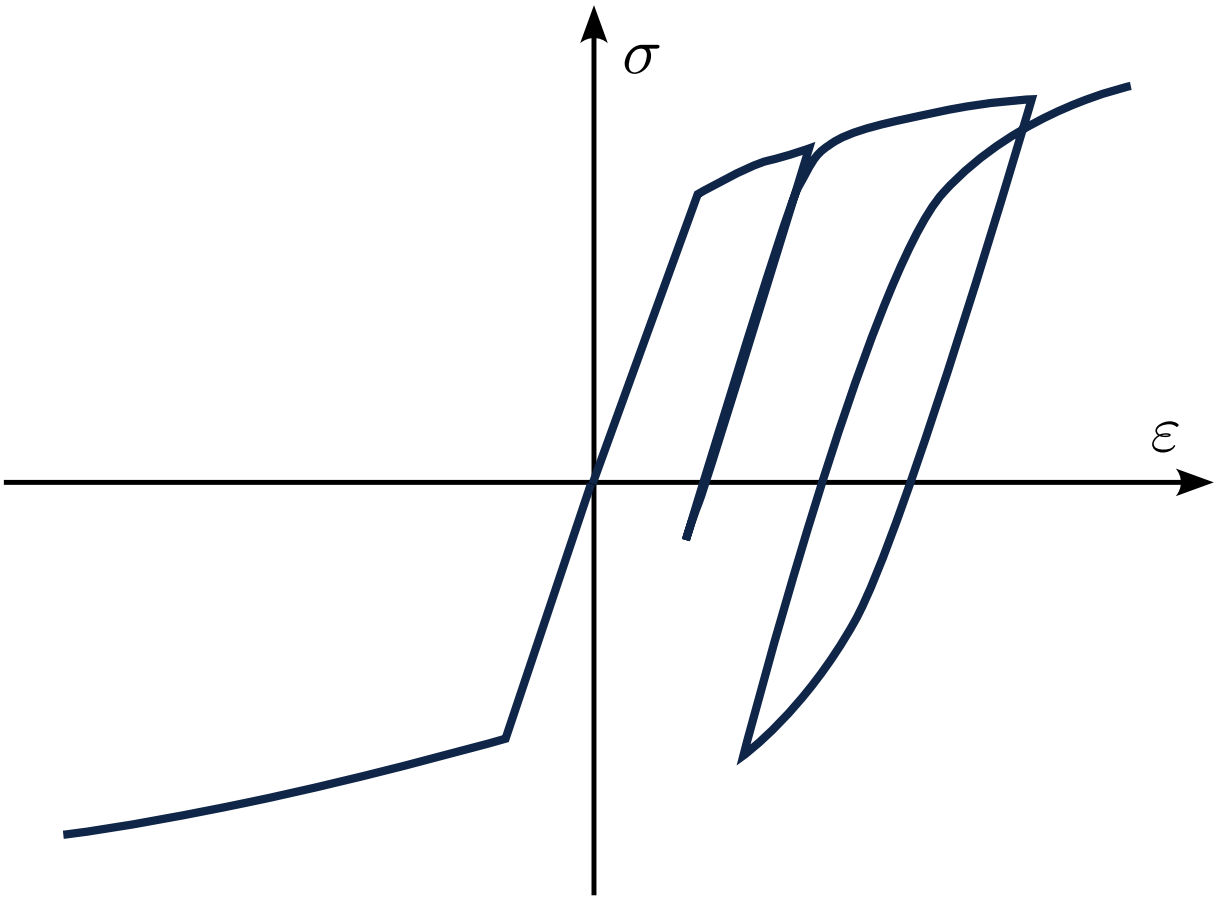

Contents

1 Phenomenological aspects of elastoplasticity **19**

2 Mathematical theory of elastoplastic constitutive modelling **21**

2.1 Additive decomposition of the strain tensor 21

2.2 Free energy potential and elastic law 21

2.3 Yield surface 22

2.4 Plastic flow rule and hardening law 23

2.5 Plastic multiplier 24

2.6 Rate form and elastoplastic tangent operator 25

3 Overview of classical constitutive models **25**

3.1 Classical yield criteria, plastic flow rules and hardening laws . 25

3.1.1 Yield criteria 25

3.1.2 Plastic flow rules 26

3.1.3 Hardening laws 26

3.2 Other typical effects and constitutive models 28

4 Elastoplastic problem resolution **30**

4.1 Elastoplastic problem 30

4.1.1 Temporal and spatial discretisation 30

4.1.2 Discretised mechanical equations 30

4.1.3 Constitutive incremental boundary value problem . 31

4.2 Resolution of the incremental problem 31

4.2.1 Return-mapping procedure 32

4.2.2 One-dimensional algorithm 33

5 Summary **34**

The present manuscript is concerned with the numerical prediction of inelasticity, and in particular elastoplasticity, *i.e.* irreversible, nonlinear, rate-independent material response.

This chapter recalls the most important concepts of the mathematical theory of elastoplasticity for solids subjected to infinitesimal deformations. Phenomenological aspects that may occur during service of elastoplastic parts are first explained, followed by mathematical hypotheses and definitions. Some classical models are then presented. Finally, the incremental problem is formulated and the return-mapping algorithm is detailed for solving elastoplastic problems in a one-dimensional setting.

The following is widely inspired by the textbooks of Lubliner (2008 [54]) for phenomenology and De Souza Neto *et al.* (2008 [21]) for mathematical methods.

1 Phenomenological aspects of elastoplasticity

> A large number of engineering materials, such as metals, concrete, rocks, clays and soils in general, may be modelled as plastic under a wide range of circumstances of practical interest. Lubliner (2008 [54])

Modern plasticity theory was primarily developed to describe the mechanical response of ductile metals, where plastic deformation is a consequence of the movement of dislocations, or *slip*, on crystallographic planes. However, various physical mechanisms are responsible for this type of behaviour in other materials. For instance, plasticity of soils is caused primarily by particles sliding over one another and strongly depends on the microstructure, chemical composition and water content. Alternatively, plasticity in brittle materials like rocks and concrete foremost occurs due to the opening and closing of microcracks. Many approximations for metals may not hold for these materials; we will thus restrict the present study to ductile solids.

Important phenomenological properties about plasticity can be inferred from the uniaxial tensile test in Fig. II.1:

- elastic domains delimited by the yield stresses σ_y, corresponding to segments O_0Y_0 and Y_1O_1,
- plastic yielding, which occurs when the material at the yield stress is further loaded, goes along with an evolution of plastic strains,
- hardening, which corresponds to the evolution of the yield stress between points Y_0 and Y_1.

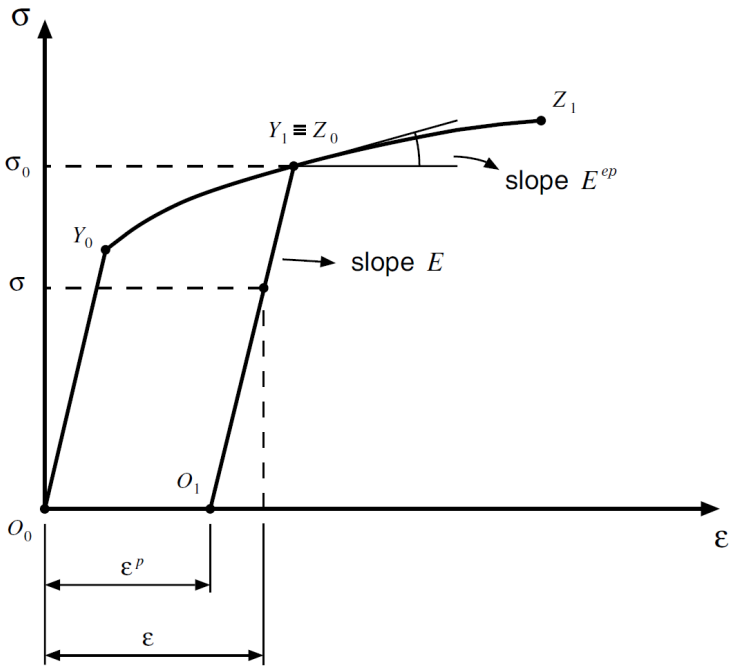

Figure II.1: Uniaxial tension experiment. Mathematical model. From De Souza Neto *et al.* (2008 [21])

In addition, most polycrystalline metals undergo a phenomenon known as Bauschinger effect (Fig. II.2): when subjected to increasing compressive stress, the yield stress in compression lowers if the material has previously been subjected to increasing tensile stress and then unloaded.

The following sections provide basic features and algorithms for computational plasticity. Widely applied in engineering, the approach is based on a continuous strain-stress relation called constitutive model, which depends on multiple parameters and can take different forms to accurately represent various materials.

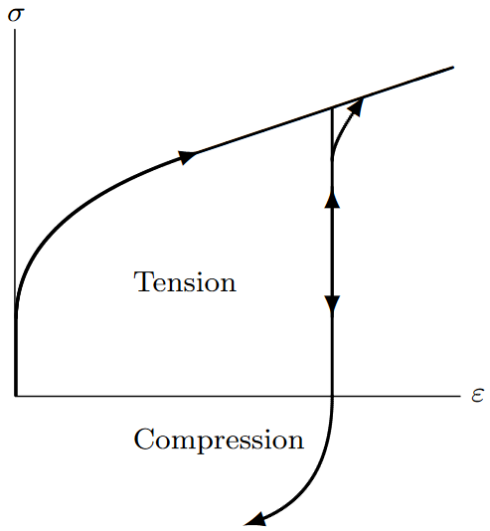

Figure II.2: Classical Bauschinger effect (from Lubliner (2008 [54]))

2 Mathematical theory of elastoplastic constitutive modelling

2.1 Additive decomposition of the strain tensor

One of the principal hypotheses of the small strain theory of plasticity is the decomposition of the strain tensor into the sum of a reversible elastic strain $\boldsymbol{\varepsilon}^{\mathrm{e}}$ and a permanent plastic strain $\boldsymbol{\varepsilon}^{\mathrm{p}}$,

$$\boldsymbol{\varepsilon} = \boldsymbol{\varepsilon}^{\mathrm{e}} + \boldsymbol{\varepsilon}^{\mathrm{p}}, \tag{II.1}$$

and its corresponding time-derivative form,

$$\dot{\boldsymbol{\varepsilon}} = \dot{\boldsymbol{\varepsilon}}^{\mathrm{e}} + \dot{\boldsymbol{\varepsilon}}^{\mathrm{p}}. \tag{II.2}$$

2.2 Free energy potential and elastic law

In plasticity theories, the free energy ψ introduced in Eq. I.9 is a function of the form:

$$\psi(\boldsymbol{\varepsilon}, \boldsymbol{\varepsilon}^{\mathrm{p}}, \boldsymbol{\alpha}), \tag{II.3}$$

where $\boldsymbol{\alpha}$ is a set of internal variables describing the hardening phenomenon.

Following this definition, the Clausius-Duhem inequality writes:

$$D = \left(\boldsymbol{\sigma} - \rho \frac{\partial \psi}{\partial \boldsymbol{\varepsilon}^{\mathrm{e}}} \right) : \dot{\boldsymbol{\varepsilon}} + \rho \frac{\partial \psi}{\partial \boldsymbol{\varepsilon}^{\mathrm{p}}} : \dot{\boldsymbol{\varepsilon}}^{\mathrm{p}} - \boldsymbol{A} * \dot{\boldsymbol{\alpha}} \geqslant 0, \tag{II.4}$$

with $*$ symbolising the appropriate product depending on internal variables dimensions and D the intrinsic dissipation. We have also introduced the hardening thermodynamical force $\boldsymbol{A}$ as:

$$\boldsymbol{A} = \rho \frac{\partial \psi}{\partial \boldsymbol{\alpha}}. \tag{II.5}$$

The elastic law obtained from the above inequality is:

$$\boldsymbol{\sigma} = \rho \frac{\partial \psi}{\partial \boldsymbol{\varepsilon}^{\mathrm{e}}} = \mathbb{D}^{\mathrm{e}} : \boldsymbol{\varepsilon}^{\mathrm{e}}, \tag{II.6}$$

where $\mathbb{D}^{\mathrm{e}} = \partial^2 \psi / \partial \boldsymbol{\varepsilon}^2$ is the standard isotropic elastic tensor.

The condition of non-negative plastic dissipation then reduces to:

$$D(\boldsymbol{\sigma}, \boldsymbol{A}; \dot{\boldsymbol{\varepsilon}}^{\mathrm{p}}, \dot{\boldsymbol{\alpha}}) = \boldsymbol{\sigma} : \dot{\boldsymbol{\varepsilon}}^{\mathrm{p}} - \boldsymbol{A} * \dot{\boldsymbol{\alpha}} \geqslant 0. \tag{II.7}$$

2.3 Yield surface

The occurrence of plastic flow is described by means of a non-positive scalar yield function which depends on the stress tensor and the set of hardening thermodynamical forces $\boldsymbol{A}$:

$$\Phi(\boldsymbol{\sigma}, \boldsymbol{A}) \leqslant 0. \tag{II.8}$$

Plastic flow may occur when the yield function reaches zero, while only elastic deformation is possible if it is negative. The elastic domain is defined as the set:

$$\{ \boldsymbol{\sigma} \mid \Phi(\boldsymbol{\sigma}, \boldsymbol{A}) < 0 \}, \tag{II.9}$$

i.e. the set of stresses for which plastic yielding is not possible. On the opposite, the set of stresses for which plastic yielding may occur, called yield locus, is the boundary of the elastic domain:

$$\{ \boldsymbol{\sigma} \mid \Phi(\boldsymbol{\sigma}, \boldsymbol{A}) = 0 \}. \tag{II.10}$$

2.4 Plastic flow rule and hardening law

In order to completely characterise the plasticity model, the evolution laws for the plastic strain tensor and the set $\boldsymbol{\alpha}$ of hardening variables must be defined. The plastic flow rule and hardening law are postulated as:

$$\dot{\boldsymbol{\varepsilon}}^{\mathrm{p}} = \dot{\gamma}\boldsymbol{N}(\boldsymbol{\sigma}, \boldsymbol{A}), \tag{II.11a}$$

and

$$\dot{\boldsymbol{\alpha}} = \dot{\gamma}\boldsymbol{H}(\boldsymbol{\sigma}, \boldsymbol{A}), \tag{II.11b}$$

where $\dot{\gamma}$ is a plastic multiplier, $\boldsymbol{N}$ is the flow vector and $\boldsymbol{H}$ is the hardening modulus which defines the evolution of the hardening variables. The loading/unloading conditions complement these evolution equations by defining when evolution of plastic strains and internal variables may occur:

$$\Phi \leqslant 0, \quad \dot{\gamma} \geqslant 0, \quad \Phi\dot{\gamma} = 0. \tag{II.12}$$

The flow rule, and possibly the hardening law, may be defined in terms of a flow, or plastic, potential $\Psi(\boldsymbol{\sigma}, \boldsymbol{A})$ from which derives the flow vector as

$$\boldsymbol{N} = \frac{\partial \Psi}{\partial \boldsymbol{\sigma}} \ , \tag{II.13}$$

and the hardening law as

$$\boldsymbol{H} = -\frac{\partial \Psi}{\partial \boldsymbol{A}} \ . \tag{II.14}$$

In that case, the plastic potential Ψ is a non-negative convex function of $\boldsymbol{\sigma}$ and $\boldsymbol{A}$, such that

$$\Psi(\boldsymbol{0}, \boldsymbol{0}) = 0, \tag{II.15}$$

to ensure that the dissipation inequality (Eq. II.7) is satisfied *a priori* by Eqs. II.11a and II.11b, and thus takes the form:

$$D(\boldsymbol{\sigma}, \boldsymbol{A}; \dot{\gamma}) = \dot{\gamma}\left(\boldsymbol{\sigma}\frac{\partial \Psi}{\partial \boldsymbol{\sigma}} + \boldsymbol{A}\frac{\partial \Psi}{\partial \boldsymbol{A}}\right) \geqslant 0. \tag{II.16}$$

2.5 Plastic multiplier

The determination of the plastic multiplier $\dot{\gamma}$ during plastic yielding was initially left aside: Eq. II.12 only ensures that it vanishes during elastic straining while it may assume any non-negative value during plastic flow. It should first be noted that the value of the yield function remains constant whenever plastic yielding occurs,

$$\Phi = 0. \tag{II.17}$$

From this comes the additional complementary condition,

$$\dot{\Phi}\dot{\gamma} = 0, \tag{II.18}$$

which implies that the rate of Φ vanishes during plastic yielding, *i.e.* when $\dot{\gamma} \neq 0$:

$$\dot{\Phi} = 0. \tag{II.19}$$

However it may assume any value during elastic straining, *i.e.* when $\dot{\gamma} = 0$. Eq. II.19 is called consistency condition.

The combination of the additive split of the strain tensor II.1, the elastic law II.6 and the plastic flow rule II.11a gives the stress rate:

$$\dot{\boldsymbol{\sigma}} = \mathbb{D}^{\mathrm{e}} : (\dot{\boldsymbol{\varepsilon}} - \dot{\boldsymbol{\varepsilon}}^{\mathrm{p}}) = \mathbb{D}^{\mathrm{e}} : (\dot{\boldsymbol{\varepsilon}} - \dot{\gamma}\boldsymbol{N}). \tag{II.20}$$

Together with the definition of $\boldsymbol{A}$ as a function of the free-energy potential II.5 and the evolution laws II.11, this gives the time-derivative of the yield function as:

$$\begin{aligned} \dot{\Phi} &= \frac{\partial \Phi}{\partial \boldsymbol{\sigma}} : \mathbb{D}^{\mathrm{e}} : (\dot{\boldsymbol{\varepsilon}} - \dot{\boldsymbol{\varepsilon}}^{\mathrm{p}}) + \frac{\partial \Phi}{\partial \boldsymbol{A}} * \rho \frac{\partial^2 \psi}{\partial \boldsymbol{\alpha}^2} * \dot{\boldsymbol{\alpha}} \\ &= \frac{\partial \Phi}{\partial \boldsymbol{\sigma}} : \mathbb{D}^{\mathrm{e}} : (\dot{\boldsymbol{\varepsilon}} - \dot{\gamma}\boldsymbol{N}) + \dot{\gamma} \frac{\partial \Phi}{\partial \boldsymbol{A}} * \rho \frac{\partial^2 \psi}{\partial \boldsymbol{\alpha}^2} * \boldsymbol{H}. \end{aligned} \tag{II.21}$$

Finally, the expression for the plastic multiplier is obtained by combination with the consistency condition II.19:

$$\dot{\gamma} = \frac{\partial \Phi / \partial \boldsymbol{\sigma} : \mathbb{D}^{\mathrm{e}} : \dot{\boldsymbol{\varepsilon}}}{\partial \Phi / \partial \boldsymbol{\sigma} : \mathbb{D}^{\mathrm{e}} : \boldsymbol{N} - \partial \Phi / \partial \boldsymbol{A} * \rho \partial^2 \psi / \partial \boldsymbol{\alpha}^2 * \boldsymbol{H}} \ . \tag{II.22}$$

2.6 Rate form and elastoplastic tangent operator

The rate form of the constitutive equation in the elastic regime is simply obtained from Eq. II.6 and reads:

$$\dot{\boldsymbol{\sigma}} = \mathbb{D}^{\mathrm{e}} : \dot{\boldsymbol{\varepsilon}}. \tag{II.23}$$

Under plastic yielding, the rate equation is of the form:

$$\dot{\boldsymbol{\sigma}} = \mathbb{D}^{\mathrm{ep}} : \dot{\boldsymbol{\varepsilon}}, \tag{II.24}$$

where $\mathbb{D}^{\mathrm{ep}}$ is the elastoplastic tangent modulus obtained by combining Eqs. II.20 and II.22 and assuming the symmetry of the elasticity tensor.

3 Overview of classical constitutive models

3.1 Classical yield criteria, plastic flow rules and hardening laws

3.1.1 Yield criteria

A yield criterion commonly used in engineering practice to describe metals is the isotropic, pressure-insensitive criterion of von Mises [56] that postulates plastic yielding begins when the J_2 stress deviator invariant reaches a critical value. The mathematical equation to represent this condition is:

$$\Phi = J_2 - R(\alpha), \tag{II.25}$$

where R is the critical value assumed to be a function of the hardening internal variable α. The stress deviator $\boldsymbol{s}$ and J_2 invariant are defined as:

$$\boldsymbol{s} = \boldsymbol{\sigma} - \frac{1}{3}(\mathrm{tr}(\boldsymbol{\sigma}))\boldsymbol{I}, \tag{II.26}$$

and

$$J_2 = \frac{1}{2}\|\boldsymbol{s}\|^2, \tag{II.27}$$

with $\boldsymbol{I}$ the identity matrix.

Tresca criterion is another common yield criterion for metals, while Mohr-Coulomb and Drucker-Prager yield criteria, that consider pressure-sensitivity, are often used for

soils, rocks and concrete.

3.1.2 Plastic flow rules

Plasticity models are classified as associative if the yield function is taken as a flow potential, and non-associative otherwise. In associative plasticity, the evolution equations defined in Eqs. II.11a and II.11b are written:

$$\dot{\boldsymbol{\varepsilon}}^{\mathrm{p}} = \dot{\gamma}\frac{\partial \Phi}{\partial \boldsymbol{\sigma}}, \tag{II.28a}$$

and

$$\dot{\boldsymbol{\alpha}} = -\dot{\gamma}\frac{\partial \Phi}{\partial \boldsymbol{A}}, \tag{II.28b}$$

implying normality of the plastic strain rate tensor to the yield surface in stress space and symmetry of the elastoplastic tangent operator.

A classical example of associative flow rule is the Prandtl-Reuss plasticity law that assumes a flow potential equal to the von Mises yield function. The flow rule thus becomes:

$$\dot{\boldsymbol{\varepsilon}}^{\mathrm{p}} = \dot{\gamma}\frac{\partial}{\partial \boldsymbol{\sigma}}\left[\sqrt{3J_2(\boldsymbol{s})}\right] = \dot{\gamma}\sqrt{\frac{3}{2}}\frac{\boldsymbol{s}}{\|\boldsymbol{s}\|}. \tag{II.29}$$

The assumption of associative plastic flow is particularly suited to the description of metals. Nevertheless, the use of non-associative laws is essential to predict the mechanical response of soils and granular materials in general.

3.1.3 Hardening laws

The dependence of yield stress level upon the history of plastic straining is represented by changes in the hardening thermodynamical force $\boldsymbol{A}$ during plastic yielding. These changes generally affect the size, shape and orientation of the yield surface.

Isotropic hardening corresponds to a uniform, or isotropic, expansion of the initial yield surface. Then, the set $\boldsymbol{\alpha}$ of internal variables normally contains a single scalar variable, which determines the size of the yield surface. A typical example is the von

Mises accumulated plastic strain:

$$p = \int_0^t \sqrt{\frac{2}{3}\dot{\boldsymbol{\varepsilon}}^{\mathrm{p}} : \dot{\boldsymbol{\varepsilon}}^{\mathrm{p}}}\,\mathrm{d}t = \int_0^t \sqrt{\frac{2}{3}}\|\dot{\boldsymbol{\varepsilon}}^{\mathrm{p}}\|\,\mathrm{d}t. \tag{II.30}$$

The corresponding rate evolution equation reads:

$$\dot{p} = \sqrt{\frac{2}{3}\dot{\boldsymbol{\varepsilon}}^{\mathrm{p}} : \dot{\boldsymbol{\varepsilon}}^{\mathrm{p}}} = \sqrt{\frac{2}{3}}\|\dot{\boldsymbol{\varepsilon}}^{\mathrm{p}}\|, \tag{II.31}$$

an equivalent formulation of which is given by the Prandtl-Reuss flow rule (Eq. II.29),

$$\dot{p} = \dot{\gamma}. \tag{II.32}$$

Kinematic hardening, alternatively, describes a translation of the yield surface in stress space without change in shape and size, also called Bauschinger effect [5]. The kinematically hardening von Mises yield function has the form,

$$\Phi(\boldsymbol{\sigma}, \boldsymbol{\chi}) = \sqrt{3J_2\left[\boldsymbol{s}(\boldsymbol{\sigma}) - \boldsymbol{\chi}\right]} - \sigma_y, \tag{II.33}$$

where $\boldsymbol{\chi}$ is the symmetric deviatoric back-stress tensor that represents the translation. A common evolution equation is Prager's linear kinematic hardening rule [65], where $\boldsymbol{\chi}$ is conjugated to the internal variable $\boldsymbol{\varepsilon}^{\mathrm{p}}$,

$$\boldsymbol{\chi} = \frac{2}{3}H\boldsymbol{\varepsilon}^{\mathrm{p}}. \tag{II.34}$$

Mixed isotropic-kinematic hardening enables a better reproducibility of real-life phenomena by combining both hardening types: under plastic straining, the yield surface deforms and translates simultaneously in stress space.

Summary of the one-dimensional elastoplastic constitutive model The general model developed above can be simplified to a one-dimensional model, in which all values are scalars. In particular, the isotropic elastic tensor $\mathbb{D}^{\mathrm{e}}$ reduces to the Young's modulus E and $\sigma_{y,0}$ is the initial yield stress, *i.e.* before hardening occurred. The resulting equations for linear kinematic hardening are summarised in Box II.1.

1. Elastoplastic split of the axial strain

$$\varepsilon = \varepsilon^{\mathrm{e}} + \varepsilon^{\mathrm{p}}$$

2. Uniaxial elastic law

$$\sigma = E\varepsilon^{\mathrm{e}}$$

3. Yield function

$$\Phi(\sigma, \chi) = |\sigma - \chi| - \sigma_{y,0}$$

4. Associated plastic flow rule

$$\dot{\varepsilon}^{\mathrm{p}} = \dot{\gamma}\mathrm{sign}\,(\sigma - \chi)$$

5. Kinematic hardening law

$$\chi = \chi(\varepsilon^{\mathrm{p}})$$

6. Loading/unloading conditions

$$\Phi \leqslant 0, \quad \dot{\gamma} \geqslant 0, \quad \Phi\dot{\gamma} = 0$$

7. Elastoplastic tangent modulus

$$E^{\mathrm{ep}} = \frac{EH}{E + H}$$

Box II.1: One-dimensional elastoplastic constitutive model with kinematic hardening

3.2 Other typical effects and constitutive models

Some phenomena that happen in plasticity cannot be accurately predicted by the classical constitutive models summarised in Section 3.1. For instance, the mechanical response under cyclic loading conditions exhibits additional specific effects, such as anisotropy and ratcheting.

Anisotropy usually occurs even in initially isotropic materials due to the hardening response on continued loading after yielding. The tensile yield strength is then different in the loading direction and in the direction normal to it. As for ratcheting (see Fig. II.3), which is an accumulation of plastic strain, it results in a change in mean strain during

one loading cycle with respect to the value obtained during the preceding cycle (Hübel, 1996 [38]).

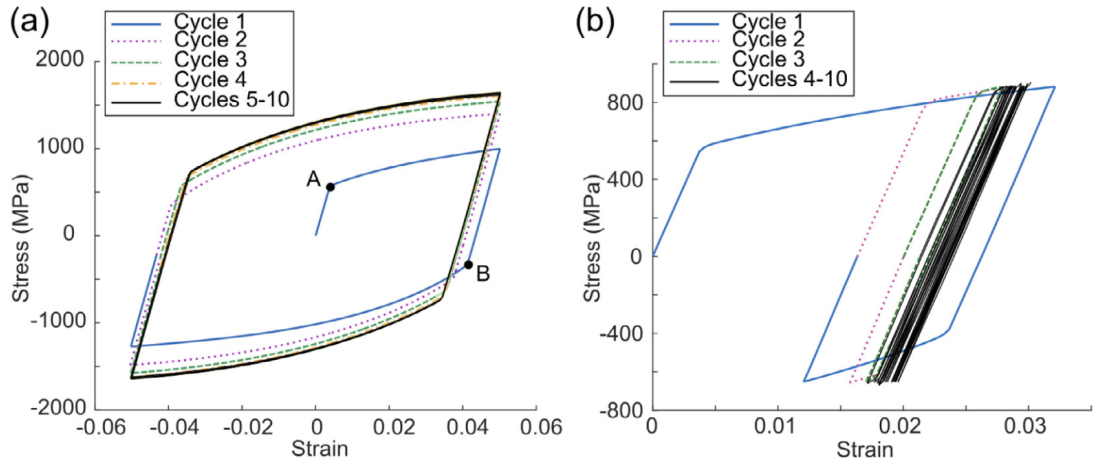

Figure II.3: Demonstration of the model with both isotropic and kinematic hardening. (a) Cyclic response under symmetric strain bounds. (b) Ratcheting response under asymmetric stress bounds. From Paranjape *et al.* (2018 [60])

In his review, Chaboche (2008 [11]) goes through different theories to account for anisotropy and ratcheting. These include anisotropic yield surfaces, *e.g.* Hill (1948 [36]), Barlat *et al.* (2003 [3]), combined with mixed isotropic and kinematic hardening laws, as Frederick *et al.* (2007 [28]). Alternatives are also suggested, *e.g.* multi-surface models introduced by Mróz (1967 [57]).

These models are continuously improved to better fit experiments (Paranjape *et al.*, 2018 [60]), account for additional phenomena (Mahan *et al.*, 2011 [55]), etc., which also results in higher complexity. Therefore, the more complex the models get, the more powerful the computational methods have to be to run accurate numerical simulations.

4 Elastoplastic problem resolution

4.1 Elastoplastic problem

4.1.1 Temporal and spatial discretisation

The resolution of the elastoplastic problem with the common Finite Element (FE) method involves two major numerical approximations:

- a time discretisation[1], which transforms time-continuum constitutive equations into incremental counterparts,
- a FE discretisation of the original body into a mesh composed of finite elements associated with shape functions.

The constitutive problem is then reduced to a set of incremental FE equations to be solved incrementally at each time step.

4.1.2 Discretised mechanical equations

We now consider a body $\Omega \in \mathbb{R}^d$ (with d the space dimension) and its FE discretisation ${}^h\Omega \in \mathbb{R}^d$ composed of N nodes and M integration points, used for the numerical resolution of the integral form of the BVP with Gaussian quadratures (see De Souza Neto *et al.* (2008 [21]) for more details). Within a time-discrete setting, we seek to approximate solutions of the elastoplastic problem at times $\{t_0, \dots, t_k, t_{k+1}, \dots T\}$.

The discrete body ${}^h\Omega$ undergoes displacements $\boldsymbol{u} = \{\boldsymbol{u}_a\}_{a=1}^N$ and loads $\boldsymbol{f} = \{\boldsymbol{f}_a\}_{a=1}^N$. At time t_k, the internal state of the discrete body is subjected to the discrete compatibility and equilibrium constraints defined by Eqs. I.2 and I.4. With the spatio-temporal discretisation, these equations transform into an Incremental Boundary Value Problem (IBVP):

$$\begin{cases} \boldsymbol{\varepsilon}_{e,k+1} = \boldsymbol{B}_e \boldsymbol{u}_{k+1}, \ \forall e = 1 \dots M, & \text{(II.35a)} \\ \sum_{e=1}^{M} w_e \boldsymbol{B}_e^{\mathsf{T}} \boldsymbol{\sigma}_{e,k+1} = \boldsymbol{f}_{k+1}, & \text{(II.35b)} \end{cases}$$

with w_e the weights of the integration points. $\boldsymbol{B}_e$ is the discrete symmetric gradient operator matrix related to integration point e that encodes the derivatives of the shape

1. As we consider time-independent material behaviours only, t is a pseudo-time and is used here as a convenient way to describe history.

functions.

4.1.3 Constitutive incremental boundary value problem

In linear elasticity, the stress tensor is expressed as a linear function of the strain tensor (Eq. II.6). The discrete BVP can be solved directly by substituting $\boldsymbol{\sigma}$ in the equilibrium equation (Eq. II.35b).

In elastoplasticity however, the material nonlinearity combined with path-dependency calls for adequate numerical resolution schemes for integration of the rate constitutive equations, which cannot be solved analytically when complex paths are involved.

The solution to the incremental elastoplastic problem depends on the prescribed incremental strain $\Delta\boldsymbol{\varepsilon}$ for the time interval $[t_k, t_{k+1}]$. All quantities of interest can also be expressed at time t_k, initial values $\boldsymbol{\varepsilon}^{\mathrm{e}}_k$ and $\boldsymbol{\alpha}_k$ being known. The constitutive IBVP thus consists in finding $\boldsymbol{\varepsilon}^{\mathrm{e}}_{k+1}$, $\boldsymbol{\alpha}_{k+1}$, $\Delta\gamma$ for the elastic strain, hardening internal variables set and increment of plastic multiplier, such that the plastic flow rule (Eq. II.11a), hardening law (Eq. II.11b) and loading/unloading conditions (Eq. II.12) are satisfied for $[t_k, t_{k+1}]$.

4.2 Resolution of the incremental problem

The resolution of the IBVP within a time increment $[t_k, t_{k+1}]$ requires two fundamental operations:

- update $\boldsymbol{\sigma}_{k+1}$ and $\boldsymbol{\alpha}_{k+1}$, respectively stress and internal variables at time t_{k+1} such that
$$\begin{cases} \boldsymbol{\sigma}_{k+1} = \hat{\boldsymbol{\sigma}}(\boldsymbol{\alpha}_k, \boldsymbol{\varepsilon}_{k+1}), \\ \boldsymbol{\alpha}_{k+1} = \hat{\boldsymbol{\alpha}}(\boldsymbol{\alpha}_k, \boldsymbol{\varepsilon}_{k+1}). \end{cases}$$
- compute the tangent operator $\mathbb{D}$, used to solve the nonlinear FE equilibrium equations.

The first operation is performed with the so-called elastic predictor/plastic corrector, or return-mapping algorithm, described in the following. The tangent operator,

$$\mathbb{D} = \frac{\partial \hat{\boldsymbol{\sigma}}}{\partial \boldsymbol{\varepsilon}_{k+1}}, \tag{II.36}$$

is the derivative of the implicit function defined by the return-mapping equations.

4.2.1 Return-mapping procedure

The return-mapping algorithm solving the IBVP is composed of three main steps, illustrated in Fig. II.4:

1. trial elastic state: compute the trial stress as if the behaviour was elastic during the increment,
2. compute the yield function and check whether the loading/unloading conditions are satisfied,
3. compute the effective stress and internal variables:
   - elastic transition: the stress equals the trial stress,
   - plastic yielding: project the trial stress onto the updated yield surface.

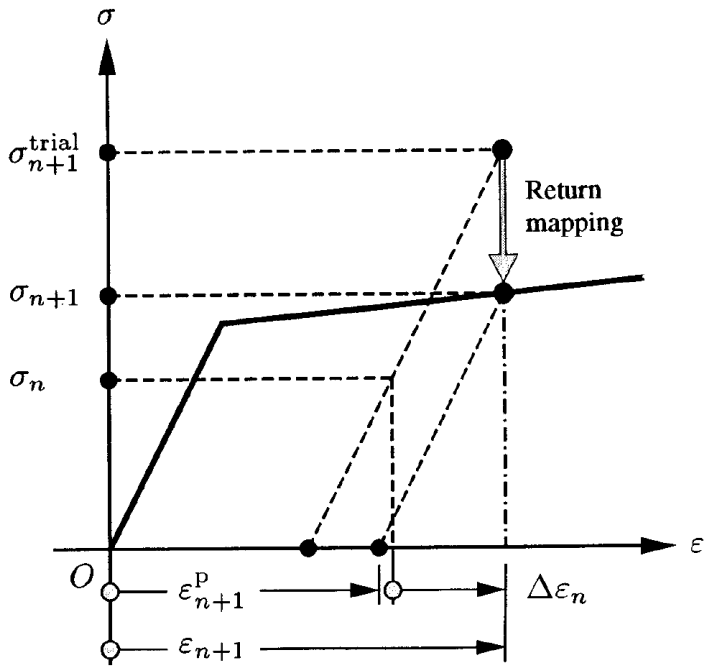

Figure II.4: The final stress is obtained by "returning" the trial stress to the yield surface through a scaling, hence, the denomination return mapping. From Simo *et al.* (1998 [71])

4.2.2 One-dimensional algorithm

This section presents the classical method for solving elastoplastic problems in a one-dimensional setting, as will be used in the third part of this manuscript to compute reference solutions. In this context, all quantities of interest are scalar.

The return-mapping algorithm procedure is provided in Alg. 1 for the constitutive model with linear kinematic hardening detailed in Box II.1. For a linear hardening law of the form

$$\chi(\varepsilon^{\mathrm{p}}) = H\varepsilon^{\mathrm{p}}, \tag{II.37}$$

the free energy of this model writes:

$$\psi(\varepsilon, \varepsilon^{\mathrm{p}}) = \frac{1}{2}E(\varepsilon - \varepsilon^{\mathrm{p}})^2 + \frac{1}{2}H(\varepsilon^{\mathrm{p}})^2. \tag{II.38}$$

Finally, dissipation is given by:

$$D = \sigma_{y,0}|\dot{\varepsilon}^{\mathrm{p}}|. \tag{II.39}$$

Algorithm 1 Return-mapping algorithm for elastoplasticity with linear isotropic hardening: compute response at step $k+1$

Input: $E, H, \sigma_{y,0}, \varepsilon_k, {\varepsilon_k}^{\mathrm{p}}, D_k, \varepsilon_{k+1}$.

$\sigma^{\mathrm{trial}} = E(\varepsilon_{k+1} - {\varepsilon_k}^{\mathrm{p}})$ ▷ *Elastic trial stress*

$\Phi = |\sigma^{\mathrm{trial}} - H{\varepsilon_k}^{\mathrm{p}}| - \sigma_{y,0}$ ▷ *Test for plastic yielding*

if $\Phi \leqslant 0$ **then** ▷ *Elastic straining*

  $\varepsilon^{\mathrm{p}}_{k+1} = \varepsilon^{\mathrm{p}}_k$

  $\sigma_{k+1} = \sigma^{\mathrm{trial}}$

else ▷ *Plastic yielding*

  $\Delta\varepsilon^{\mathrm{p}} = \mathrm{sign}\left(\sigma^{\mathrm{trial}}\right)\dfrac{\Phi}{E+H}$

  $\varepsilon^{\mathrm{p}}_{k+1} = \varepsilon^{\mathrm{p}}_k + \Delta\varepsilon^{\mathrm{p}}$

  $\sigma_{k+1} = E(\varepsilon_{k+1} - \varepsilon^{\mathrm{p}}_{k+1})$

  $D_{k+1} = D_k + \sigma_{y,0}|\Delta\varepsilon^{\mathrm{p}}|$

end if

Output: ${\sigma_{k+1}, \varepsilon^{\mathrm{p}}}_{k+1}, D_{k+1}$

5 Summary

Plasticity is a complex phenomenon involved in the mechanical behaviour of a large number of engineering materials. Constitutive modelling of elastoplasticity was primarily developed for metals, but because of the various physical mechanisms behind plastic deformation, many approximations may not hold for other materials. We restrict our study to classical plasticity in the small strain framework.

Besides the additive decomposition of the strain tensor into an elastic and a plastic part, the three main ingredients composing elastoplastic constitutive models are the yield function, the plastic flow rule and the hardening law. The first one establishes the conditions for the onset of plastic yielding, while the latter govern the evolution of the yield function during plastic yielding.

Some classical models have been presented in the third section, which are yet too restrictive for many applications. For instance, cyclic plasticity involves additional effects, as anisotropy and ratcheting, that cannot be predicted by these models. Ongoing research still aims to improve them to better reflect experiments, coming along with higher mathematical complexity of the related numerical methods.

The resolution of the FE incremental problem involves numerical methods to treat material non linearities and path-dependency. In particular, the return-mapping algorithm was detailed to solve incremental problems in a one-dimensional setting. It basically consists in computing an elastic trial state, which can then be corrected if it exceeds the elastic range by projection onto the yield surface. In a more general case, computing the material tangent operator is one of the tedious operations required.

Chapter III

Data and data-driven approaches in computational mechanics

Contents

1 Model-based methods **36**

2 Model-free methods **37**

2.1 Material data in model-free computational mechanics 37

2.2 Fundamental philosophical differences with constitutive modelling 38

3 Summary **39**

During the last decades, major breakthroughs in data science have led to a turning point in the way we create and use data in multiple domains, from medicine to economics, and even our everyday life.

The field of computational mechanics has also greatly benefited from the development of Machine Learning (ML), both to generate and handle data. The scientific community has embraced these tools to develop new methods in solid mechanics, the advancements of which are closely tied to progress in computer science. This field is therefore very active and constantly evolving. Various approaches emerged, which can be classified into two main trends: model-based and model-free methods.

1 Model-based methods

In these approaches, ML is used to discover or improve material models. The philosophy is similar to that of constitutive modelling, but aims to overcome two central limiting factors: the complexity of models and low computational efficiency of simulations.

Bock *et al.* (2019 [6]) published an overview of the application of ML in continuum mechanics. Their work looks over various ML methods that have been employed in materials research and classifies them by position in the process-structure-property-performance chain. The most popular tools are Artificial Neural Networks (ANNs) and their derivatives, Feedforward Neural Networks (FFNNs) and Recurrent Neural Networks (RNNs). The term ANN refers to "a simple one-layer neural network and [is] used as a linear classifier" [6]. Its simplest modern form is a FFNN, a unidirectional stack of layers, *i.e.* "in which each neuron computes an output based on inputs from the previous layer" [6], while a RNN is a bi-directional stack of ANNs.

More recently, a review by Dornheim *et al.* (2023 [24]) focussed solely on ANNs for learning constitutive behaviour. The authors went over about 200 papers, published between 1991 and 2022 except for a few posterior yet important contributions, presenting methods ranging from physical models to purely data-driven models. What results from this study is the variety of approaches, making them difficult to compare against each other. Furthermore, challenges remain regarding knowledge integration (*e.g.* from mechanical equations), extrapolation and interpretability of ANN constitutive model predictions.

2 Model-free methods

In parallel, Kirchdoerfer *et al.* (2016 [43]) proposed a new paradigm that completely bypasses constitutive models and their inherent bias. In this original approach, the material behaviour is encoded directly as a discrete set of data points, the "material database". Based on a FE discretisation, the model-free solver seeks to minimise the distance between the latter and a set of mechanical constraints. The solution to the problem is thus twofold: on the one side, mechanical fields fulfilling kinematic compatibility and equilibrium, and on the other side, material fields, which belong to the material database.

Model-free methods divide into two branches: Data-Driven Computational Mechanics (DDCM) and Data-Driven Identification (DDI).

- DDCM is a tool for structural analysis: the material database contains data points lying in a constitutive space, *e.g.* the strain-stress space. The solver can predict the mechanical response of a structure under various loading conditions in regions of the constitutive space sampled by the material database, *e.g.* the strain range covered by the material database in elasticity. The accuracy of the prediction depends on the constitutive space sampling.
- DDI is an identification method that, from experimental full-field strain measurements, aims to identify stresses. DDI has been introduced and investigated by Leygue *et al.* (2018 [52]) and Dalémat *et al.* (2019 [20]), who first developed coupled experimental and numerical tools for elastic materials. Unlike DDCM, the problem unknowns are mechanical and material stresses. In this method, material states are obtained by clustering analysis and constitute a sampling of the mechanical response evaluated by mechanical states. Besides, mechanical strains are measured by Digital Image Correlation (DIC) (Grédiac *et al.*, 2012 [31]) while stresses are estimated by DDI.

2.1 Material data in model-free computational mechanics

Contrarily to model-based approaches, material data is neither inter- nor extrapolated in DDCM and DDI. Therefore, appropriate data generation and constitutive space coverage is a fundamental question. In practice, data can be of different types:

- **Numerical data,** *e.g.* obtained from microscopic constitutive models, which allows

to summon data when, where and as densely as needed (see for instance Platzer (2020 [62]), Karapiperis *et al.* (2021 [42]), Gorgogianni *et al.* (2023 [30])). These adaptive/dynamic routines implemented into a multiscale setting provide an efficient alternative to the very expensive multilevel finite element approach (FE^2). While the latter requires evaluations of both micro- and macroscopic elements at every step, multiscale DDCM only invokes microscopic simulations when the regions of the constitutive space which are called for the macroscopic problem are too sparsely sampled.

- **Experimental data** obtained by DDI. An example is given by Stainier *et al.* (2019 [72]), whose article details a procedure for generating the material database with DDI and then solving a BVP with DDCM. Generating dense material databases thus calls for new experiments to gain knowledge about the mechanical response of the material under multiaxial loading conditions, as discussed in the thesis by Costecalde (2023 [19]).

2.2 Fundamental philosophical differences with constitutive modelling

A fundamental difference between model-based and model-free approaches emphasised in the previous section is the absence of data inter- and extrapolation in the latter. In addition, these approaches differ in the way various classes of material behaviours are treated.

Model-based methods are based on classifications of material behaviours as described in Chapter I and Chapter II. Constitutive models are designed for a given type of mechanical response. Solvers also adapt to and are designed for each category.

This is unnecessary in model-free approaches. For instance, as will be shown in the following sections, the same algorithm can be used in linear or nonlinear elasticity. Furthermore, there is no need to differentiate between history-dependent behaviours. We will take advantage of this distinctive feature of DDCM, which motivates the graph-based formulation for inelasticity developed in Chapter VI.

3 Summary

Recent advances in data science led to major breakthroughs in computational mechanics. Thanks to ML methods, simulations can be performed that involve complex models and require high computing capacity. In this context, ANN-based tools are particularly widespread for learning constitutive models and the variety of developed approaches reflects their popularity.

In parallel, model-free approaches emerged, introduced by Kirchdoerfer *et al.* (2016 [43]), which aim to replace constitutive models with a discrete "material database". This paradigm aims to bypass any inter-/extrapolation of the observed material behaviour. Two methods are currently developed: DDI for material identification and DDCM for structural analysis, which is the subject of this thesis.

Chapter IV

Model-free data-driven computational mechanics

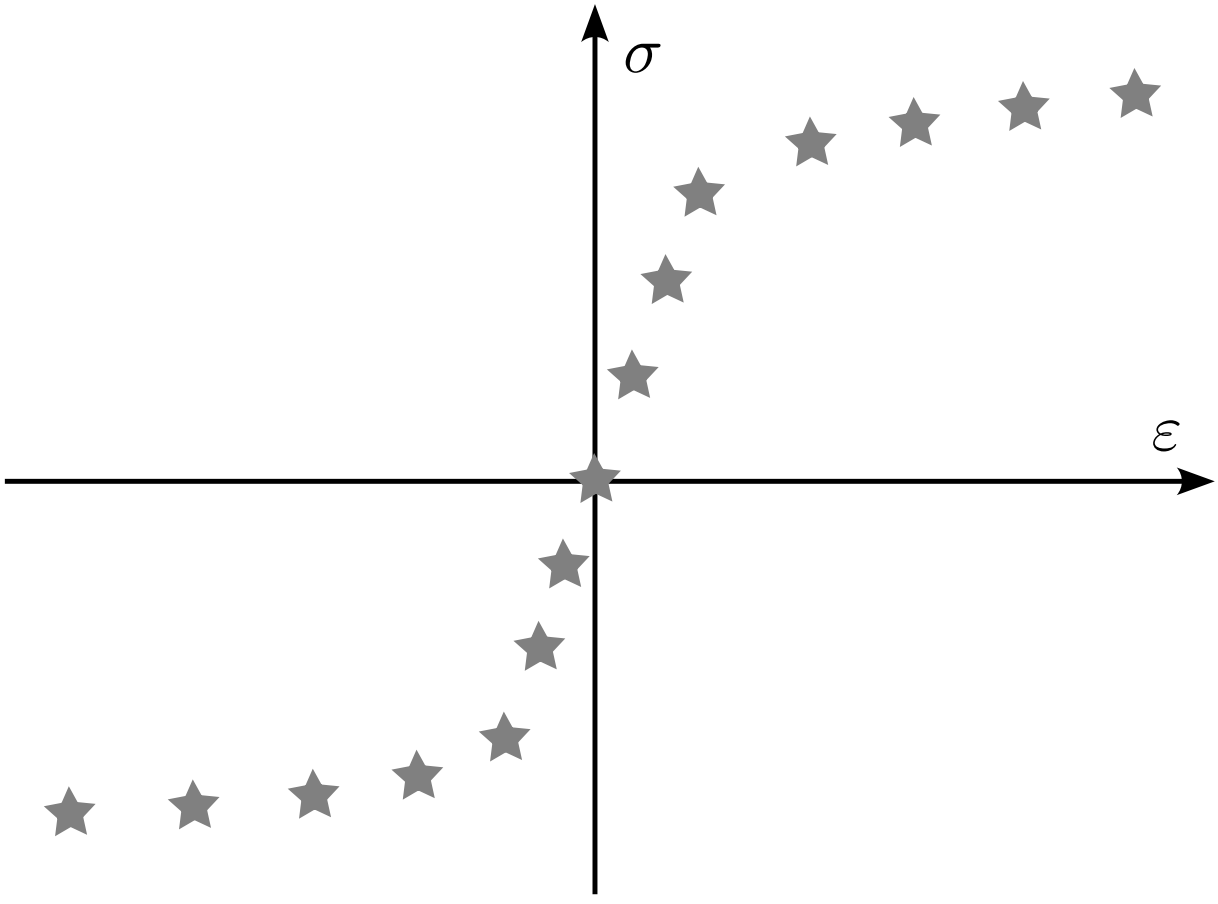

Contents

1 Data-Driven Computational Mechanics in elasticity **43**
1.1 Mathematical framework 43
1.2 Original algorithm 46
2 Extension to inelasticity **47**
2.1 Fundamental mathematical framework 47
2.2 History representation 48
2.3 Other approaches 49
3 Overview of related works **50**
3.1 Noisy data sets, insufficient data and uncertainty quantification 50
3.2 Extension to other classes of problems 52
4 Summary **54**

1 Data-Driven Computational Mechanics in elasticity

This section recalls the mathematical framework for data-driven elasticity introduced by Kirchdoerfer *et al.* (2016 [43]) and consolidated by Conti *et al.* (2018 [16]). The first subsection presents the FE discrete formulation and the numerical data-driven solver is listed in the second one.

1.1 Mathematical framework

We consider an inelastic body $\Omega \in \mathbb{R}^d$ and its discrete representation ${}^h\Omega \in \mathbb{R}^d$ composed of N nodes and M integration points, which undergoes displacements $\boldsymbol{u} = \{\boldsymbol{u}_a\}_{a=1}^N$ and loads $\boldsymbol{f} = \{\boldsymbol{f}_a\}_{a=1}^N$. The internal state of the discrete body is subjected to compatibility and equilibrium constraints:

$$\begin{cases} \boldsymbol{\varepsilon}_e = \boldsymbol{B}_e \boldsymbol{u} \ \forall e = 1 \dots M, & \text{(IV.1a)} \\ \sum_{e=1}^{M} w_e \boldsymbol{B}_e^{\mathsf{T}} \boldsymbol{\sigma}_e = \boldsymbol{f}, & \text{(IV.1b)} \end{cases}$$

with w_e the weights of the integration points and $\boldsymbol{B}_e$ the discrete kinematic operator matrix related to integration point e. Eqs. IV.1a and IV.1b correspond to the space-discretised form of Eqs. (I.2) and (I.4).

A local state z_e describing the internal condition of the system at each integration point is defined as:

$$z_e = (\boldsymbol{\varepsilon}_e, \boldsymbol{\sigma}_e) \in \mathcal{Z}_e, \tag{IV.2}$$

with $\mathcal{Z}_e$ the local constitutive space, such that $\mathcal{Z}_e = \mathbb{R}^{m_e} \times \mathbb{R}^{m_e}$, and with m_e the dimension of the tensors at integration point e. In a three-dimensional setting $m_e = 6$ in Voigt notation, while $m_e = 1$ for bar elements. The global state $z = \{(\boldsymbol{\varepsilon}_e, \boldsymbol{\sigma}_e)\}_{e=1}^M \in \mathcal{Z}$ represents the whole system in the global constitutive space $\mathcal{Z} = \bigotimes_{e=1}^{M} \mathcal{Z}_e$, with $\bigotimes$ meaning the tensor product of spaces.

The mechanical admissibility of a state is material-independent and given by Eqs. IV.1a and IV.1b. A first subset $\mathcal{E}$ of the global constitutive space, the set of mechanical con-

straints, can thus be defined as:

$$\mathcal{E} = \{z \in \mathcal{Z} \mid \text{ Eqs. IV.1a and IV.1b}\} \subset \mathcal{Z}. \tag{IV.3}$$

In small strain elasticity, the system Eq. II.35a is usually solved using a constitutive relation of the following type:

$$\boldsymbol{\sigma} = \check{\boldsymbol{\sigma}}(\boldsymbol{\varepsilon}), \tag{IV.4}$$

with $\check{\boldsymbol{\sigma}} : \mathbb{R}^{m_e} \to \mathbb{R}^{m_e}$ describing a potentially nonlinear relation between $\boldsymbol{\sigma}$ and $\boldsymbol{\varepsilon}$ and *a priori* bijective.

In the data-driven approach, the formulation of a constitutive relation between stress and strain is bypassed by reformulating the BVP into a minimisation problem. Instead of a mathematical law, the material response is described by collections of states, obtained for instance through experiments or numerical simulations at a finer material scale. These local material databases write:

$$\mathcal{D}_e = \{y_i = (\boldsymbol{\varepsilon}_i, \boldsymbol{\sigma}_i) \in \mathcal{Z}_e,\ i = 1 \dots N^*\} \subset \mathcal{Z}_e, \tag{IV.5}$$

with N^* a finite number of strain-stress pairs. The resulting global material database is $\mathcal{D} = \bigotimes_{e=1}^{M} \mathcal{D}_e$, second subset of $\mathcal{Z}$.

We then associate a norm to the local constitutive space:

$$\|z_e\|_{\mathbb{C}} = \left[\frac{1}{2}(\mathbb{C}_e : \boldsymbol{\varepsilon}_e) : \boldsymbol{\varepsilon}_e + \frac{1}{2}(\mathbb{C}_e^{-1} : \boldsymbol{\sigma}_e) : \boldsymbol{\sigma}_e\right]^{1/2}, \tag{IV.6}$$

with the data-driven metric tensor $\mathbb{C}_e$ a positive-definite 4th-order tensors that is not related to any material property and can be updated during the simulation. Hence the squared distance between two states[1] $z_e, y_e \in \mathcal{Z}_e$ is:

$$d^2_{\mathbb{C}}(z_e, y_e) = \|z_e - y_e\|^2_{\mathbb{C}}\ . \tag{IV.7}$$

The extension to the global constitutive space $\mathcal{Z}$ gives the global distance, also called

1. For clarity and when applicable, we will keep the same notations throughout this manuscript for mechanical states, denoted z, and states of the material database, denoted y.

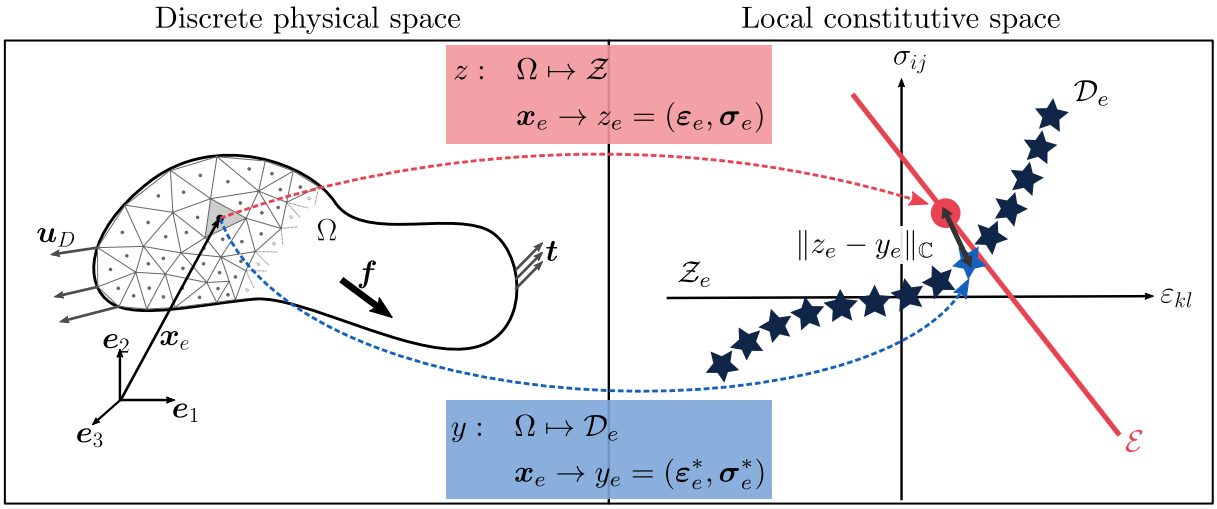

Figure IV.1: Functional spaces of the data-driven FE formulation. The mechanical state z_e (red circle) of the integration point can only move along the constraint set (red solid line). The material state y_e (light blue star) of the integration point is the closest material data point selected from the material database $\mathcal{D}_e$ (dark blue stars), according to the local distance $\|z_e - y_e\|_{\mathbb{C}}$ defined Eq. IV.14. From Platzer (2020 [62])

objective function of the DDCM problem:

$$d^2_{\mathbb{C}}(z, y) = \sum_{e=1}^{M} w_e d^2_{\mathbb{C}}(z_e, y_e) \ . \tag{IV.8}$$

Finally, the DDCM problem is formulated as a double minimisation problem, whose solution is given by:

$$\mathcal{S} = \arg \min_{z \in \mathcal{E}} \min_{y \in \mathcal{D}} d^2_{\mathbb{C}}(z, y), \tag{IV.9}$$

i.e. the pair (z, y) of states, respectively mechanically admissible and from the material database, which are closest to each other with respect to distance $d_{\mathbb{C}}$. It is worth noting that the algorithm remains unchanged for linear and nonlinear behaviours.

Fig. IV.1, taken from Platzer (2020 [62]) with adapted notations, illustrates the above definitions and minimisation problem with a constitutive space schematic representation in two dimensions. In the small strain regime and for loading conditions independent of the motion, the constraint set $\mathcal{E}$ subject to linear compatibility and equilibrium equations results in a linear manifold. The local material database $\mathcal{D}_e$ represents a nonlinear elastic behaviour.

1.2 Original algorithm

In this work, the DDCM solution is obtained by alternating minimisation over continuous (z) and discrete (y) variables, as illustrated in Fig. IV.2. This algorithm consists in the fixed-point iteration:

$$z^{(i+1)} = P_{\mathcal{E}} P_{\mathcal{D}} z^{(i)} \tag{IV.10}$$

with i the iteration number, $y^{(i)} = P_{\mathcal{D}} z^{(i)}$ the closest point projection onto $\mathcal{D}$, which consists in searching for the nearest neighbour of $z^{(i)}$ in $\mathcal{D}$, and $P_{\mathcal{E}} y^{(i)}$ the projection of a material state onto $\mathcal{E}$. The latter operation is a constrained minimisation problem with a quadratic function to be minimised and a linear constraint. From the nature of the metric tensor $\mathbb{C}$, similar to the elasticity tensor, yields a simple pseudo-elastic problem typically solved with the method of Lagrange multipliers.

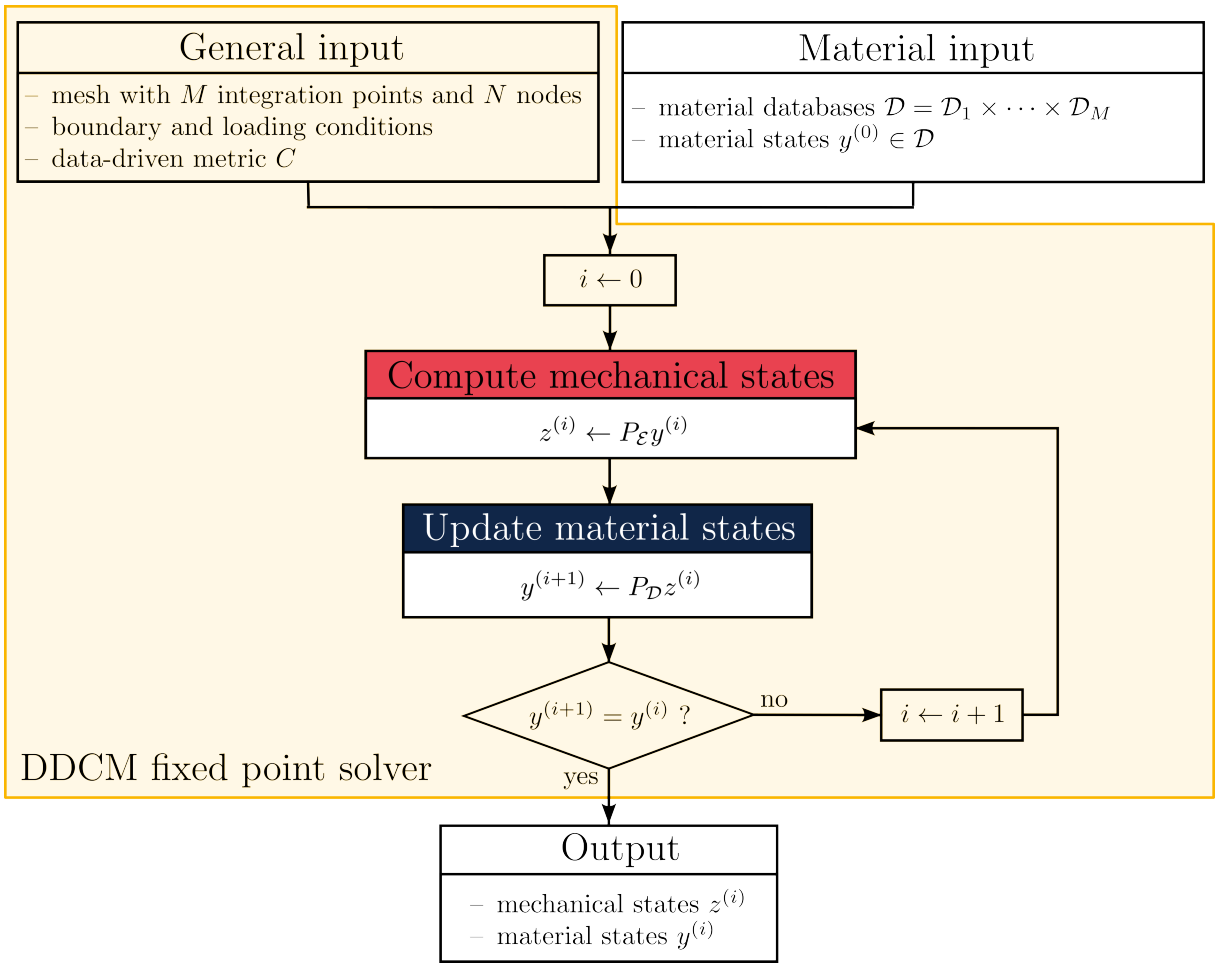

Figure IV.2: DDCM algorithm for elastic material response

2 Extension to inelasticity

The characteristic of inelastic behaviours in the broadest sense is the irreversibility of the material response. As opposed to elasticity, where the material response can be described as a manifold that can be freely and entirely scanned to get the solution of the DDCM problem, inelasticity implies a significant dependence on past history. Strain-stress pairs are therefore not sufficient to unequivocally identify material points.

The original DDCM framework introduced in 2016 has been extended a few years later by Eggersmann *et al.* (2019 [25]) to inelasticity, of which elastoplasticity is a special case. Section 2.1 recalls the main outlines of their work, while Section 2.3 briefly presents concurrent approaches.

2.1 Fundamental mathematical framework

In order to take into account the history of strains and stresses, we switch to a time-discrete setting, where we seek to approximate solutions at times $\{t_0, \dots, t_k, t_{k+1}, \dots\}$.

As described in Chapter II, time discretisation transforms Eqs. IV.1a and IV.1b into Eqs. II.35a and II.35b, recalled here:

$$\begin{cases} \boldsymbol{\varepsilon}_{e,k+1} = \boldsymbol{B}_e \boldsymbol{u}_{k+1}, \ \forall e = 1 \dots M, \\ \sum_{e=1}^{M} w_e \boldsymbol{B}_e^{\mathsf{T}} \boldsymbol{\sigma}_{e,k+1} = \boldsymbol{f}_{k+1}. \end{cases}$$

They provide the instantaneous set of mechanical constraints:

$$\mathcal{E}_{k+1} = \{z \in \mathcal{Z} \mid \text{ Eqs. (II.35a) and (II.35b)}\} \subset \mathcal{Z}_{k+1}. \tag{IV.11}$$

The local material database for a given element at a specific time step reads:

$$\mathcal{D}_{e,k+1} = \{y_i = (\boldsymbol{\varepsilon}_i, \boldsymbol{\sigma}_i) \in \mathcal{Z}_{e,k+1}, \ i = 1 \dots N^* \mid \text{past local history}\} \subset \mathcal{Z}_{e,k+1}. \tag{IV.12}$$

Also, the norm, the squared local and global distances read respectively:

$$\|z_{e,k+1}\|_{\mathbb{C}} = \left[\frac{1}{2}(\mathbb{C}_{e,k+1} : \boldsymbol{\varepsilon}_{e,k+1}) : \boldsymbol{\varepsilon}_{e,k+1} + \frac{1}{2}(\mathbb{C}_{e,k+1}^{-1} : \boldsymbol{\sigma}_{e,k+1}) : \boldsymbol{\sigma}_{e,k+1}\right]^{1/2}, \tag{IV.13}$$

$$d^2_{\mathbb{C}}(z_{e,k+1}, y_{e,k+1}) = \|z_{e,k+1} - y_{e,k+1}\|^2_{\mathbb{C}} \ , \tag{IV.14}$$

and

$$d^2_{\mathbb{C}}(z_{k+1}, y_{k+1}) = \sum_{e=1}^{M} w_e d^2_{\mathbb{C}}(z_{e,k+1}, y_{e,k+1}) \ , \tag{IV.15}$$

providing the new definition of the double minimisation problem,

$$\mathcal{S} = \arg \min_{z_{k+1} \in \mathcal{E}_{k+1}} \min_{y_{k+1} \in \mathcal{D}_{k+1}} d^2_{\mathbb{C}}(z_{k+1}, y_{k+1}). \tag{IV.16}$$

The principal challenge hence lies in the selection of local material databases $\mathcal{D}_{e,k+1}$ subject to past history.

2.2 History representation

Eggersmann *et al.* (2019 [25]) review different paradigms to represent history dependent materials in continuum mechanics. The first one, called *general materials with memory*, refers to materials that exhibit a relation between the state of stress and the history of strain of the form:

$$\boldsymbol{\sigma}_{e,k+1} = \hat{\boldsymbol{\sigma}}_e(\{\boldsymbol{\varepsilon}_{e,l}\}_{l \leqslant k+1}) \tag{IV.17}$$

with $\boldsymbol{\sigma}_{e,k+1}$ the stress at given material point and time, $\{\boldsymbol{\varepsilon}_{e,l}\}_{l \leqslant k+1}$ the history of strain (prior to t_{k+1}) and $\hat{\boldsymbol{\sigma}}_e$ a discrete hereditary function. Local material databases then read:

$$\mathcal{D}_{e,k+1} = \{(\boldsymbol{\varepsilon}_{e,k+1}, \boldsymbol{\sigma}_{e,k+1}) \mid \{\boldsymbol{\varepsilon}_{e,l}\}_{l \leqslant k}\} \tag{IV.18}$$

However, this implies to deal with long histories of strain, even in the case of fading memories.

Differential representation, a second paradigm, uses limited histories of strain and stress to represent material irreversibility. Local material data sets take the form:

$$\mathcal{D}_{e,k+1} = \{(\boldsymbol{\varepsilon}_{e,k+1}, \boldsymbol{\sigma}_{e,k+1}) \mid (\{\boldsymbol{\varepsilon}_{e,k-l}\}_{l=0}^{p-1}, \{\boldsymbol{\sigma}_{e,k-l}\}_{l=0}^{q-1})\}, \tag{IV.19}$$

with $\{\boldsymbol{\varepsilon}_{e,k-l}\}_{l=0}^{p-1}$ and $\{\boldsymbol{\sigma}_{e,k-l}\}_{l=0}^{q-1}$ the first p and q time derivatives of strain and stress respectively.

Finally, *internal variables* and *history variables* are additional variables used to char-

acterise the state at a material point. They summarise its past history, reducing local material databases to:

$$\mathcal{D}_{e,k+1} = \{(\boldsymbol{\varepsilon}_{e,k+1}, \boldsymbol{\sigma}_{e,k+1}) \mid \boldsymbol{\alpha}_{e,k}\} \tag{IV.20}$$

where $\boldsymbol{\alpha}_{e,k}$ is the array of variables at material point e and time t_k. This explicit formalism greatly simplifies the computation of data sets compared to the previous ones and has been used in Chapter II for the description of elastoplastic constitutive modelling.

The distinction between the two latter representations lies in their interpretation: while internal variables usually contain physical information that might not be observable and result from modelling assumptions, history variables "simply record partial information about the history of the material" [25].

2.3 Other approaches

The work by Eggersmann *et al.* (2019 [25]) provides a general framework for inelasticity but no practical implementation. Several authors also explored this topic and tried different approaches and assumptions.

Instead of subjecting local databases to histories, Ciftci *et al.* (2022 [14]) chose to extend the database with the tangent space information (Eggersmann *et al.*, 2021 [27]). A strain-stress pair may be associated with different tangent spaces, that can be classified as elastic or plastic subsets and essentially determined by the elastic stiffness or the hardening modulus respectively. A transition rule based on a yield function maps the modelling points to the subsets. This method also enables interpolation in sparsely sampled regions of the constitutive space. In a second publication [15], the same authors provided a guide to compute the tangent space and the yield surface in the Haigh–Westergaard space for elastoplasticity with isotropic hardening. Similarly to this approach and based on the variational formulation of DDCM (Nguyen *et al.*, 2020 [59]), Pham *et al.* (2023 [61]) developed an algorithm for J_2-plasticity with isotropic hardening.

Alternatively, Bartel *et al.* (2023 [4]) chose to keep the same database for all loading steps. However, they introduced a history surrogate, a quantity "that can be tapped along a hypothetical load path and can represent the history dependence as accurately and unambiguously as possible", and a propagator, that updates the history surrogate at each loading step. The former contains specific strain and stress values or quantities directly

derived from them and recording load reversals. The latter replaces the constitutive evolution equation and depends on the quantities chosen to define the history surrogate. The definition of data-driven distance is also updated to take history into account. This method, developed for one-dimensional elements, applies to several material classes of inelastic phenomena and is absolutely model-free. However, the extension to two- and three-dimensional problems is not straightforward, since the definition of history surrogate is not universal and even material-dependent. Poelstra *et al.* (2022 [64]) followed the same idea, but determined the appropriate history surrogate thanks to an ANN.

Finally, a preliminary study on the extension of DDI to elastoplastic behaviours with differential representation has been conducted by Langlois (2023 [49]), but lots of open questions still remain. Advances in DDCM, which constitute the subject of this thesis, might also help solving issues for identification.

3 Overview of related works

The DDCM extensions listed below have been well described in Platzer's PhD thesis (Platzer, 2020 [62]). This section provides an up-to-date version of this work with some of the latest publications on the topic.

3.1 Noisy data sets, insufficient data and uncertainty quantification

The alternated minimisation solver originally proposed by Kirchdoerfer *et al.* (2016 [43]) is still widely used in the community despite its major drawback: since the discrete nature of the material database leads to high combinatorial complexity as the number of integration points in the mesh M and the material database size N^* increase, the proportion of local minima rises too, which implies a greater probability that the solver will converge towards local minima that are far from global minima. While this effect is limited with noise-free data, it becomes of significant impact when dealing with noisy data sets where the alternated minimisation solution can be dominated by outliers.

Kanno (2019 [41]) attempted to improve robustness of the solver with respect to outliers by transforming the DDCM problem into a Mixed-Integer Quadratic Programming

(MIQP) problem that can be solved globally with a standard algorithm. However, the main drawback of this method is its computational cost that may become very large when the size of the problem increases, since the number of unknowns is the product of M and N^*.

An enhanced entropy-maximising (max-ent) solver has been developed by Kirchdoerfer *et al.* (2017 [44]) to deal with noisy databases that "assign[s] data points a variable relevance depending on distance to the solution and through maximum-entropy estimation". A simulated annealing schedule ensures that both criteria evolve reciprocally to efficiently penalise outliers and achieve robustness.

Other approaches are based on the assumption of an underlying constitutive manifold in the material data set, which comes down to coupling model-free DDCM and manifold learning techniques. The mechanical solution is projected onto the constitutive manifold to obtain the material solution. The manifold may be reconstructed with diverse methods to smooth the optimisation problem and thus reduce the influence of noise. As an example, Kanno (2018 [40]) used kernel regression, while He *et al.* (2020 [35]) performed on the fly locally convex reconstruction of the manifold and Bahmani *et al.* (2023 [2]) introduced a geometric autoencoder to recover and flatten the underlying manifold.

An additional advantage of these methods is their ability to counter the "curse of dimensionality", to which DDCM is highly sensitive. This expression refers to the difficulty of sampling all the relevant regions of the constitutive space needed to achieve the good convergence of the solver when the dimensionality of this space increases. Indeed, the constitutive space for a general 1D mechanical problem is of dimension 2, which increases to 12 for the 3D case. The contribution by Eggersmann *et al.* (2021 [27]) addresses this issue in a different manner: the authors seek to minimise the distance to a tangent space computed in an off-line step for each material point in the local data set. This method enables interpolation in poorly sampled regions of the constitutive space and proved to outperform the max-ent solver.

To handle noisy data and quantify uncertainties, other authors have preferred adopting a statistical representation of the DDCM problem. As an example, Ayensa-Jiménez *et al.* (2018 [1]) incorporated statistical uncertainty into the distance-minimising solver to account for the random nature of data, while Korzeniowski *et al.* (2019 [46]) compared stochastic and DDCM approaches. Alternatively, the concept of Uncertainty Analysis-based DDCM (UA-DDCM) was developed by Guo *et al.* (2021 [33]), who, instead of looking for a single solution, aims to find a solution set "induced by the uncertainty of the data

point characterised by a bounding interval". Huang *et al.* (2023 [37]) then improved the numerical efficiency of this approach.

Recently, Weinberg *et al.* (2023 [76]) considered game theory to formulate a new implementation of DDCM where strain and stress are players that may or may not cooperate to pursue their respective objectives. In this setting, a non-cooperative data-driven game replaces the prior cooperative strategy: "the objective of the stress player is to minimize the discrepancy to a material data set that characterizes material behavior; the objective of the strain player is to ensure the admissibility of the mechanical state, in the sense of satisfying compatibility and equilibrium" [76]. Following the philosophy behind DDCM, the connection between material data and resolution tool is direct, unsupervised and model–free. The method can also be associated with the max-ent regularisation for noisy data with outliers.

Finally, some studies focussed on improving efficiency, the point projection $P_{\mathcal{D}}$ stage being the weakest point as it requires to search the whole database. In particular, Eggersmann *et al.* (2021 [26]) compared different approximate nearest-neighbour algorithms and Korzeniowski *et al.* (2021 [47]) tried a multi-level method that first provides an approximation of the material state based on a coarse database subset, which is then adaptively refined to improve the solution.

3.2 Extension to other classes of problems

Since 2016 and the first work on DDCM for elastic behaviours, the approach has been extended to several classes of problems, a non-exhaustive overview of which is given in Fig. IV.3. Each case requires adapted balance equation, while the mathematical framework remains the same.

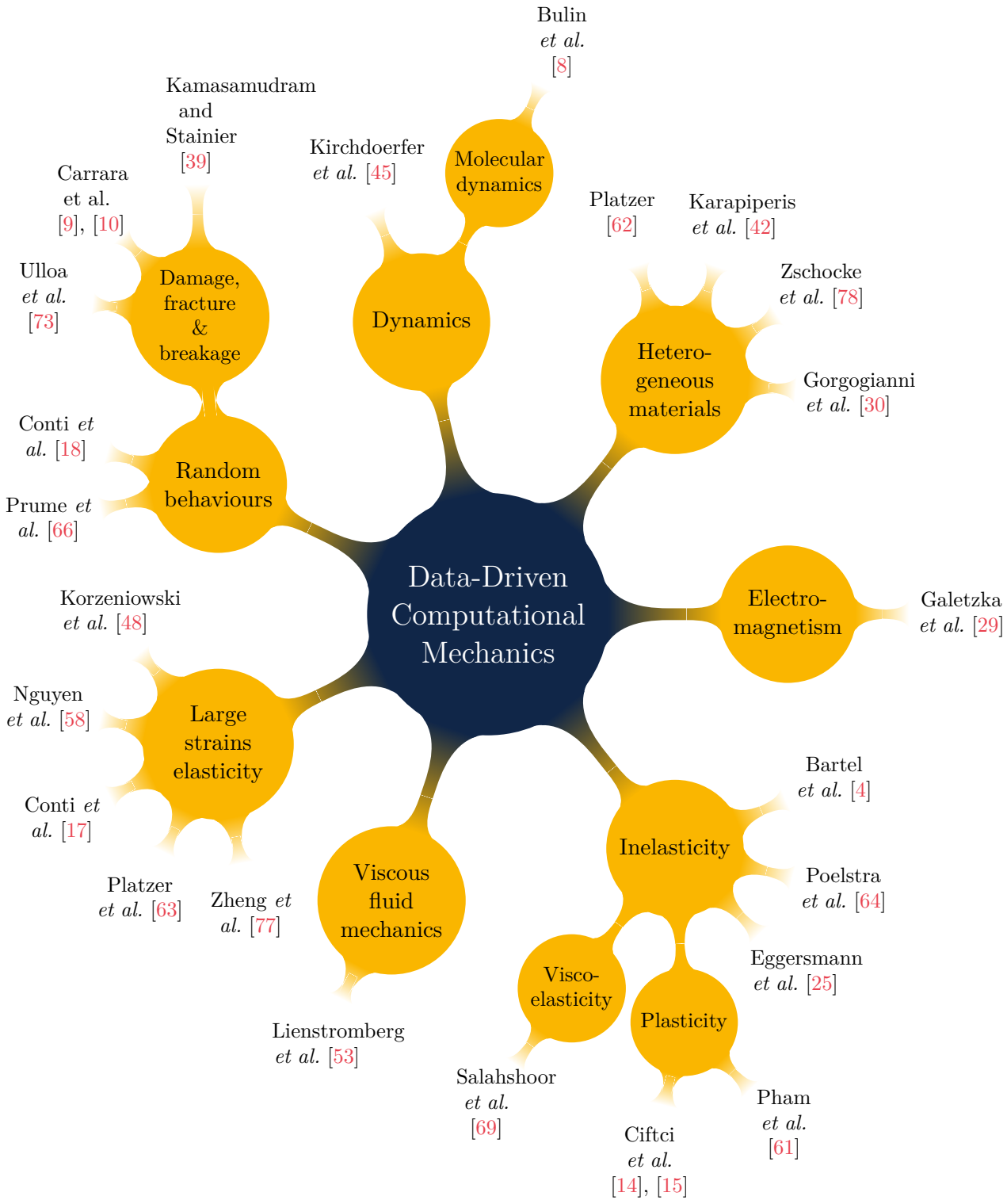

Figure IV.3: Overview of DDCM extensions

4 Summary

The broad topic "model-free data-driven computational mechanics" gathers approaches derived from the work by Kirchdoerfer *et al.* (2016 [43]). Contrary to constitutive modelling, the fundamental principle of this paradigm is a discrete representation of the material behaviour, which prevents bias induced by inter- and/or extrapolation. The data-driven solver seeks to minimise the *distance* between a discrete material database and continuous mechanical constraints, *i.e.* kinematic compatibility and equilibrium. The BVP solution is twofold:

- a *material state field*, belonging to the material database,
- a *mechanical state field* that verifies mechanical constraints.

The data-driven problem is a double minimisation problem and is usually solved with a fixed-point algorithm.

The method, originally developed in elasticity, has since then been extended to various classes of material behaviours. Additionally, improvements of the *alternated minimisation solver* have been proposed, *e.g.* to speed up convergence or deal with noisy data and outliers.

Regarding inelasticity, Eggersmann *et al.* (2019 [25]) laid the foundations for the data-driven incremental BVP. The mathematical framework transforms the definition of local material database to include path-dependency, which can be represented by a mathematical relation encoding the history of strain, or summarised by internal/history variables or differential representations.

Part B

Towards an incremental problem formulation for model-free data-driven inelasticity

Chapter V

Incremental problem formulation for inelastic data-driven simulation

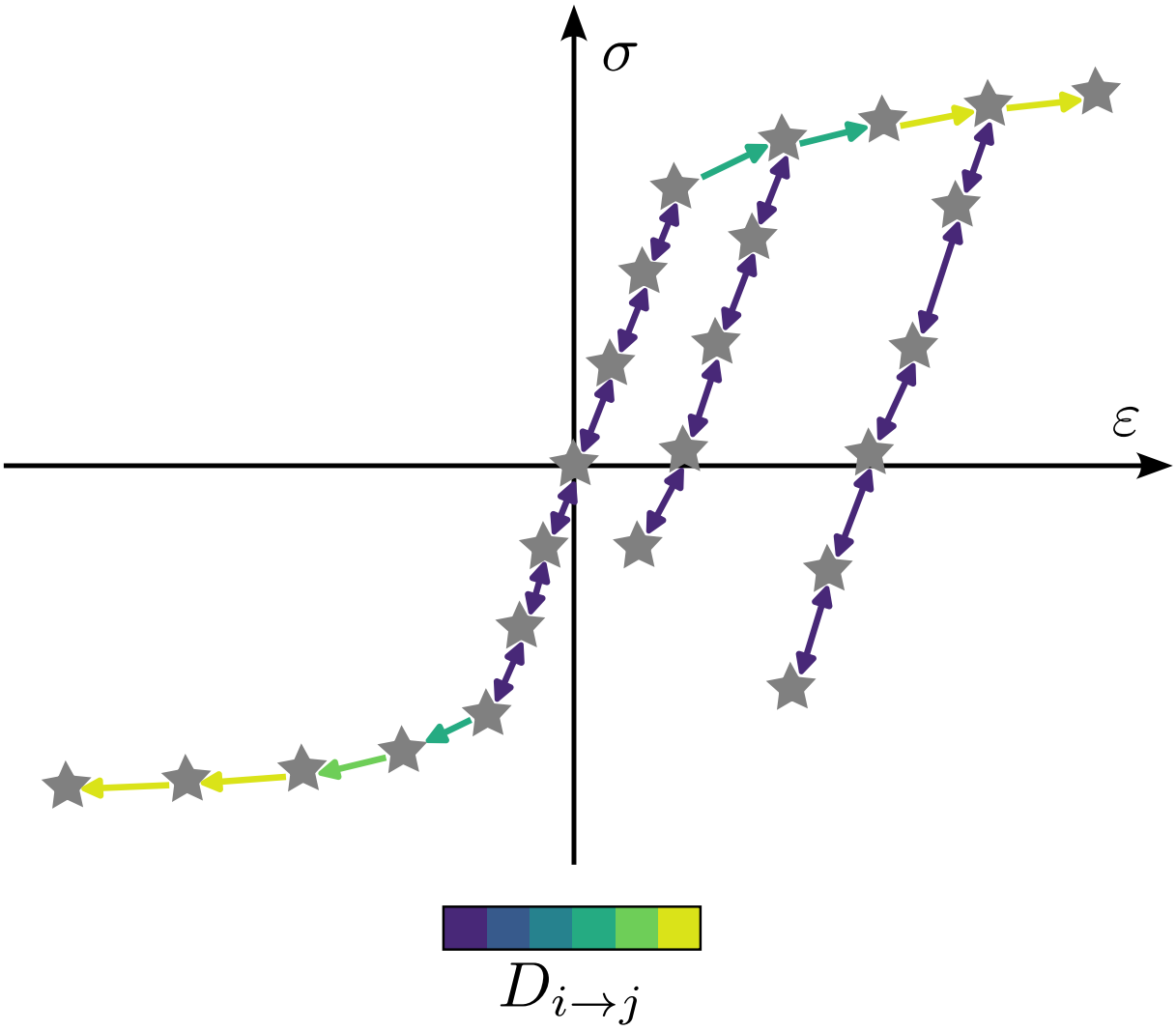

Contents

1 Challenges in model-free data-driven inelasticity **59**
1.1 General materials with memory 61
1.2 Differential representation, internal and history variables . . . 62
2 New problem formulation **63**
2.1 Structured material data 63
2.1.1 From mechanics... 63
2.1.2 ...to discrete mathematics 64
2.2 Pseudo-elastic problem 65
3 Summary **66**

1 Challenges in model-free data-driven inelasticity

As opposed to elasticity, characterised by the instantaneous reversibility of deformation, inelasticity refers to all classes of material behaviours that exhibit a sensitivity to loading path. Their mechanical response depends on time, plastic strain and/or other variables, as presented in Chapter I. Moreover, the irreversibility of inelastic behaviours usually goes hand in hand with a strongly nonlinear strain-stress relation, which makes these types of material behaviours extremely difficult to model. As a consequence, the BVP resolution is more complex and requires high-level numerical methods.

In the model-free DDCM framework, a discrete set of strain-stress pairs represents the material response. For inelastic behaviours, where there is no unicity of stress for a given strain, additional information about the history of deformation has to be considered to solve the BVP.

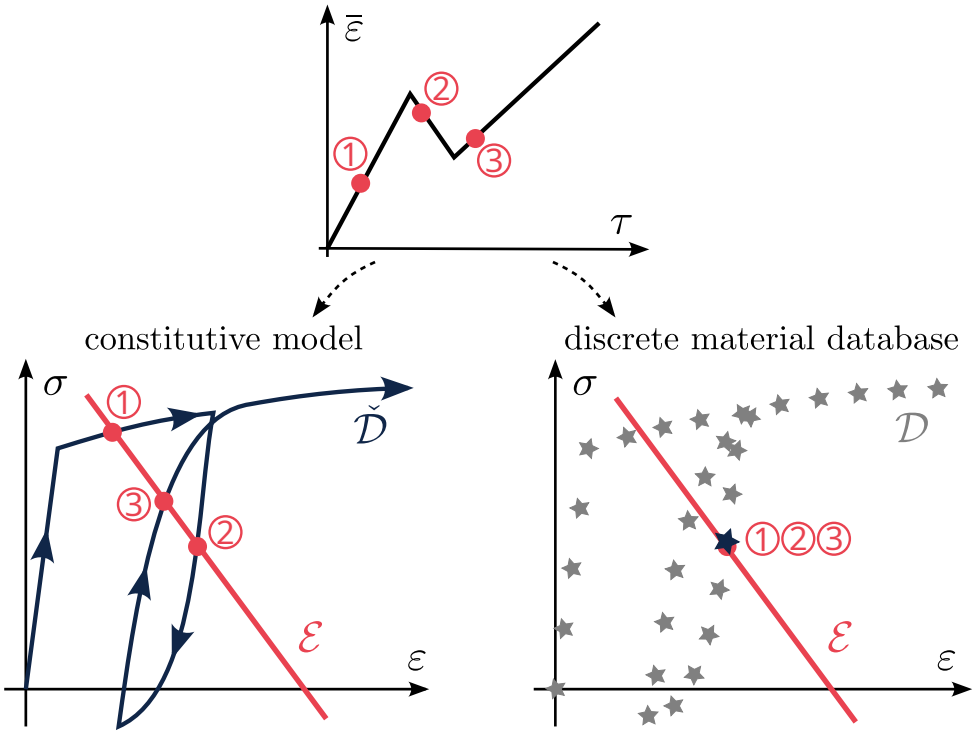

Figure V.1: Uniaxial loading applied to an elastoplastic material and graphical representation of the material response in strain-stress space with constitutive modelling and DDCM. Red dots represent mechanically admissible solutions to corresponding loadings. In constitutive modelling, they constitute the solution of the BVP and intersect the continuous material law. In model-free DDCM, the material states (dark blue stars) provide a solution effectively observed.

Fig. V.1 gives evidence of the complexity of inelastic behaviours and the challenges related to the resolution of the BVP. An elastoplastic material is subjected to elastoplastic loading, elastic unloading and elastoplastic reloading. The upper graphic illustrates this loading condition using an imposed strain $\bar{\varepsilon}$ against pseudo-time τ. Three snapshots, marked with red dots, are taken during different loading phases.

In the lower part of the figure, the graph on the left shows a mechanical constraint set (red line, as in Fig. IV.1) and a continuous constitutive relation $\check{\mathcal{D}}$ with loading, unloading and reloading (dark blue line). In constitutive modelling, the incremental problem resolution allows to retrieve the exact solutions of the system consisting of mechanical constraints and material model. Solutions at steps 1, 2 and 3, represented by red dots, are retrieved naturally.

The bottom right graphic illustrates the DDCM approach with the same symbols as in

Fig. IV.1. The inelastic material response consists in a discrete set $\mathcal{D}$ of strain-stress pairs (grey stars). In DDCM, although optimal mechanical and material solutions exist at every marked step, they are not retrieved by the standard solver that selects the closest point projection of the material database onto the constraint set[1] (red dot and dark blue star). Not only is this solution spurious for steps 1 and 3 but when loading step 3 is reached, solution 2 is no longer admissible from a thermomechanical point of view because the material underwent irreversible deformation.

This motivates the incremental approach suggested by Eggersmann *et al.* (2019 [25]), where the local database is not only specific to integration point e but also to loading step k (see Eq. IV.12), and is determined by the local history at previous steps. Consequently, the point projection step of a mechanical state $z_{e,k+1}$ onto the local material database $\mathcal{D}_{e,k+1}$ is modified. In an incremental setting, this operation writes:

$$y^{(i)}_{e,k+1} = P_{\mathcal{D}_{e,k+1}} z^{(i)}_{e,k+1} \tag{V.1}$$

with i the iteration number, and consists in searching for the nearest neighbour of $z^{(i)}_{e,k+1}$ in $\mathcal{D}_{e,k+1}$.

The authors of [25] reviewed a number of paradigms used to represent or summarise history, detailed in Chapter IV, to propose new definitions of inelastic $\mathcal{D}_{e,k+1}$. The practical application of these paradigms yet leads to major drawbacks that we discuss in the following.

1.1 General materials with memory

When considering general materials with memory, the whole history of strain is stored throughout the simulation and allows to distinguish between identical points of the constitutive space. In a model-free setting, this means that not only point-wise distances between states, but also distances between their histories must be compared: the definition of distance needs to be adapted.

A straightforward method would consist in interpolating between points of history. The distance can then be inferred by integrating the difference between interpolated

1. For clarity purposes, in the example the same solution is reached at every step. However, as the convergence of the alternating minimisation algorithm depends on multiple parameters, such as boundary conditions and metric, the solver is likely to fall into different local minima.

histories over time.

However, storing and handling whole histories is extremely expensive from a computational point of view and, as pointed out by Bartel *et al.* (2023 [4]), the choice of a realistic interpolation is difficult and contradicts the objectives of the model-free approach.

Simplified representations, which take advantage of the fading memory property of materials "whereby their instantaneous behavior is a function primarily of the recent state history and is relatively insensitive to the distant past history" (Eggersmann *et al.*, 2019 [25]), are therefore of great interest.

1.2 Differential representation, internal and history variables

A few works studied representations encoding limited histories. In particular, Langlois *et al.* (2022 [50]) implemented a differential representation based on first-order time derivatives for elastoplastic stress field identification with DDI.

Bartel *et al.* (2023 [4]) explored the idea of storing memory in a history surrogate, a quantity that "represents essential information on the history of the material behavior". The authors mention that internal variables are not suitable candidates as history surrogate, since they cannot be computed by the model-free DDCM solver. Instead, they suggest using a RNN to "gather essential information on the material behavior along a specific load path". This quantity can be considered a history variable and its dimension might increase dramatically for the high-dimensional simulation of complex materials.

These paradigms should be used cautiously in high dimensions. In fact, a characteristic of the curse of dimensionality is that in high-dimensional spaces, the notion of similarity, or proximity, vanishes. When the constitutive space dimensionality increases, possibly due to additional variables, the concept of distance becomes meaningless and all points tend to be equidistant. As an example, in a uniformly sampled p-dimensional hypercube, the pairwise-euclidean distances between points, illustrated in Fig. V.2 for different dimensions, increase with p. Apart from the inherent difficulty to determine the nature and level of accuracy of representative quantities necessary to encode history, the risk of degrading the mathematical concept of distance with such representations is also a major concern for the data-driven distance-minimising solver.

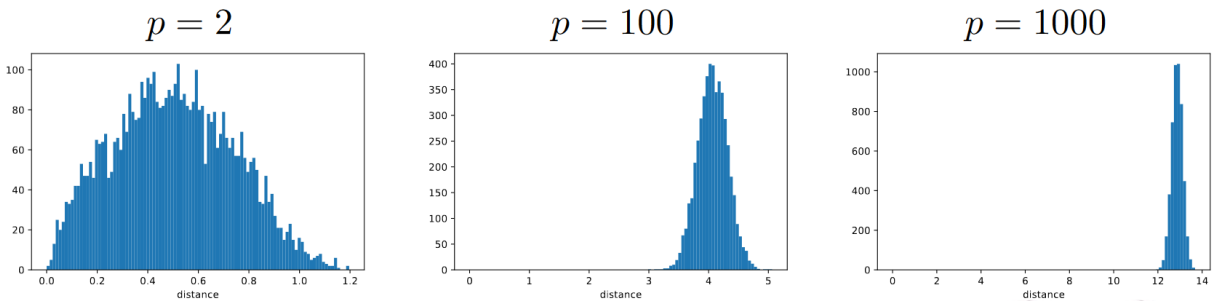

Figure V.2: Histograms of pairwise-distances between $n = 100$ points sampled uniformly in the hypercube $[0, 1]^p$, from Delon (2017 [22])

2 New problem formulation

To keep the constitutive space dimensionality to its minimum, it is important to consider a history representation paradigm that relies on few quantities, the latter being chosen such that their dimension will not increase when simulating high-dimensional problems. One way of doing this is to encode history directly in the data structure.

2.1 Structured material data

2.1.1 From mechanics...

In the model-free setting, material data is usually a discrete set of points, which samples a constitutive space $\mathcal{Z}$. We suggest augmenting this definition with an underlying data structure that enforces relationships between points, establishing a hierarchy within the material database.

Fundamentally, a state's history is an ordered sequence of visited states, which can be encoded as a predecessor list as in Fig. V.3a. However, the exact same states could be obtained with a different loading path, as in Fig. V.3b. Whether a transition from one state to another is possible or not depends on the class of material behaviour, possibly on its history, and is characterised by the laws of mechanics and thermodynamics.

From a global perspective, a material database is also a collection of states related to each other through thermodynamical constraints. For instance, in small strain elasticity, all points in the material database are related because all transitions are thermodynamically admissible. The BVP can be solved at every loading step independently without the

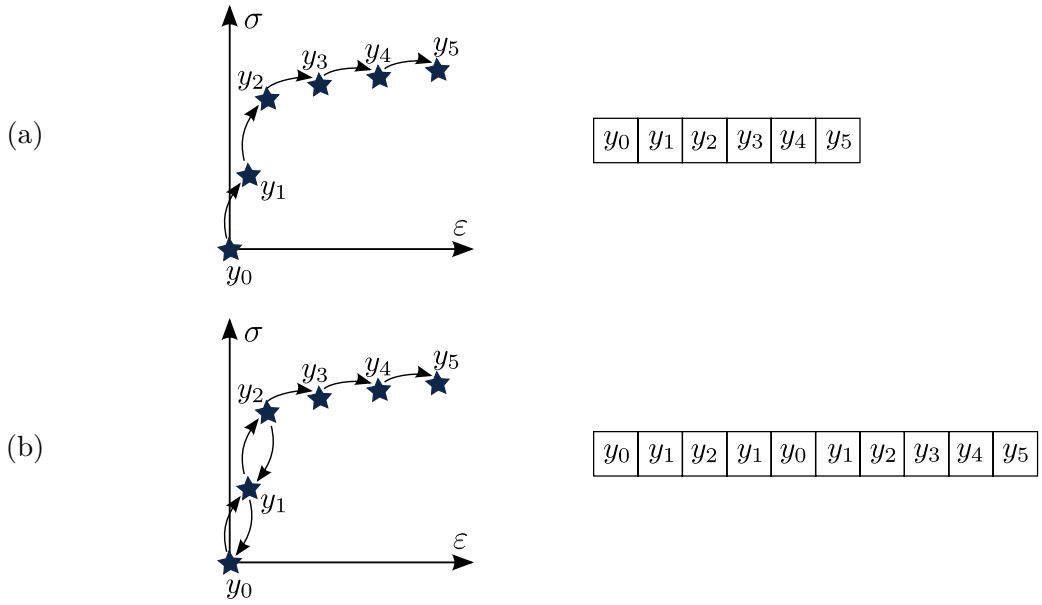

Figure V.3: Discrete history of a material loading point. The dark blue stars represent material states at time steps ranging from 0 to 5 while arrows describe transitions from one state to its successor. This history can be stored in an array where each item refers to a state.

need for an incremental formulation. In inelasticity however, the laws of thermodynamics establish which transitions are impossible. In particular, dissipation increments must be non-negative.

2.1.2 . . . to discrete mathematics

As Harary *et al.* (1965 [34]) wrote, graph theory is a branch of discrete mathematics that "is concerned with patterns of relationship among pairs of abstract elements". It provides precise vocabulary, theorems and computation techniques to gain knowledge on the properties of a system.

A graph is an abstract structure amounting to a set of objects which are pairwise related. Objects are called "vertices" or "nodes", and relationships are "edges" or "arcs". This structure, illustrated in Fig. V.4, allows for simple graphic representation and is perfectly suited to the application we target. As described in the previous section, a material database is a collection of states linked to each other through thermodynamical constraints. In the context of graph theory, material states can be seen as vertices, and

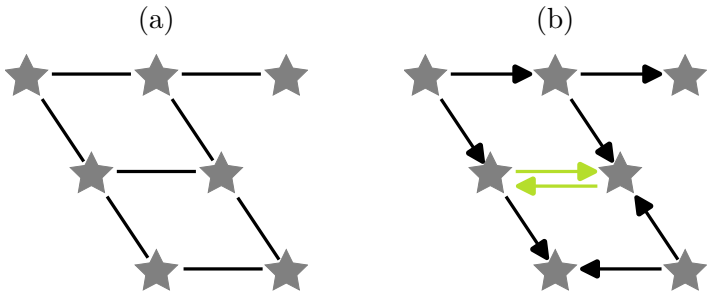

Figure V.4: A graph with 7 vertices and (a) 8 undirected edges, (b) 9 directed edges

thermodynamical links as edges. The original definition of material database $\mathcal{D}$ enriched with thermodynamics allows to encode possible transitions.

The main goal of the data structure is to distinguish between reversible and irreversible transitions between states, which in turn will make it possible to differentiate identical states with different histories. Dissipation is a good candidate as it is defined as follows:

$$\begin{cases} D_{i\to j} = 0 \text{ if transition from } y_i \text{ to } y_j \text{ is reversible,} \\ D_{i\to j} > 0 \text{ otherwise.} \end{cases} \tag{V.2}$$

Therefore, an irreversible or inelastic transition can be encoded with a single arc in the direction of positive dissipation. Conversely, two arcs with opposite directions, as green arcs in Fig. V.4b, represent a reversible or elastic transition.

2.2 Pseudo-elastic problem

In a structured version of the material database encoded with a graph, a state $y_{e,k+1}$ comes with a relative position in the structure allowing to retrieve its history and admissible futures under the form of predecessors and possible successors. A new paradigm for local database determination arises from this representation, based on searching for admissible states given local history, rather than conditioning solutions to history.

This leads to a new formulation of the data-driven problem:

0. build the thermodynamical graph associated with the material database in an offline step,
1. at each loading step, extract local databases from the graph,
2. solve step as a pseudo-elastic problem with the incremental fixed point solver.

Local databases possibly contain inelastic transitions but are treated as elastic. Although not necessarily unique, the solution is admissible in the sense of mechanics and thermodynamics.

3 Summary

Inelastic behaviours are history-dependent and highly nonlinear. These characteristics make them difficult to model; model-free methods are therefore promising alternatives.

The mathematical basis of model-free data-driven inelasticity developed by Eggersmann *et al.* (2019 [25]) transforms the elastic data-driven problem into an incremental problem that requires local databases. The latter, element- and step-dependent, are subjected to local history, which is usually represented by differential representations or internal/history variables.

DDCM is based on a distance-minimising algorithm. It is thus of greatest importance that the definition of data-driven distance remains valid in any context, *i.e.* regardless the class of material behaviour and space dimensionality. Inelastic behaviours yet imply a substantial increase of the constitutive space dimensionality, especially in 2D and 3D, conditioned by the chosen history representation paradigm and the number of additional variable that it requires.

In this work, we suggest augmenting the material database with an underlying structure, a *directed graph* encoding thermodynamical information that allows to differentiate reversible and irreversible transitions between two states. Practically, material points are the graph vertices, while directed arcs represent thermodynamical relations. History is thus used to determine local databases as admissible futures of a state and the incremental inelastic problem is solved as a pseudo-elastic problem.

Chapter VI

Graph-based representation of the material database: mathematical framework

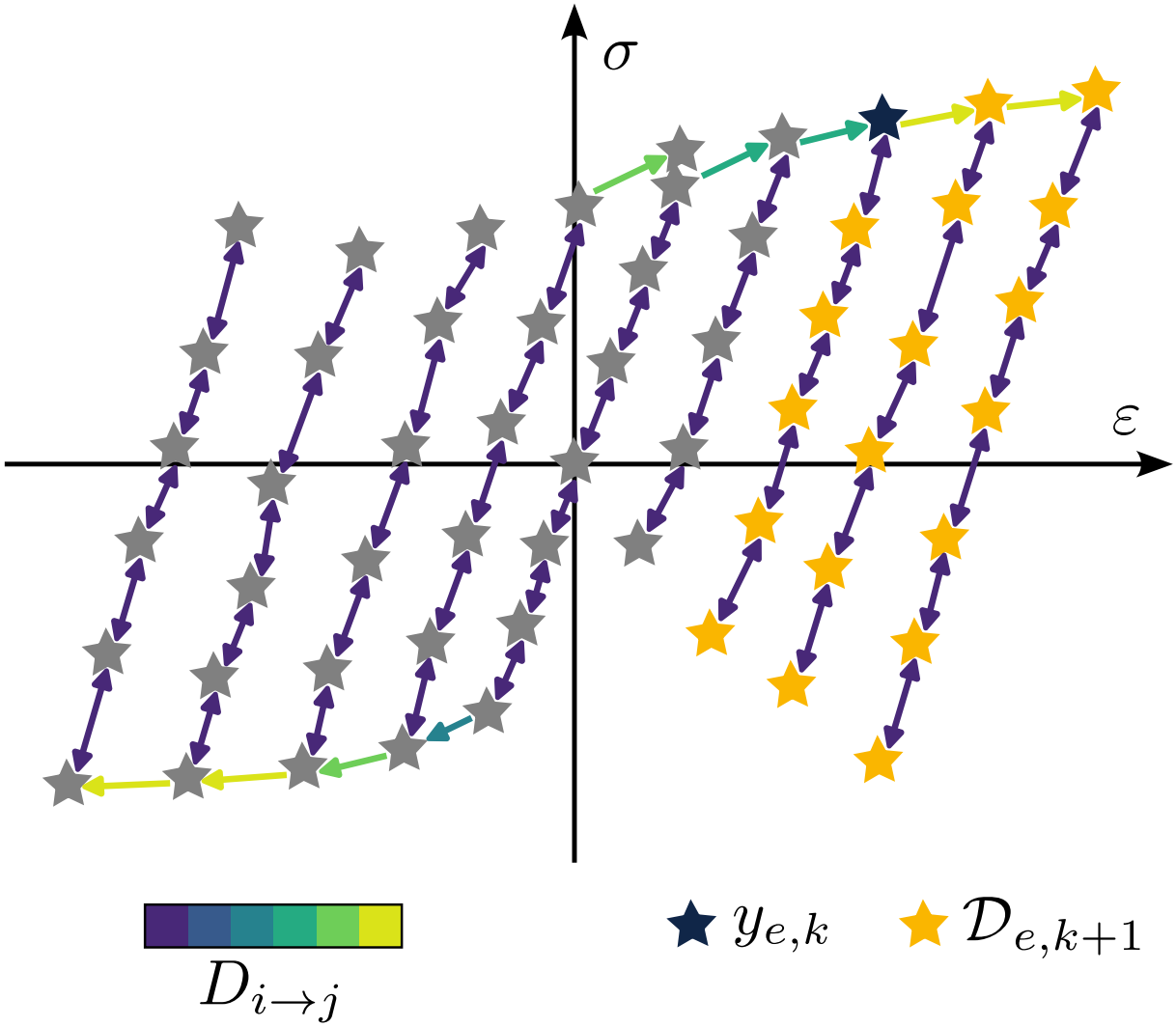

Contents

1 Elements of graph theory **69**

1.1 Definitions 69

1.1.1 Graphs and directed graphs 69

1.1.2 Special families of digraphs 70

1.1.3 Paths and cycles 70

1.1.4 Trees 71

1.2 Numerical representation of a digraph 71

1.3 Graph search 72

2 Digraph associated with the material database **73**

2.1 Representation of the discrete material behaviour with a material digraph 73

2.2 Distinction between identical states in the constitutive space . 74

3 New definition of local database **76**

3.1 Local database selection 76

3.2 Local database reduction 77

4 Numerical implementation **78**

4.1 Numerical representation of the material digraph 78

4.2 Updated algorithm 79

5 Summary **80**

1 Elements of graph theory

This section summarises the textbooks by Harary *et al.* (1965 [34]), Bondy *et al.* (2008 [7]), Rigo (2016 [67]) and Charon *et al.* (2019 [12]) to give the basics of graph theory, from encoding to graph search, which are relevant for the targeted application. Graphs can be easily represented visually, thus helping understanding many of their properties and illustrating newly introduced concepts.

1.1 Definitions

1.1.1 Graphs and directed graphs

A graph G consists of a pair $(V(G), A(G))$, or shortly, (V, A), with V a set of vertices and A a set of arcs disjoint from V. An incidence function ψ_G links each arc to a pair of vertices in V:

$$\begin{aligned} \psi_G : A &\mapsto (V, V) \\ a &\to (uv) \end{aligned} \tag{VI.1}$$

with u and v the ends of arc a, not necessarily distinct. If $u = v$, a is a loop. Arcs that share the same ends are called parallel.

A directed graph (*abbr.* digraph), as for example in Fig. VI.1[1], is a graph whose arcs are *ordered* pairs of vertices, such that u is the tail and v the head of a. A cost $c(a)$ may be assigned to each arc $a \in A$.

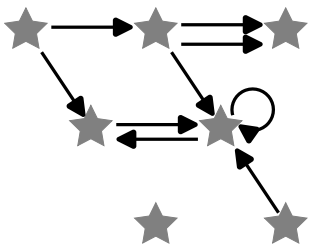

Figure VI.1: Example of digraph

1. Note that vertex positions are not significant in graph theory, the same graph can have different representations.

The number of vertices of G, denoted $|V|$[2], is referred to as the order of G, and the number of arcs, denoted $|A|$, the size of G. In this work, we will focus on finite (both vertex and arc sets are finite), nontrivial (such that $|V| \geqslant 1$) digraphs. This condition is implicit throughout the manuscript.

1.1.2 Special families of digraphs

Some atypical graphs with interesting properties are also defined and illustrated in Fig. VI.2:

(a) a strict digraph does not have any loop or parallel arc,
(b) a complete digraph or clique is a digraph in which every pair of vertices is joined by exactly two arcs, one in each direction,
(c) a connected digraph is such that, for every partition of its vertex set into two non-empty subsets X and Y, there is an arc with one end in X and the other in Y; otherwise, it is disconnected.

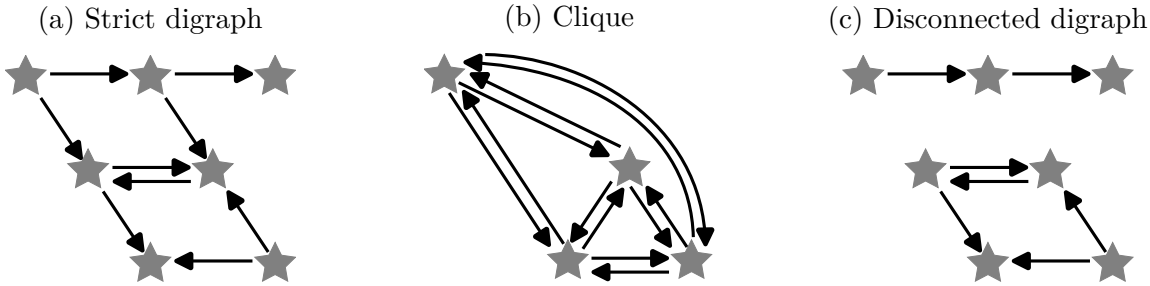

Figure VI.2: Examples of special digraphs

1.1.3 Paths and cycles

A path is a special digraph made of an ordered sequence of arcs such that the tail of each arc of the sequence coincides with the head of the preceding and where all the visited vertices are pairwise distinct. A path with the same first and last vertices is called a cycle. Conversely, an acyclic digraph does not contain any cycle.

We also introduce the concept of path cost defined as the sum of every arc's cost:

$$c(p) = \sum_{a \in A(p)} c(a), \tag{VI.2}$$

2. The symbol $|\bullet|$ denotes the cardinality of a set.

with p a specific path and $A(p)$ the set of its arcs. A minimum cost path is the shortest path with respect to cost $c(\bullet)$ and is denoted $[u, v]_c$ with u and v the tail and head vertices respectively. Fig. VI.3 illustrates this definition.

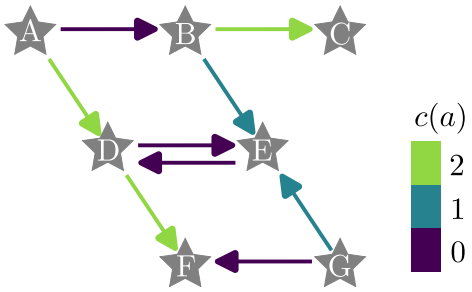

Figure VI.3: A digraph with a cost assigned to each arc: the minimum cost path between vertices A and F is A–B–E–D–F; the path D–E–D is a cycle.

1.1.4 Trees

A tree is a connected graph that contains no cycles. As for digraphs, trees can be written in terms of coupled sets of arcs and vertices as $T = (V(T), A(T))$. Starting from a root $r \in V(G)$, a tree $T(r)$ contains all vertices of G that can be reached from r and the arcs leading to them, as shown in Fig. VI.4. Hence a vertex $v \in V(G)$ belongs to $V(T)$ if there is a path in G leading from r to v.

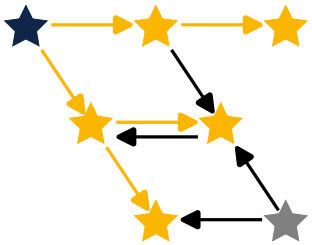

Figure VI.4: A tree (yellow and dark blue vertices, yellow arcs) obtained by taking the dark blue vertex as root

1.2 Numerical representation of a digraph

Drawings might be convenient for representing and understanding graphs, but they are not suitable for storing in computers, nor studying their properties when their size increases. A digraph is usually encoded by a matrix, which makes it easier to process.

The adjacency matrix A_G is a square matrix of dimension the order of the digraph that represents adjacent vertices of the digraph. A component A_{uv} usually equals the number of arcs joining vertices u and v. In the present work, we encode the cost directly in the adjacency matrix and set $A_{uv} = \exp(c(uv))$, as shown in Fig. VI.5b. The exponential function allows to differentiate the absence of arc from a zero-cost arc.

(a)

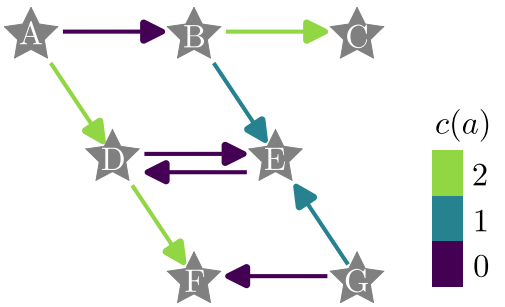

(b)

	A	B	C	D	E	F	G
A	0	e^0	0	e^2	0	0	0
B	0	0	e^2	0	e^1	0	0
C	0	0	0	0	0	0	0
D	0	0	0	0	e^0	e^2	0
E	0	0	0	e^0	0	0	0
F	0	0	0	0	0	0	0
G	0	0	0	0	e^1	e^0	0

Figure VI.5: (a) A digraph and (b) the corresponding adjacency matrix

1.3 Graph search

Frequent problems in combinatorial optimisation are for instance finding the shortest (in terms of cost or number of arcs) path between two vertices, determining whether a graph is connected or computing a minimum spanning tree, *i.e.* a tree that connects all the vertices together and with the minimum possible total arc cost. Graph search algorithms handle these problems in different ways. This work does not aim to review existing solvers or perform highly efficient computations. Nevertheless, the large variety of tools available in the literature gives substantial potential for progress in these areas.

In this thesis, we will use Dijkstra's algorithm [23], a common shortest path algorithm that restricts to digraphs with positive costs and finds the shortest path from a root vertex in the graph to every others. Different data structures exist for storing and querying solutions, which are sorted by cost from the start. In SciPy's implementation (Virtanen *et al.*, 2020 [75]), a Fibonacci heap is used, optimising the running time complexity to $O(|A| + |V| \times \log(|V|))$.

2 Digraph associated with the material database

In this section, we use graph theory to generalise the material database to the concept of material digraph.

2.1 Representation of the discrete material behaviour with a material digraph

We note $G = (V, A)$ the digraph encoding the material behaviour, illustrated in Fig. VI.6. Its vertices are the material states and its arcs are thermomechanically consistent transitions between these states such that G contains no isolated vertex. Given an arc $(y_i y_j) \in A$ between vertices $y_i, y_j \in V$, the cost $c_D(y_i y_j)$ is the dissipative cost of the transition from states y_i to y_j:

$$c_D(y_i y_j) = D_{i \to j}, \tag{VI.3}$$

with $D_{i \to j}$ the dissipation level of the transition. In this way, a non-dissipative or reversible transition is such that $c_D(y_i y_j) = 0$ and is encoded with two symmetric arcs in the digraph, *i.e.* $(y_i y_j)$ and $(y_j y_i)$, while an irreversible transition is represented with one arc directed such that $c_D(y_i y_j) > 0$.

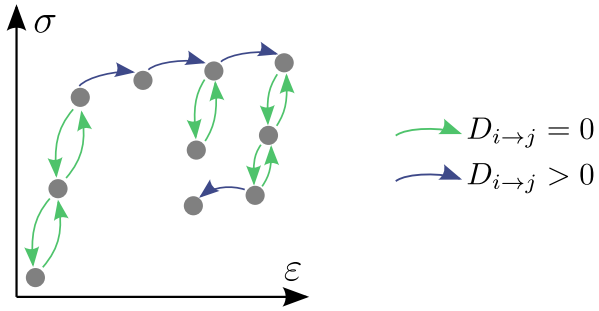

Figure VI.6: A digraph G for an elastoplastic material response with loading and unloading

We define a non-dissipative directed subgraph $E = (V(E), A(E)) \subseteq G$ such that $A(E)$ is the set of non-dissipative arcs of $A(G)$ and $V(E)$ the set of vertices joined by arcs in $A(E)$. E might be disconnected and all the vertices belonging to the same connected component can be linked together via zero-cost arcs only (see Fig. VI.7a). As a result, each connected component is associated with an elastic domain, which fundamentally

corresponds to a clique, *i.e.* a digraph in which every pair of vertices is joined by exactly two arcs, one in each direction.

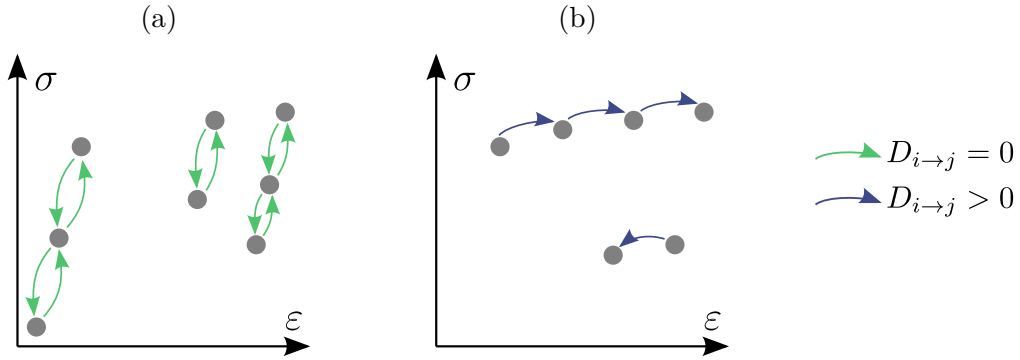

Figure VI.7: Subgraphs of G (Fig. VI.6): (a) non-dissipative subgraph E, (b) dissipative subgraph P

Furthermore, we define the dissipative directed subgraph $P = (V(P), A(P)) \subseteq G$ such that $A(P) = A(G) \setminus A(E)$ and $V(P)$ has no isolated vertex. $A(P)$ thus contains all thermodynamically irreversible transitions: all arcs in $A(P)$ have strictly positive dissipative cost, as in Fig. VI.7b.

For a database representing a purely elastic material behaviour, the digraph G is a clique and is equal to the non-dissipative subgraph E. Therefore, the local database $\mathcal{D}_{e,k+1}$ contains all material states.

From this point on, we will use the terms of computational mechanics and graph theory interchangeably to refer to a state of the material database or the corresponding vertex in the digraph and a thermomechanical transition or the equivalent arc. We also call *material digraph* and write G the digraph associated with the material data set.

2.2 Distinction between identical states in the constitutive space

Let us now consider two identical states in the constitutive space $y_k = (\boldsymbol{\varepsilon}, \boldsymbol{\sigma})$ and $y_\varkappa = (\boldsymbol{\varepsilon}, \boldsymbol{\sigma})$ but with different histories of strain and stress, denoted $\{y_l\}_{l\leqslant k}$ and $\{y_\lambda\}_{\lambda\leqslant\varkappa}$ respectively.

Histories $\{y_l\}_{l\leqslant k}$ and $\{y_\lambda\}_{\lambda\leqslant\varkappa}$ exist in the digraph as paths whose vertices are the states of histories. Yet according to its definition, P is acyclic. Thus, if either $\{y_l\}_{l\leqslant k}$ or $\{y_\lambda\}_{\lambda\leqslant\varkappa}$ or both contain any arcs $a_k \in A(P)$ and $a_\varkappa \in A(P)$ that belong to different connected

components of P, then y_k and $y_\varkappa$ are different vertices of G (see Fig. VI.8). Otherwise, y_k and $y_\varkappa$ belong to the same elastic domain and are strictly equal (same characteristics in the constitutive space and same loading histories).

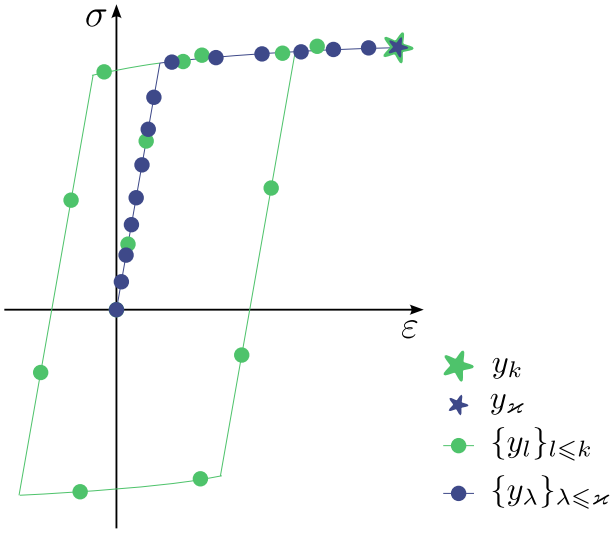

Figure VI.8: Identical states y_k and $y_\varkappa$ in constitutive space $(\boldsymbol{\varepsilon}, \boldsymbol{\sigma})$ but with different histories

In conclusion, the digraph framework makes it possible to distinguish between states with the same localisation in the constitutive space but different past histories and thus to represent complete and repeated loading cycles with various loading directions without any modification in the formalism. In that case, simulating the material response is only achievable in the sampled areas of the constitutive space with adequate dissipation levels. For example, to predict the mechanical behaviour for a loading-unloading-reloading cycle, the material digraph must encode the material response for at least one cycle and for the same strain range as implied by the applied loading.

3 New definition of local database

3.1 Local database selection

The solution of the data-driven problem at time step $k+1$ and integration point e is given by the pair $(z_{e,k+1}, y_{e,k+1})$ of respectively mechanical and material states computed with Eq. IV.16. This first requires knowing the local material database $\mathcal{D}_{e,k+1}$, which contains all the admissible states in the data set given the history of e.

As shown in Section 2.1, the history of a state is encoded in the global material database digraph. Therefore, selecting $\mathcal{D}_{e,k+1}$ now comes down to searching for admissible futures in the material database or equivalently to searching for existing paths in the digraph. To tackle this problem, we use the concept of tree defined in Section 1.1.4.

Knowing that G encodes the thermodynamically admissible transitions between states of material database $\mathcal{D}$ and given a root $y_{e,k}$, we build a rooted tree from this vertex and denote it $T(y_{e,k})$. Finally, the local material database at $k+1$, illustrated in Fig. VI.9, contains the local states corresponding to the vertices of $T(y_{e,k})$:

$$\mathcal{D}_{e,k+1} = \{y_i, \forall y_i \in V(T(y_{e,k}))\}\,. \tag{VI.4}$$

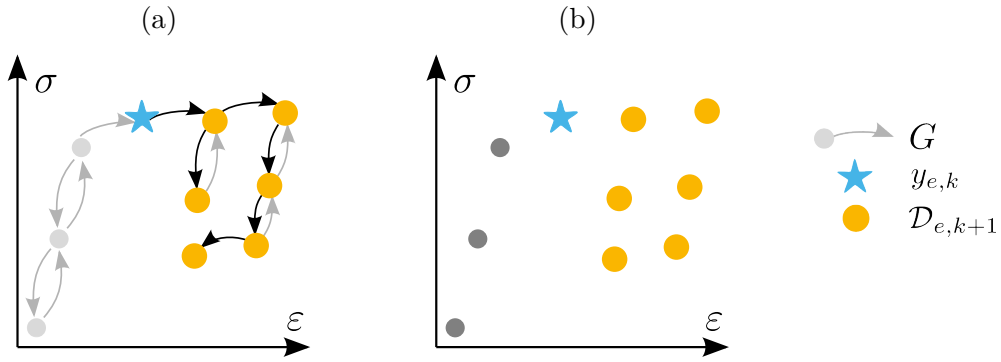

Figure VI.9: (a) Tree $T(y_{e,k})$ built from G (Fig VI.6) and (b) material database, root $y_{e,k}$ and local database $\mathcal{D}_{e,k+1}$

3.2 Local database reduction

The alternating minimisation solver used for elastic problems is highly sensitive to local minima (Kirchdoerfer *et al.*, 2017 [44]), the number of which increases in inelasticity. In the incremental problem developed above, we usually consider small loading increments. We therefore assume small increments of the material solution at a material point e both in terms of distance in the constitutive space and dissipative cost of the transition.

To this end, we use the concept of path cost defined in Section 1.1.3. As a reminder, a minimum cost path is the shortest path with respect to cost $c(\bullet)$ and is denoted $[u, v]_c$ with u the tail and v the head of a. As part of an elastoplastic local database, u is always a tree's root and v is a vertex of $T(u)$, which ensures that there is at least one path from u to v.

Finally, three conditions on the states belonging to $\mathcal{D}_{e,k+1}$ as defined in Eq. VI.4 are applied to reduce local material databases:

1. squared data-driven distance:

$$d^2_{\mathbb{C}}(y_{e,k}, y_i) \leqslant \texttt{TOL1}, \tag{VI.5}$$

   where $y_{e,k}$ is the root of $T(y_{e,k})$ and y_i is any vertex of the tree,
2. cumulated squared data-driven distance along the path:

$$c_{\mathbb{C}}(p = [y_{e,k}, y_i]_{\mathbb{C}}) = \sum_{a \in A(p)} c_{\mathbb{C}}(a) \leqslant \texttt{TOL2}, \tag{VI.6}$$

   with $c_{\mathbb{C}}(a) = d^2_{\mathbb{C}}(\text{tail}(a), \text{head}(a))$,
3. path dissipative cost:

$$c_D(p = [y_{e,k}, y_i]_D) = \sum_{a \in A(p)} c_D(a) \leqslant \texttt{TOL3}, \tag{VI.7}$$

   with $c_D(a) = D_{\text{head}(a) \to \text{tail}(a)}$.

It should be noted that the first two conditions involve algorithmic criteria while the latter is a material criterion that adds entire elastic domains to the local database. Furthermore, for any path from $y_{e,k}$ to y_i, the data-driven distance is always smaller or equal to the distance along the path used in condition 2.

Fig. VI.10 illustrates conditions 2 and 3, the effect of these criteria and their combinations will be discussed in more details in the next chapter.

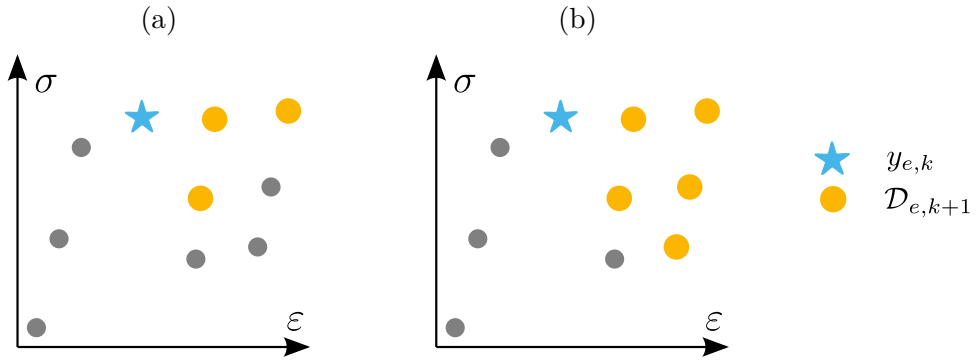

Figure VI.10: For G from Fig VI.6, reduced local databases with limited: (a) $c_{\mathbb{C}}$ (condition 2, cumulated data-driven distance) (b) c_D (condition 3, dissipation)

4 Numerical implementation

4.1 Numerical representation of the material digraph

In the present work, the numerical representation of the material digraph G is an $N^* \times N^*$ adjacency matrix $A_{ij} = \exp(c(y_i y_j))$ where N^* is the number of points in the data set and $c(y_i y_j)$ is the cost of arc $(y_i y_j)$. We use two matrices to encode the costs defined in the previous section:

- data-driven distance adjacency matrix: $A^{\mathbb{C}}_{ij} = \exp(c_{\mathbb{C}}(y_i y_j))$,
- dissipative cost adjacency matrix: $A^{D}_{ij} = \exp(c_D(y_i y_j))$.

Both matrices represent the same material digraph (same vertices and same arcs) but with different arcs' costs. Therefore they have the same sparsity pattern, which can be stored only once.

As we will see in Chapter IX, it is to be noted that the material digraph should be designed in such a way that it contains a sufficient number of arcs to provide enough information about the material behaviour and thus improve the solver's precision, and yet as few arcs as possible to ensure adjacency matrices' sparsity and speed up computations (*e.g.* graph search). In particular, cliques should not be fully encoded as such:

a necessary and sufficient condition is that at least one path exists between all vertices of the corresponding elastic domain. For instance, an enhanced representation of cliques could be developed to speed up computations.

Finally, local databases can be obtained thanks to generic graph search or shortest-path algorithms as discussed in Section 1.3. We implement the reduction criteria introduced in Section 3.2 within the chosen routine as a boundary or limit of path cost.

4.2 Updated algorithm

The new data-driven procedure for the incremental inelastic problem is detailed in Fig. VI.11. As stated by Eggersmann *et al.* (2019 [25]), the difference with the elastic case lies in the definition of local databases while the following algorithmic steps remain the same.

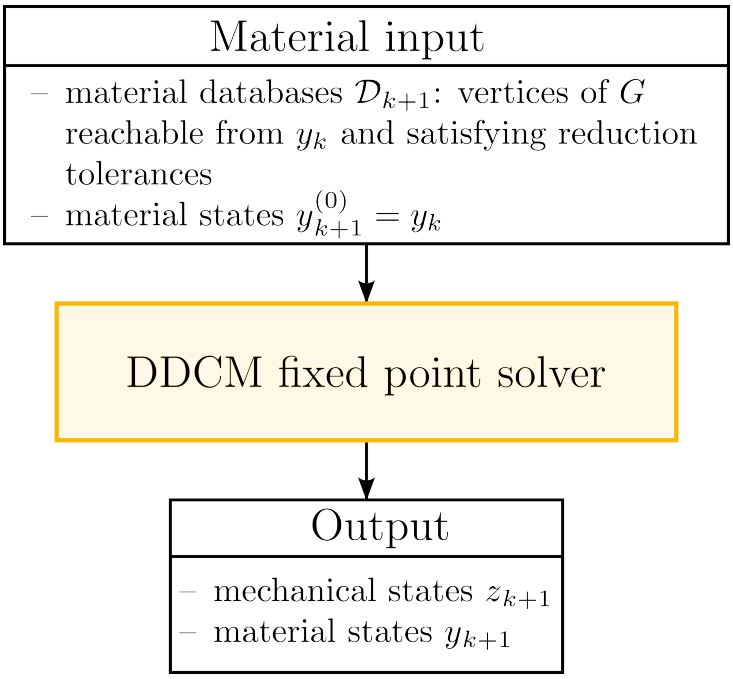

Figure VI.11: DDCM algorithm for rate-independent elastoplastic material response at loading step $k+1$

5 Summary

This chapter presents the mathematical background for a model-free representation of history-dependent data sets with a material digraph $G = (V(G), A(G))$.

The material points correspond to vertices of the digraph, stored in the set $V(G)$. Their thermodynamical relationships, determined by the non-negativity of dissipation increments, are symbolised by directed arcs in the direction of flow and stored in $A(G)$. Reversible, or non-dissipative, transitions are encoded by two arcs with opposite directions; two vertices linked by one arc only are related by irreversible, or dissipative, transitions. This definition of the so-called material digraph ensures that similar points in the strain-stress space can effectively be distinguished.

Local databases are the vertices of a rooted tree, built by searching the material digraph. Thus, from a material state $y_{e,k}$ taken as the root, we follow one arc after the other and store the traversed vertices in $\mathcal{D}_{e,k+1}$. Depending on the material history, stored here in the tree's root, local databases may be extremely large. For instance, at first time step, $\mathcal{D}_{e,1} = V(G)$. We have therefore introduced reduction criteria, whose role is to eliminate solutions that are highly unlikely because of their distance to the root, the term "distance" referring here to the data-driven distance of a path from root to any searched vertex, and/or dissipative cost of the path.

The material digraph is encoded in an off-line stage as an adjacency matrix, a compact numerical representation that enables efficient graph algorithms to be used. Then, new local databases are selected at each time step with a graph search tool and the incremental problem is finally solved as a pseudo-elastic problem.

Part C

Application to one-dimensional elastoplasticity

Chapter VII

Numerical implementation and investigation of a single element problem

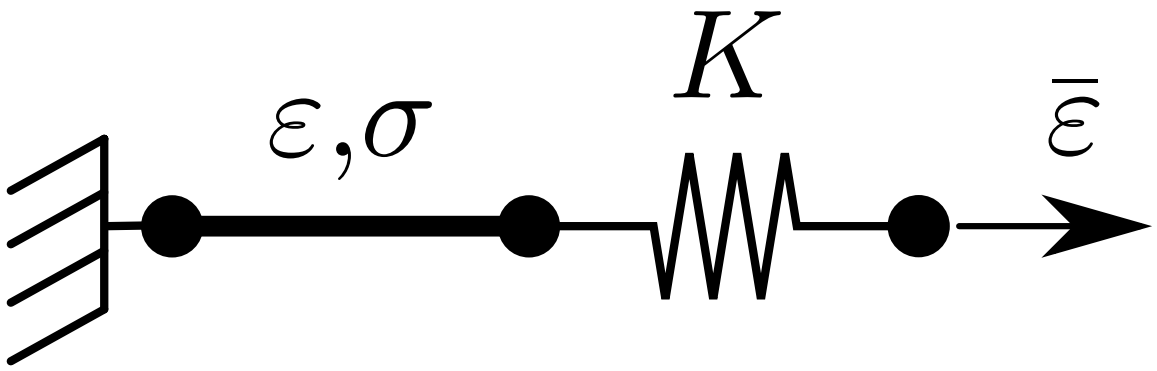

Contents

1 Numerical example **85**
1.1 Description of the BVP 85
1.2 Discussion on the influence of database density 85
1.2.1 Elastic material data sets and parameters 86
1.2.2 Results 87
1.2.3 Discussion and perspectives 89
2 Pre- and post-processing **90**
2.1 Material digraph and local database reduction 90
2.1.1 Material digraph construction 90
2.1.2 Influence of local database reduction criteria 92
2.2 Evaluation of results quality 93
3 Resolution of the elastoplastic problem **95**
4 Discussion about the efficiency of the solver **97**
5 Summary **98**

In this chapter, we put aside the combinatorial issues arising from the alternating minimisation solver by modelling the behaviour of a single element. We seek to demonstrate the method's potential for generating a suitable material database from the material digraph to solve a simple problem.

The first section describes the spring-bar element system studied and brings some considerations on the influence of the problem parameters. The second section provides the numerical methods for elastoplastic data generation, construction of the associated material digraph and evaluation of results independent of data sparsity. Finally, we present qualitative and quantitative assessments of the data-driven solution to the numerical problem.

1 Numerical example

1.1 Description of the BVP

The BVP, shown in Fig. VII.1, is composed of a bar with one integration point and a spring in series subjected to an imposed strain $\bar{\varepsilon}$. The equilibrium of the system writes:

$$K(\bar{\varepsilon} - \varepsilon) = \sigma, \tag{VII.1}$$

with K the spring stiffness and the strain-stress pair (ε, σ) describing the internal state of the bar.

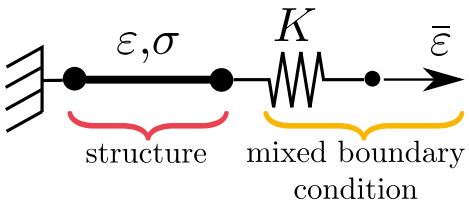

Figure VII.1: Spring-bar element system

1.2 Discussion on the influence of database density

As extensively discussed in Chapter IV, the data-driven alternated minimisation solver is sensitive to the sparsity pattern of the material database. In elastoplasticity, gen-

erating an adequate and regular sampling of the constitutive space to study numerical convergence gets more complicated due to the diversity of possible loading paths. As the choice of discretisation always influences the results, evaluating the impact of the new representation, *i.e.* with a material digraph, would be extremely demanding.

In this section, we will momentarily come back to reversible behaviours and solve the DDCM spring-bar problem in elasticity. Because of its simplicity, this example is convenient to illustrate the solver's accuracy for different data set densities, and the influence of the data-driven metric on the results. To reproduce the challenges arising in elastoplasticity in a reversible context, we will focus on material data sets mimicking an elastoplastic response with linear hardening, *i.e.* with a strong slope discontinuity, which we consider to be a worst-case scenario.

1.2.1 Elastic material data sets and parameters

Simulations are performed for a spring stiffness $K = 2l_0E$, a bar length $l_0 = 1$ m and an applied strain $\bar{\varepsilon} = 0 \dots 4 \times 10^{-2}$ with increments $\Delta\bar{\varepsilon} = 1.2 \times 10^{-3}$. The metric takes values $C = \{E, E/10\}$ and material data is generated synthetically up to $\varepsilon = 5 \times 10^{-2}$ using the piecewise linear function:

$$\sigma = \begin{cases} ① & E\varepsilon & \text{if } \sigma \leqslant \sigma_y, \\ ② & \dfrac{E}{E+H}(\sigma_y + H\varepsilon) & \text{otherwise,} \end{cases} \tag{VII.2}$$

with parameters $E = 1$ Pa, $H = E/200$ and $\sigma_y = E/100$. For practical reasons, we also call ① and ② the data set parts corresponding to each piece of the function. Two different sampling increments are used for the data sets:

- ε-DB, with fixed strain increment $\Delta\varepsilon \times \sqrt{E} = 10^{-5}$,
- σ-DB, with fixed stress increment $\Delta\sigma/\sqrt{E} = 10^{-5}$.

Therefore, the space discretisation is the same in zone ① for both data sets, shown on Fig. VII.2. Finally, the problem is solved incrementally: at every time step t_k, the material state is initialised with the state reached at t_{k-1} to ensure a good convergence of the algorithm.

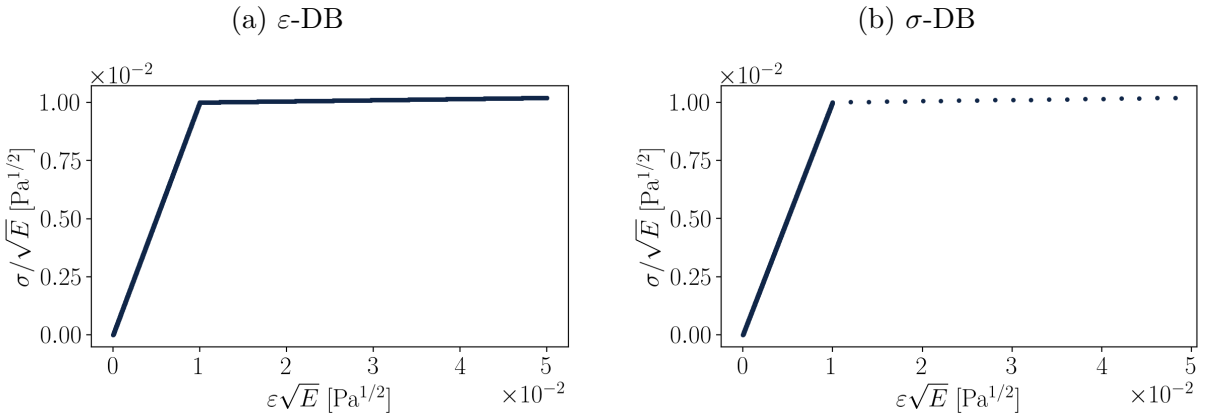

Figure VII.2: Material data sets for the elastic resolution of the spring-bar problem

1.2.2 Results

Fig. VII.3 gives the mechanical and material states, as well as the FE reference solution obtained at every time step with metric $C = E$. While in part ① all states seem to be perfectly superimposed, in part ② the data sparsity pattern has a major impact on the results: sparse σ-DB provides a less accurate solution than dense ε-DB, as noticeable in Fig. VII.3b.

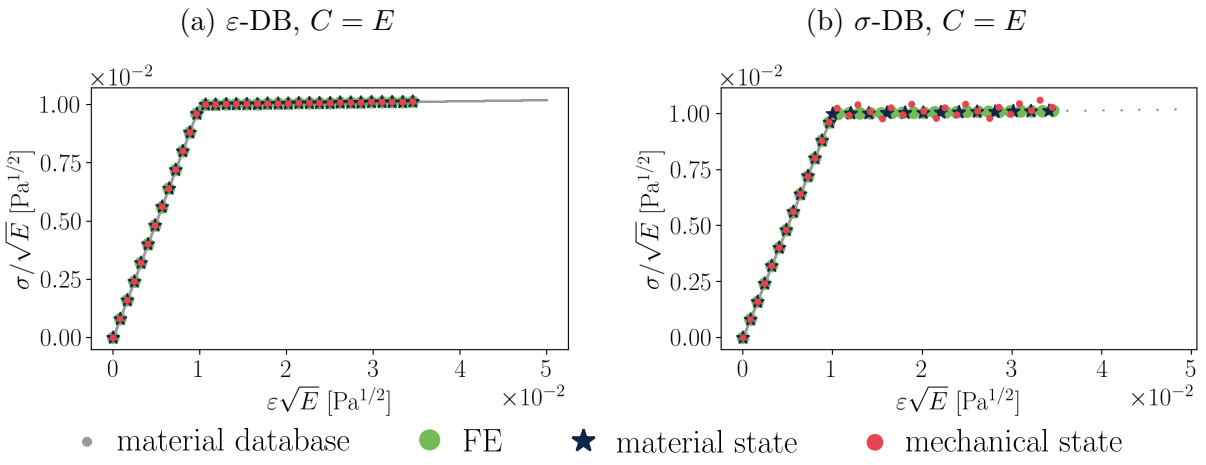

Figure VII.3: Mechanical and material solutions obtained for the elastic spring-bar problem

A quantitative evaluation of the results is given by Fig. VII.4, which shows absolute errors between DDCM mechanical states and FE reference solution, defined by:

$$\begin{aligned} \mathrm{err}_\varepsilon &= |\varepsilon_k - \varepsilon_k^{\mathrm{ref}}| \ , \\ \mathrm{err}_\sigma &= |\sigma_k - \sigma_k^{\mathrm{ref}}| \ . \end{aligned} \tag{VII.3}$$

In part ①, the lowest errors (of order 10^{-6}) are reached when the metric is equal to the slope factor E (Fig. VII.4a and Fig. VII.4b). In part ②, the order of magnitude of absolute errors is lower when $C = E/10$, *i.e.* closer to the actual slope factor: 10^{-10} for ε-DB (Fig. VII.4c), 10^{-8} for σ-DB (Fig. VII.4d).

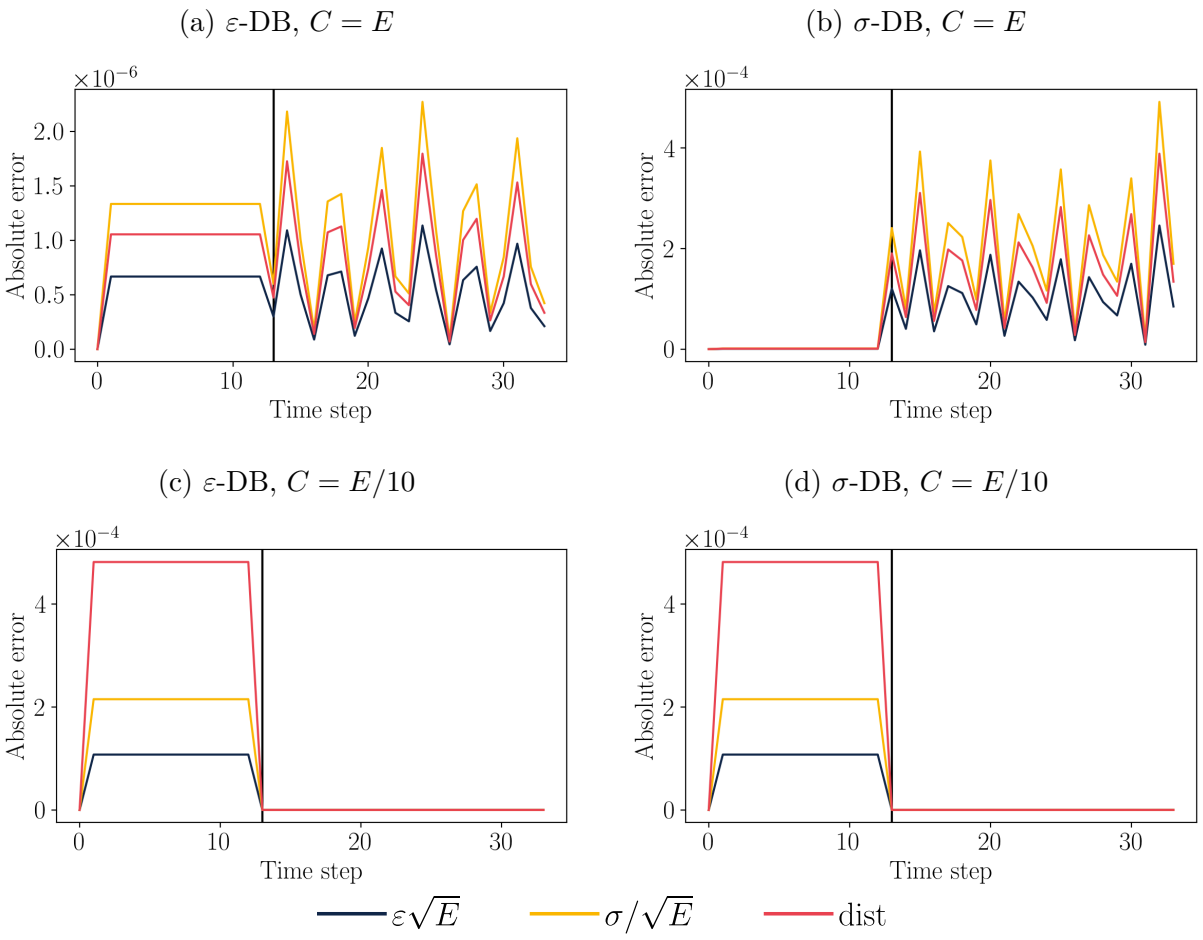

Figure VII.4: Absolute errors between mechanical states and FE reference solution for the elastic spring-bar problem, the black vertical line identifies the slope change

1.2.3 Discussion and perspectives

Accuracy depends on multiple factors, among which data sparsity and metric play a major role. Discretising an elastoplastic constitutive law to generate a regular database requires to set at least an elastic strain increment $\Delta\varepsilon^{\mathrm{e}}$ and a plastic strain increment $\Delta\varepsilon^{\mathrm{p}}$, defined in Chapter II, which can vary on different parts of the database, as shown in Fig. VII.5. In general, an appropriate elastoplastic database is dense in the "original", or non-hardened, elastic domain (part ①) and in the dissipative, or hardening, part (part ②). This condition is applied in Section 2.1.1.

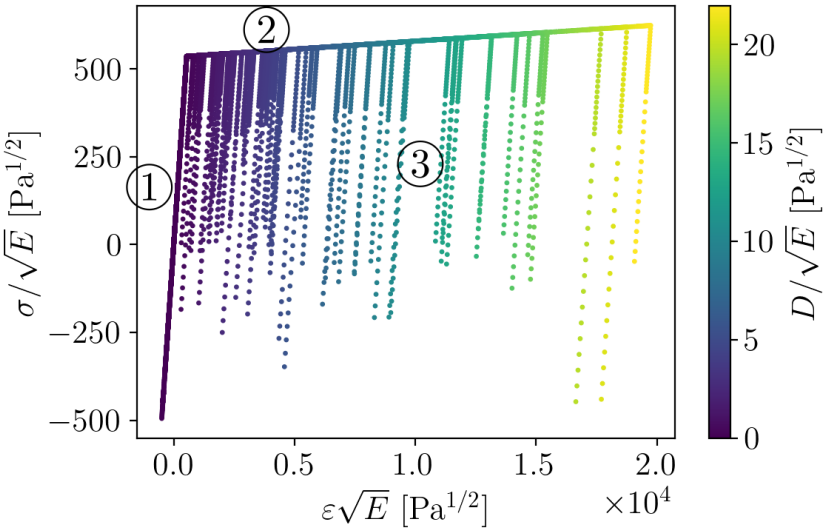

Figure VII.5: Material data set from FE simulation with loading and unloading, $\Delta\varepsilon^{\mathrm{e}}$ and $\Delta\varepsilon^{\mathrm{p}}$ are lower in part ③ than in ① and ②

The influence of data sparsity has to be taken into account when evaluating the results. A proper convergence study should be conducted to clearly identify the impact of the material representation and those of the alternating minimisation solver. However, as pointed out previously, such a study would be very demanding. Additionally, convergence could be improved by an enhanced solver, *e.g.* through game theory as suggested by Weinberg *et al.* (2023 [76]).

This first work about material digraphs aims to demonstrate the ability of the new graph-based approach to represent the mechanical solution independently of the convergence study, which motivates the introduction of the sparsity-independent indicator in Section 2.2.

In the following, we made the choice to keep the metric constant and equal to the Young's modulus throughout the simulation. However, we showed this hypothesis is not optimal when reaching the dissipative part of the data set. Different approaches, *e.g.* the one developed by Pham *et al.* (2023 [61]), rely on multiple metrics and could be used in the future to enhance our solver.

2 Pre- and post-processing

The following restricts to one-dimensional rate-independent elastoplastic behaviours. In this context, all quantities of interest are scalar, which simplifies graphical representations and constitutive space sampling. DDCM computations are performed with synthetic regular data sets for which the material digraph construction is straightforward.

2.1 Material digraph and local database reduction

2.1.1 Material digraph construction

A synthetic database is generated thanks to an elastoplastic material model with linear kinematic hardening. The yield function is given by:

$$f(\sigma, \varepsilon^{\mathrm{p}}) = |\sigma - H\varepsilon^{\mathrm{p}}| - \sigma_y \tag{VII.4}$$

with hardening modulus H, yield limit σ_y and plastic strain ε^{p}.

We build a regular data set representing the material response under elastoplastic loading, elastic unloading and plastic reloading. The strain increment in the non-hardened elastic domain and the first dissipative part is 0.01 %. Unloading and reloading paths are generated with $\Delta\varepsilon^{\mathrm{p}} = 0.2$ % and $\Delta\varepsilon^{\mathrm{e}} = 0.04$ %.

The arcs of the material digraph are defined as follows:

- elastic domains, or sets of states that could be represented by cliques, are encoded as minimum spanning subgraphs with respect to the data-driven distance, *i.e.* such that all vertices are connected in both directions and with arcs that minimise the total (data-driven) cost of each connected component,

- elastic domains are linked together with dissipative arcs that encode irreversibility, *i.e.* such that

$$\int_0^t |\dot{\varepsilon}^{\mathrm{p}}| dt > 0.$$

We rely on the order of the generated sequence of material points and on the dissipation level to determine the arcs' direction and whether they should be encoded. The final digraph is similar to the example presented in Fig. VI.6. According to the definition, superimposed states in the (ε, σ) configuration (see Fig. VII.6a) might have different histories and dissipation levels (see Fig. VII.6b) and are different vertices of the material digraph.

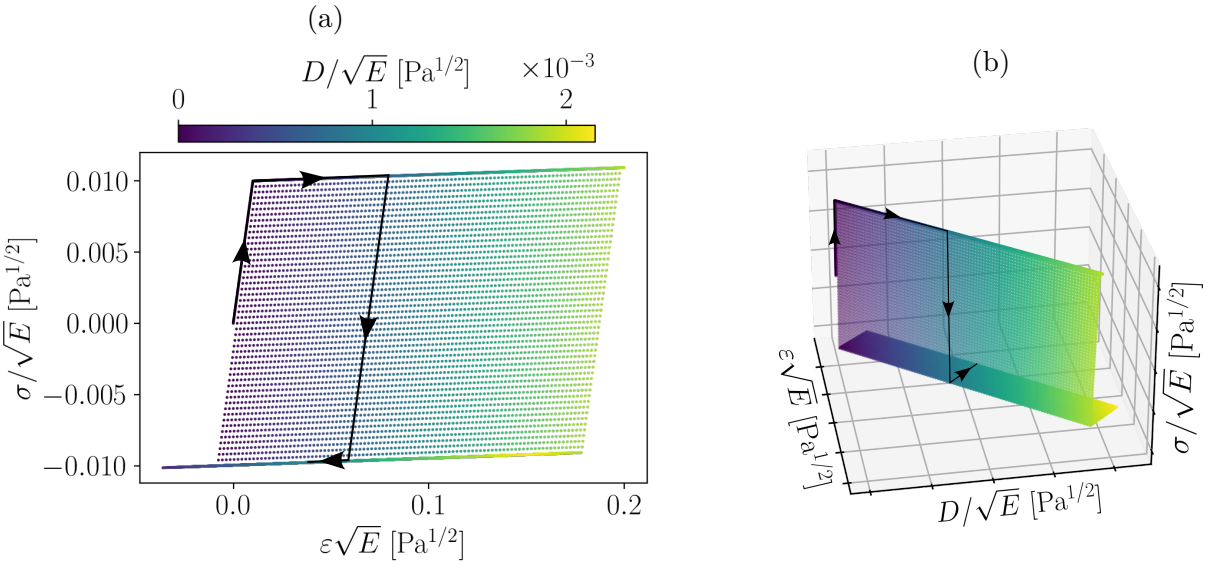

Figure VII.6: Regular material data set under loading, unloading and reloading conditions. The black solid line represents an example of history: strain and stress reach a maximum before decreasing, while dissipation only increases. Colouring symbolises the dissipation state. Representation in (a) strain-stress space and (b) strain-stress-dissipation space

2.1.2 Influence of local database reduction criteria

A local database contains potential states for a given loading increment. The criteria defined in Chapter VI tighten eligibility conditions and therefore downsize the database.

- The data-driven distance criterion is implemented with `sklearn`'s Nearest Neighbor algorithm and a maximum radius equal to $\overline{\texttt{TOL1}}$[1]. Since the original routine computes the euclidean distance, the data-driven distance is recovered by feeding the solver non-dimensional data, *i.e.* in space $(\varepsilon\sqrt{C}, \sigma/\sqrt{C})$.
- The path distance and cost conditions are computed with Dijkstra's algorithm implementation from Python library `scipy.sparse.csgraph` and graph adjacency matrices $A^{\mathbb{C}}$ and A^{D} encoding respectively data-driven distance and transition dissipation as arcs' cost. Again, $\overline{\texttt{TOL2}}$ and $\overline{\texttt{TOL3}}$ represent the maximum admissible path cost for the last node of the sequence to be in the local database.

Fig. VII.7 shows local databases for different reduction criteria in space $(\varepsilon\sqrt{E}, \sigma/\sqrt{E})$, which has the same dimensions as the constitutive space. In this representation and because we set the DDCM parameter C equal to Young's modulus, data-driven and euclidean distance are equivalent. Criterion 1 expresses a maximum data-driven radius centred on the root and is represented by a circle in these coordinates (see Fig. VII.7b).

The second criterion limits the data-driven distance along the shortest path from the root to any vertex in the local database (see Fig. VII.7c). Note that the notion of path included in this definition excludes points corresponding to plastic unloading, contrarily to the latter criterion. It is equivalent to a radius in the graph space and seems more suitable to our study as it reflects the loading path effectively leading to a given state.

Finally, the dissipative criterion in Fig. VII.7d adds all vertices in elastic domains obtained with dissipative increments lower than the chosen tolerance to the database. It is used in the following simulations in association with the second criterion. Other criteria could also be developed, for instance, to explicitly forbid non-monotonic increments (in dissipation). This assumption is implicit in the classical return-mapping algorithm for elastoplastic constitutive modelling.

1. We use relative tolerances taken with respect to the chosen metric C, such that $\texttt{TOL}= \overline{\texttt{TOL}} \times C$, where $\overline{\texttt{TOL}}$ is a non-dimensional parameter.

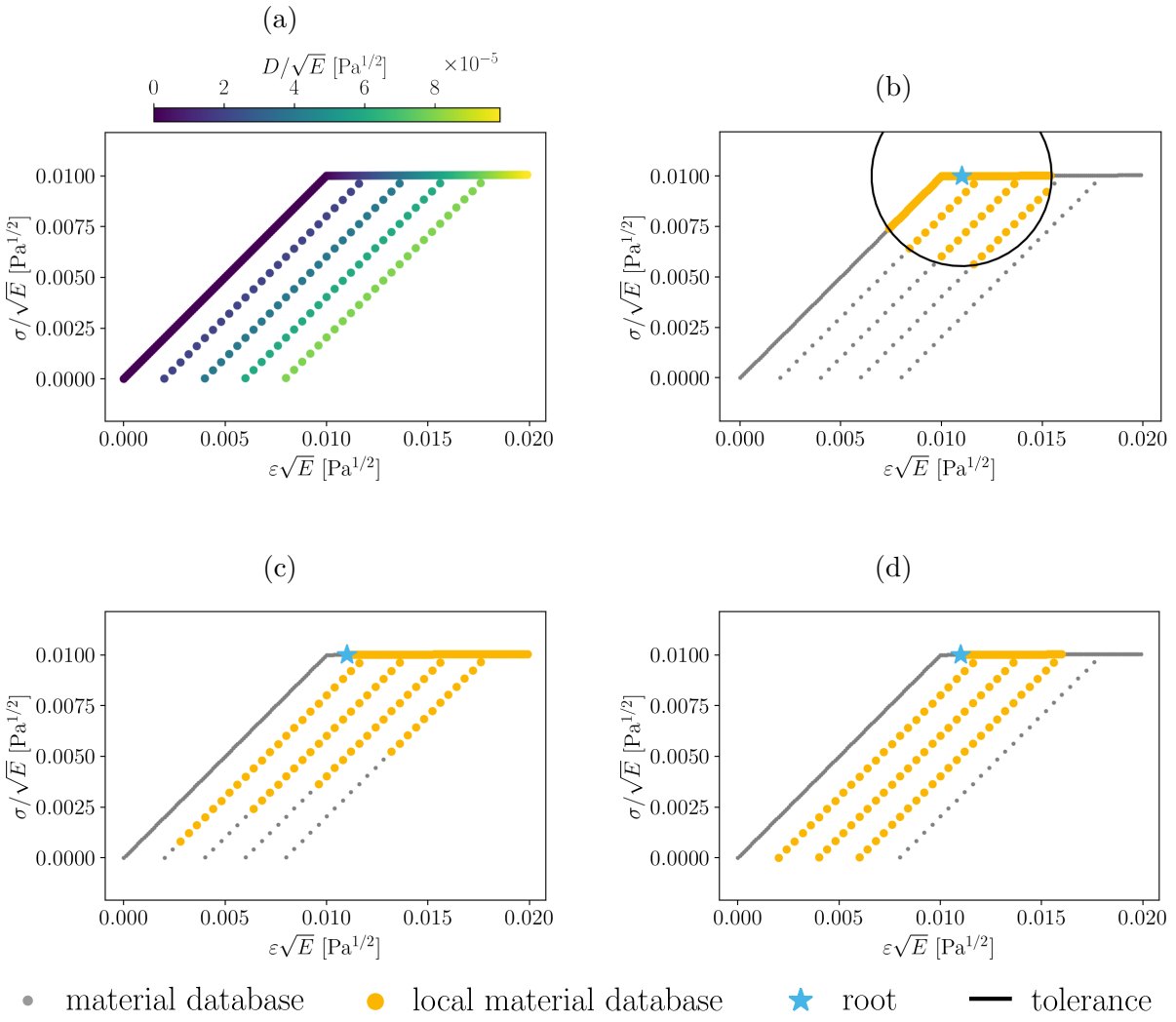

Figure VII.7: Material database (detail) and effect of reduction criteria on the local database. (a) Material database. (b) Data-driven distance, `TOL1`$=10^{-5} \times C$. (c) Cumulated data-driven distance along the path, `TOL2`$=10^{-2} \times C$. (d) Path dissipative cost, `TOL3`$=5 \cdot 10^{-5} \times C$.

2.2 Evaluation of results quality

As discussed in Section 1.2.3, DDCM solution is strongly dependent on database sparsity, especially when the metric C is not optimised. This is the case here as we choose a fixed value for this parameter throughout the simulation despite slope discontinuities in the material data.

To decouple the influence of these parameters, we seek to limit the data set's density impact by filtering the FE reference solution with the data set. We therefore introduce a new indicator: the data-driven projection of the reference solution onto the material database. This value is computed in two steps:

1. projecting the FE solution z^{ref} onto the material database (*reference material states*),

$$y^{\text{ref}} = P_{\mathcal{D}} z^{\text{ref}} \ ,$$

2. re-projecting the reference material states onto equilibrium (*projected reference mechanical states*),

$$z^{\text{proj}} = P_{\mathcal{E}_{k+1}} y^{\text{ref}}.$$

Projected states represent the best solution achievable by a data-driven solver with given data and chosen metric. As an example, Fig. VII.8 shows the DDCM solution obtained in Section 1.2 with σ-DB and $C = E$, which gave errors up to 10^{-4}. Yet when compared to projected mechanical reference states, absolute errors are null except at time step 32, where the solver reached a local minimum.

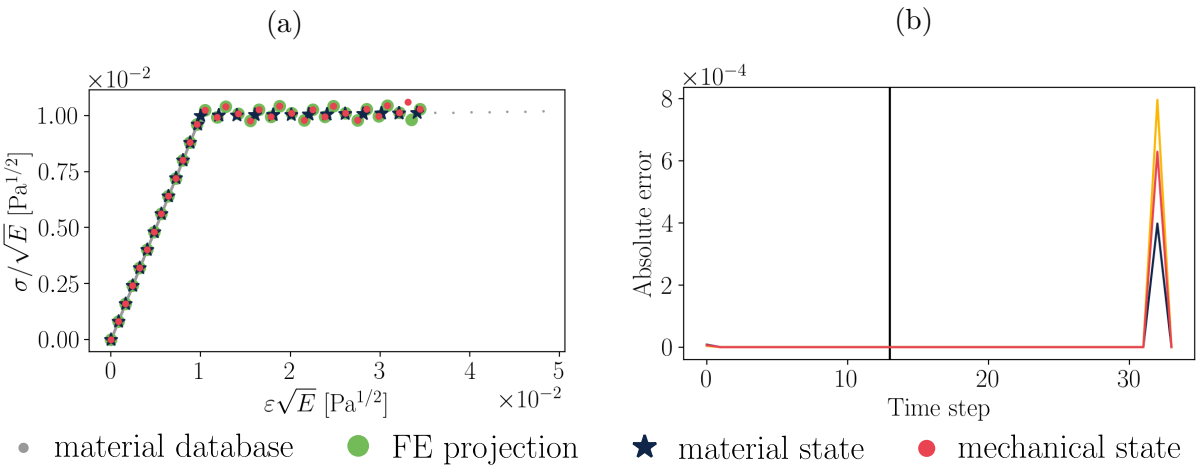

Figure VII.8: Mechanical and material solutions obtained for the elastic spring-bar problem with σ-DB, $C = E$, in comparison with projected mechanical reference states

The distance between DDCM and projected reference solutions provides a neutral indicator regarding data sparsity and is used in the following to evaluate the results accuracy. It is yet noteworthy that this indicator is not completely independent of the database density, since the convergence of the fixed point algorithm depends on this density.

3 Resolution of the elastoplastic problem

We illustrate the graph-based approach with the one-dimensional spring-bar element system subjected to a strain $\bar{\varepsilon}$ up to 15 % followed by elastic unloading and plastic reloading in compression with $\bar{\varepsilon}$ down to 10 % (see Fig. VII.9).

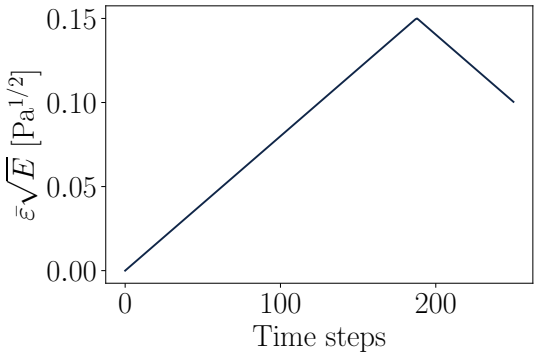

Figure VII.9: Spring-bar element system: applied strain

As in Section 1.2, the spring stiffness is $K = 2l_0E$ and the bar length is $l_0 = 1$ m. The material data set is synthetically generated with constitutive model parameters $E = 1$ Pa, $H = E/200$ and $\sigma_y = E/100$ and the material digraph built following Section 2.1.1. The data-driven metric is set to $C = E$. Fig. VII.10 illustrates the FE solution of the problem and the projected reference mechanical states.

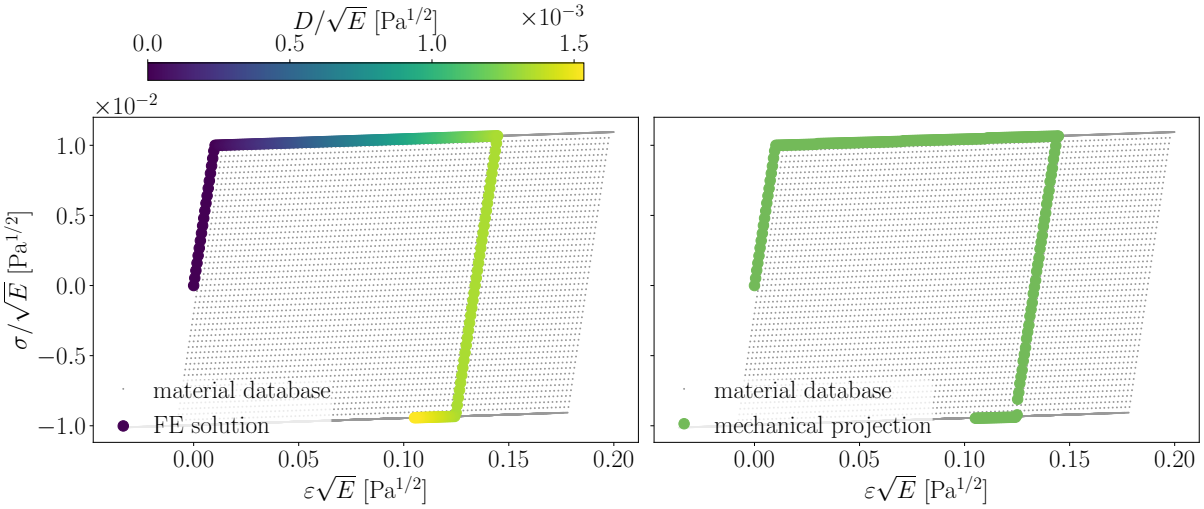

Figure VII.10: Material data set and (left) FE solution, (right) projected reference mechanical states

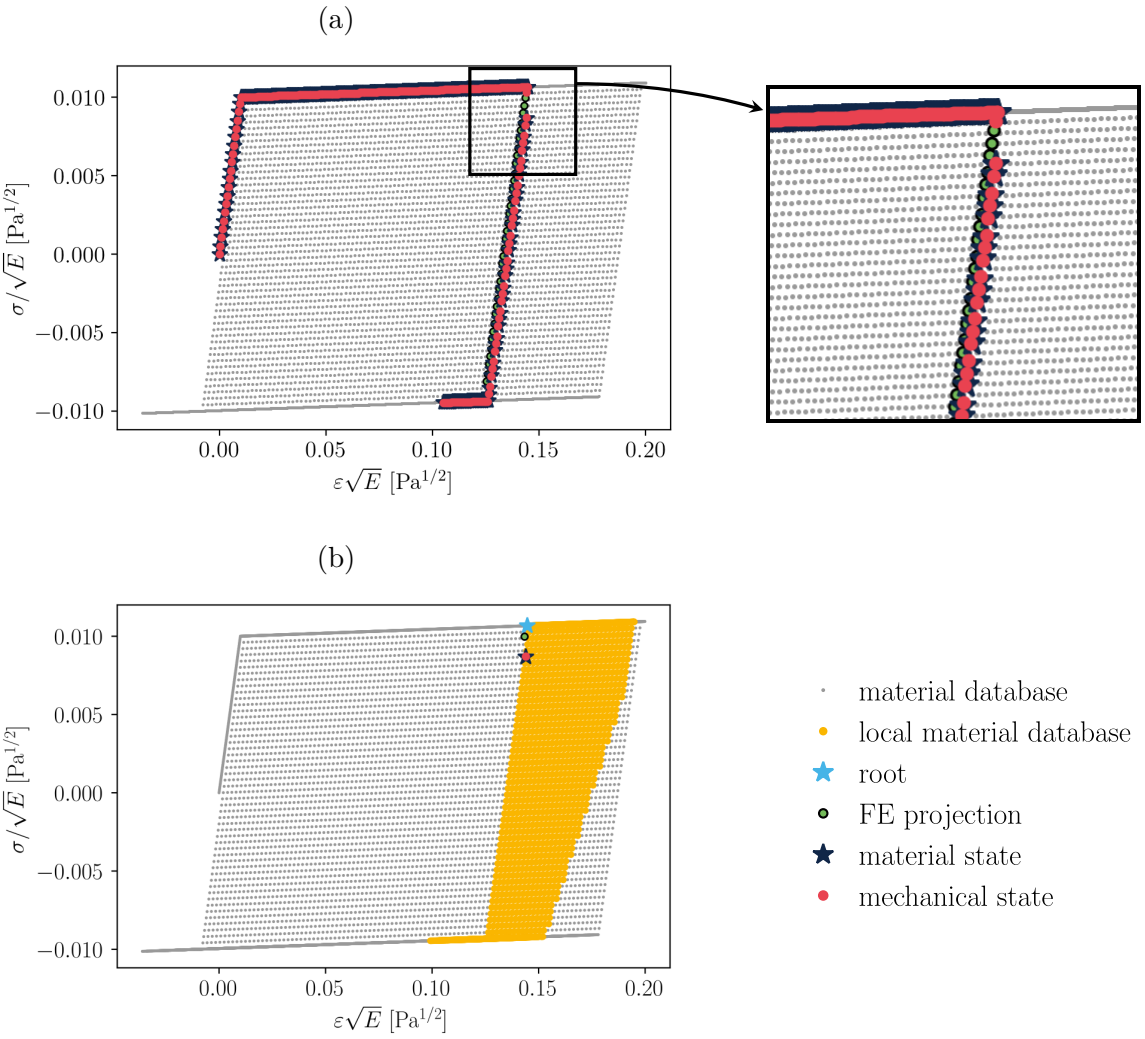

Figure VII.11: (a) Mechanical and material solutions for the spring-bar element model under loading, unloading and reloading. (b) Local material database, DDCM solution (blue star and red point) and projected reference mechanical state (green point) at maximum loading

Fig. VII.11a shows the mechanical and material states obtained at all time steps. The DDCM solver is able to retrieve a good approximation of the path shape even during the unloading phase, where the material database does not contain points with the exact reference dissipation level. The projected reference solution is well recovered except from the onset of unloading (time step 188) until reloading (time step 225) where the distance between DDCM mechanical states and projected reference mechanical states increases (see Fig. VII.12).

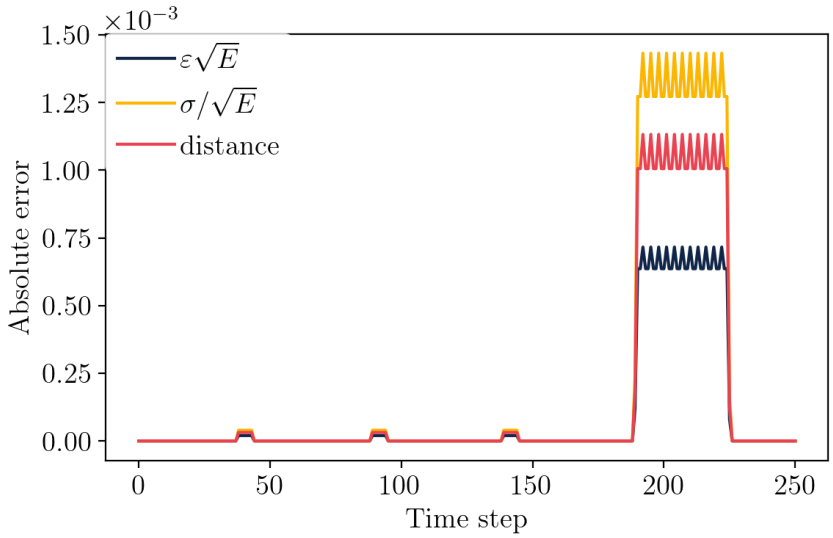

Figure VII.12: Errors between DDCM and projected reference mechanical states for the spring-bar element model under loading, unloading and reloading

Fig. VII.11b provides detailed results at step 188: the dark blue star symbolises the material state at step 187 and local database's root, the mechanical (red dot) and material (dark blue star) states look superimposed but ahead of the projected reference mechanical state (green dot). This phenomenon is repeated during the whole unloading phase and explains the high distance and absolute errors observed in Fig. VII.12. These errors are taken with respect to projected reference mechanical states and computed as:

$$\begin{aligned} \mathrm{err}_\varepsilon &= |\varepsilon_k - \varepsilon_k^{\mathrm{proj}}| \ , \\ \mathrm{err}_\sigma &= |\sigma_k - \sigma_k^{\mathrm{proj}}| \ . \end{aligned} \tag{VII.5}$$

4 Discussion about the efficiency of the solver

The current bottleneck in the proposed solver is the local database selection operation, since it requires to search the whole digraph for connected vertices. This operation is performed once for every point of the material digraph that is selected as a local material state computed between the first and the second to last loading steps.

The local database represents every possible future states that are compatible with the thermomechanical history. It therefore contains states that might be distant regarding different criteria. A reduction of the local database has been proposed by filtering states

according to three of those criteria. Additional conditions could also be introduced to filter states obtained from dissipation-wise non-monotonic paths. This restriction, similar to the hypothesis used by the classical return-mapping algorithm in constitutive modelling, would ensure that the local database only contains states belonging either to the same elastic domain as the root or to a linked dissipative part of the material database.

Furthermore, the efficiency of this selection operation can be improved with optimised graph search algorithms. For instance, considering a worst case scenario for a loading step where the local database selection operation has to be repeated at every integration point, Dijkstra's algorithm (with Fibonacci heap) running time complexity is in $O(|A| + |V| \times \log(|V|))$. The reduction criteria yet restrict the graph search to the root's neighbourhood, decreasing time cost. Alternatively, a Breadth-First Search (BFS) algorithm with a complexity in $O(|A| + |V|)$ could be used to explore the vertices from one depth to the next, starting from the root (as opposed to Depth-First Search (DFS), which explores a complete branch before moving to the next). The less flexible BFS Scipy routine was not used in the current study because it did not permit a direct implementation of the reduction criteria.

5 Summary

This chapter provides numerical results to illustrate the new graph-based material representation and evaluate the accuracy of the associated data-driven procedure. A simple problem consisting in a spring-bar element system, and thus involving no combinatorial issues, has been investigated to dig up potential challenges.

A preliminary study of the BVP in elasticity highlighted the limits of the alternating minimisation solver when material data exhibits slope discontinuities, as is the case in elastoplasticity.

Furthermore, the impact of the reduction criteria for local databases, introduced in the previous chapter, is illustrated for a regular elastoplastic material data set. The most suitable criteria, based on data-driven distance and dissipation level of the path from root to any vertex in the local database, are applied to the data-driven simulation.

The elastoplastic problem is solved under loading, unloading and plastic reloading boundary conditions. The results are compared with a newly introduced indicator com-

puted by projecting the reference FE solution onto the material database, and then again onto equilibrium. The obtained projected reference mechanical field is used for comparison and evaluation of the DDCM prediction.

The solver is able to predict the mechanical response of the structure with high accuracy. Even from the onset of unloading, where the constitutive space is sparsely sampled and contains no data points with the dissipation level required to get the exact solution.

Chapter VIII

Numerical experiments on a truss problem

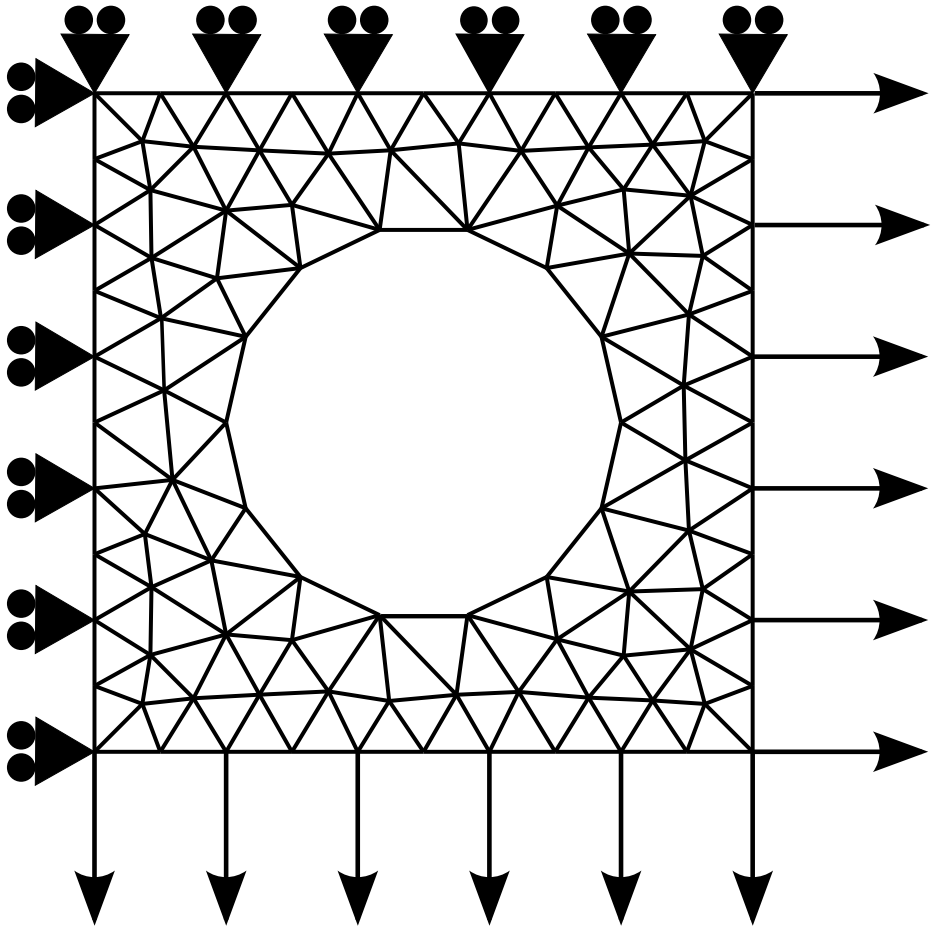

Contents

1 Numerical problem and preliminary results **103**
1.1 Description of the BVP 103
1.2 Data-driven results in elasticity 104
1.3 Preliminary results in elastoplasticity 106
2 Predictor-corrector algorithm **109**
2.1 Description of the enhanced algorithmic procedure 109
2.2 Numerical results 111
3 Summary **113**

The simulation of a continuous body is a combinatorial problem that involves coupled minimisations of mechanical and material states at every integration point. The DDCM alternating minimisation solver ensures global convergence but is likely to fall into local minima, which could lead to a completely unreliable solution both at local and global scales.

This chapter aims to illustrate and address this challenge through the example of a truss structure. First, a comparison of the DDCM solution in elasticity and elastoplasticity allows to decouple the influence of the algorithm from that of the material behaviour. Second, an enhanced solver is proposed to improve the results.

1 Numerical problem and preliminary results

1.1 Description of the BVP

The geometry is a square plate of side length 1 m with a hole of radius 0.5 m. The plate discretisation with 1D elements provides a 2D truss, shown in Fig. VIII.1a and composed of 102 nodes and 252 elements, subjected to displacement-driven boundary conditions. The top and left boundaries are fixed while right and bottom nodes are subjected to the same displacement up to 7 mm and back to 6 mm with 135 increments, as illustrated in Fig. VIII.1b.

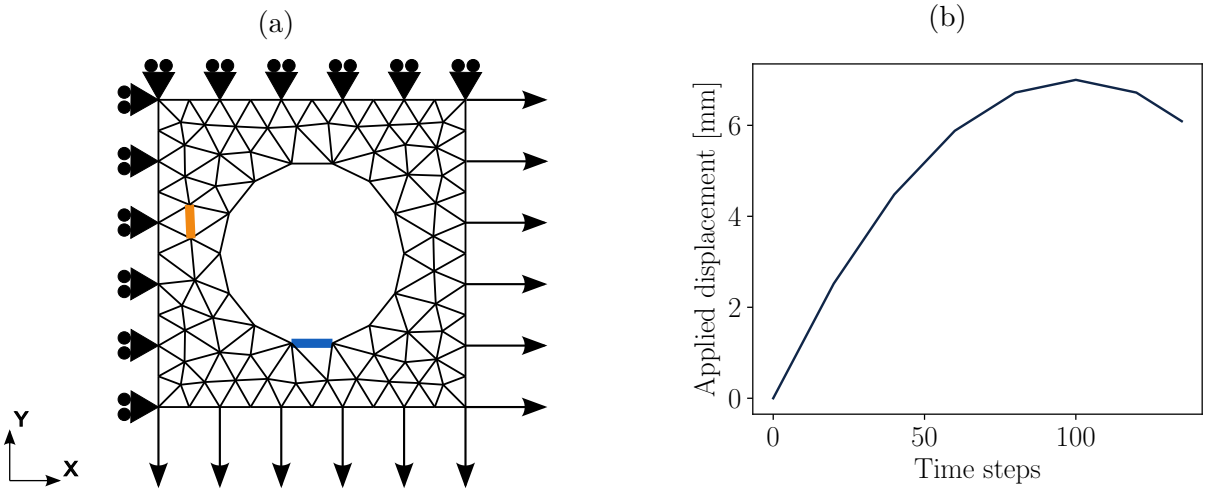

Figure VIII.1: (a) Truss geometry and boundary conditions, (b) applied displacement (unloading starts at time step 100)

Regular material data sets are generated synthetically as described in Chapter VII with constitutive model parameters $E = 217.5$ GPa, $H = 1$ GPa, $\sigma_y = 250$ MPa. These parameters are representative of steel and close, in non-dimensional form, to those used for the single element problem in the previous chapter. The data-driven metric is set to $C = E$.

1.2 Data-driven results in elasticity

Like in the previous chapter, we start this numerical investigation with a nonlinear elastic behaviour whose shape mimics an elastoplastic material response. Once again, this hypothesis aims to emphasise accuracy issues and challenges arising from the combinatorial complexity of DDCM, and later on, put the results obtained with the graph-based representation into perspective.

The simulation is performed with an elastic material data set that samples the constitutive space for strains ranging from -0.1 % to 5 % with constant steps of 0.001 % computed as in Chapter VII.

The mechanical states obtained at all loading steps for two plastically deformed elements of the mesh are illustrated on Fig. VIII.2 for comparison with the projected reference mechanical states. In addition to visible stress overestimations, higher strains are largely underestimated. Moreover, although the behaviour is reversible, the mechanical state field at loading and unloading are not superimposed. As explained in Chapter VII, this effect can be corrected by enriching the material database.

Besides, Fig. VIII.3a highlights the median of relative strain and stress errors, calculated as:

$$\begin{aligned} \mathrm{err}_\varepsilon &= |\varepsilon_{e,k} - \varepsilon_{e,k}^{\mathrm{proj}}|/\varepsilon_{e,k}^{\mathrm{proj}} \ , \\ \mathrm{err}_\sigma &= |\sigma_{e,k} - \sigma_{e,k}^{\mathrm{proj}}|/\sigma_{e,k}^{\mathrm{proj}} \ . \end{aligned} \tag{VIII.1}$$

The difference in magnitude between strain and stress medians is consistent with the strain and stress discretisation: with the data-driven distance, which transforms into the euclidean distance in space $(\varepsilon\sqrt{E}, \sigma/\sqrt{E})$, the stress range is much lower than that of strains, and stress discretisation is denser.

Fig. VIII.3b shows how relative errors are distributed in the mesh with elements sorted by increasing strain. Given the bijective nature of the material response, strain and stress

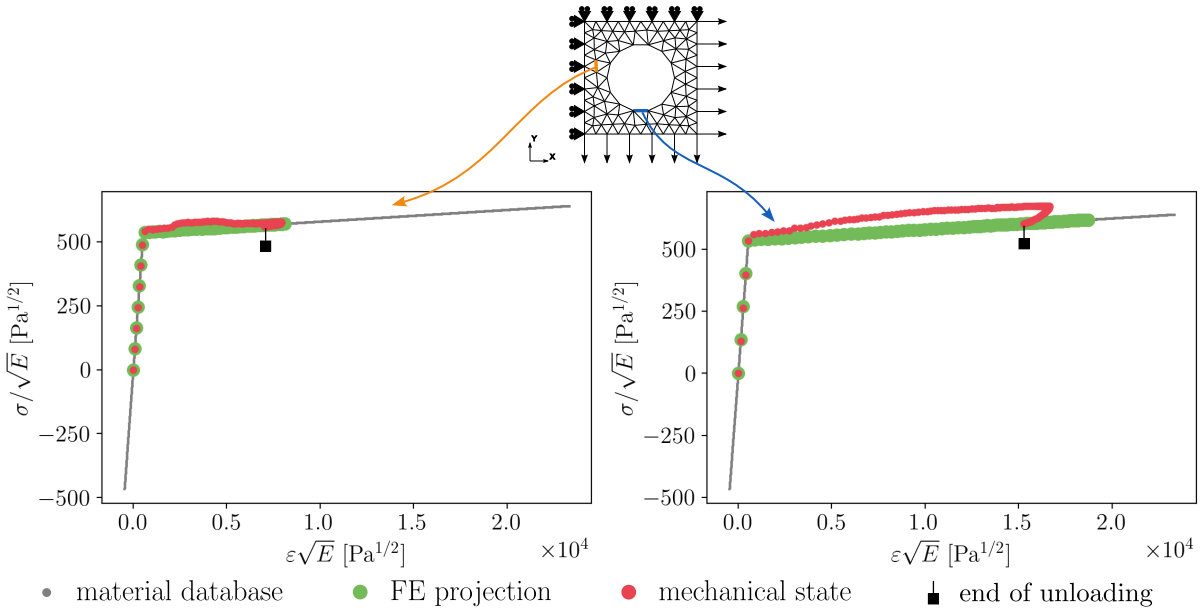

Figure VIII.2: Evolution of DDCM mechanical states and projected reference mechanical states for orange and blue elements during elastic loading

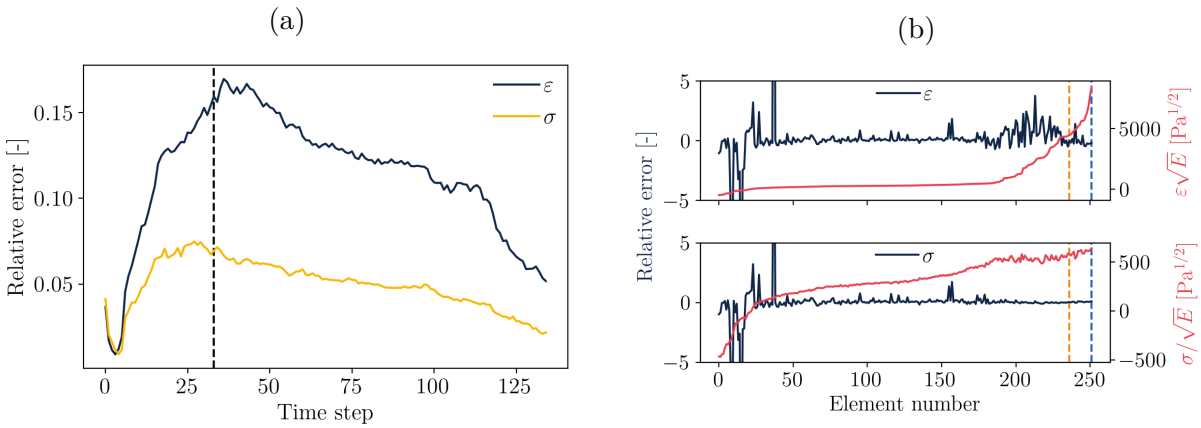

Figure VIII.3: (a) Median relative errors between DDCM and projected reference mechanical states in elasticity. (b) Relative errors at time step 33 (black dotted line on plot (a)) between DDCM and projected reference mechanical states, the orange and blue dotted lines refer to the elements highlighted on Fig. VIII.1a

should grow together. For some elements labelled in range 180-252 nonetheless, stress levels are lower than expected, which corresponds to local underestimations as highlighted in Fig. VIII.2 for the blue element. At this specific loading step, 12 % of the elements have strain relative errors greater than 100 %, half of which reaching strain levels smaller than 500 Pa$^{1/2}$ $\approx$ 0.1 %.

Conversely, combinatorial resolution optimises the global objective function to the detriment of local behaviours. The macroscopic response, illustrated in Fig. VIII.4 by the evolution of the resulting force along the truss right boundary as a function of the applied displacement, is thereby close to the FE reference solution.

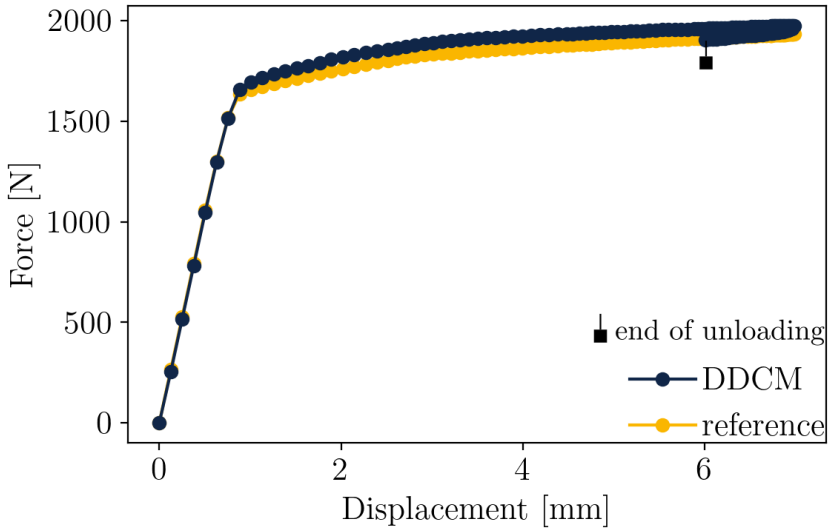

Figure VIII.4: Evolution of resulting force against displacement for the truss problem

1.3 Preliminary results in elastoplasticity

The material data set discretisation is defined with a strain increment of 0.001 % in the non-hardened elastic domain and the first dissipative part, while unloading paths are generated with $\Delta\varepsilon^{\mathrm{p}} = 0.04$ % and $\Delta\varepsilon^{\mathrm{e}} = 0.006$ %. The material database finally contains 10 478 points. The local database reduction tolerances are set to $\texttt{TOL2} = 5 \times 10^3 \times C$ and $\texttt{TOL3} = 10^{-5} \times C$. These values are chosen to ensure that a large portion of elastic domains are caught in the local database, while still considerably reducing its size (see Fig. VIII.5).

DDCM mechanical and material states obtained at all loading steps for two plastically deformed elements of the mesh are illustrated in Fig. VIII.6. Although prediction is satisfactory for the orange element, the solution computed for the blue one does not match the expected elastoplastic response. Strain "sliding" is observed for strains from 0 $\mathrm{Pa}^{1/2}$ to 6×10^3 $\mathrm{Pa}^{1/2}$ and DDCM underestimates maximum strain, even though the overall

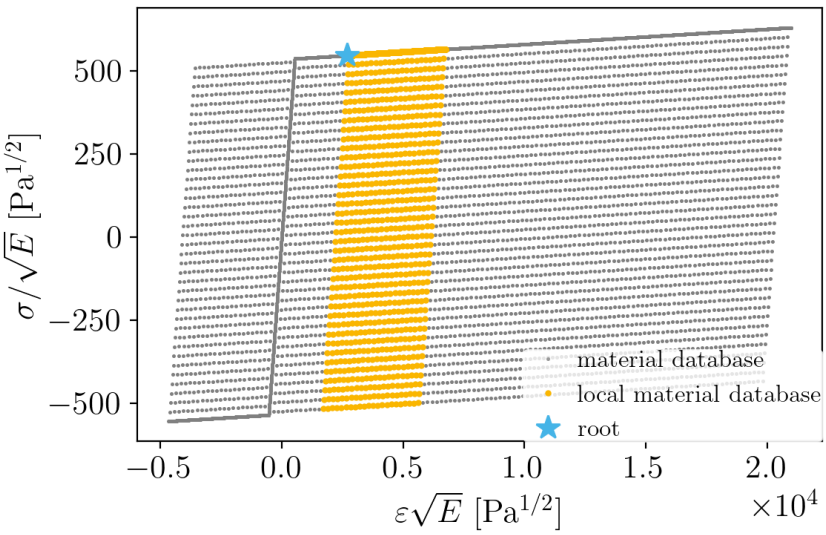

Figure VIII.5: Example of local database for the truss problem with `TOL2` $= 5 \times 10^3 \times C$ and `TOL3` $= 10^{-5} \times C$

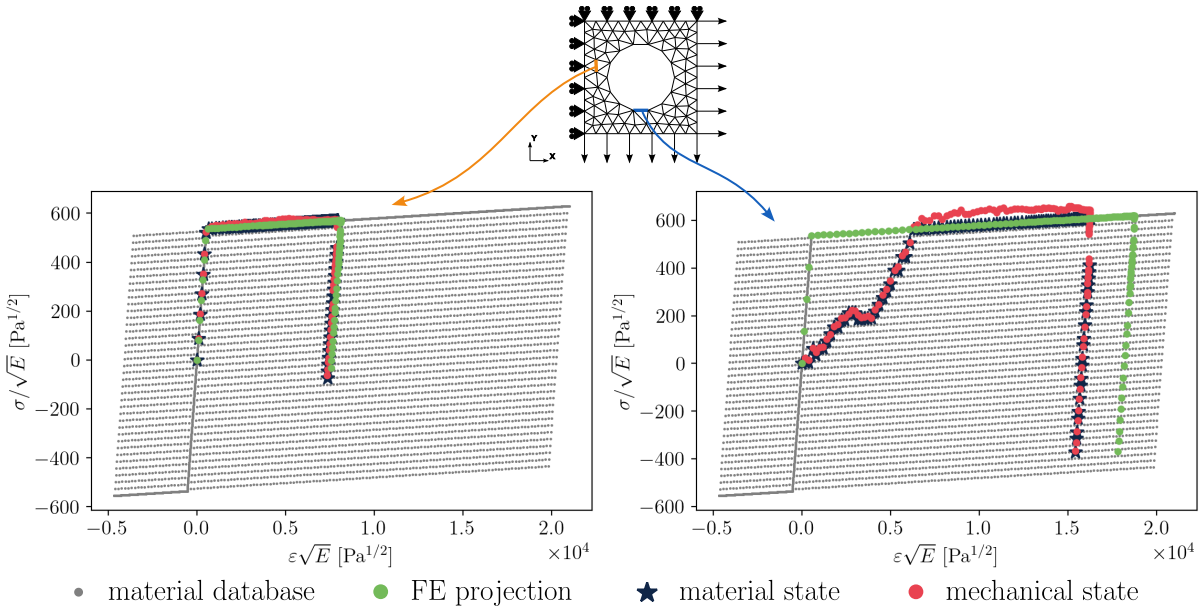

Figure VIII.6: Evolution of DDCM mechanical, material states and projected reference mechanical states for orange and blue elements during loading

path shape is consistent. These effects are related to the constitutive space discretisation with finer strain increments along with a metric value that gives strains a higher weight in the distance calculation.

As in Section 1.2, Fig. VIII.7a shows the median of relative strain and stress errors

defined in Eq. VIII.1 and Fig. VIII.7b illustrates how relative errors are distributed in the mesh with elements sorted by increasing strain. The plotted time step corresponds to the loading phase, yet for elements in range 220-252 strain and stress levels are inconsistent. This effect, already observed in elasticity, increased dramatically, and corresponds to local stress underestimations as emphasised in Fig. VIII.6 for the blue element. Additionally, at loading step 33, 19 % of the elements have strain relative errors greater than 100 %, half of which reaching strain levels smaller than 500 $\mathrm{Pa}^{1/2} \approx 0.1$ %.

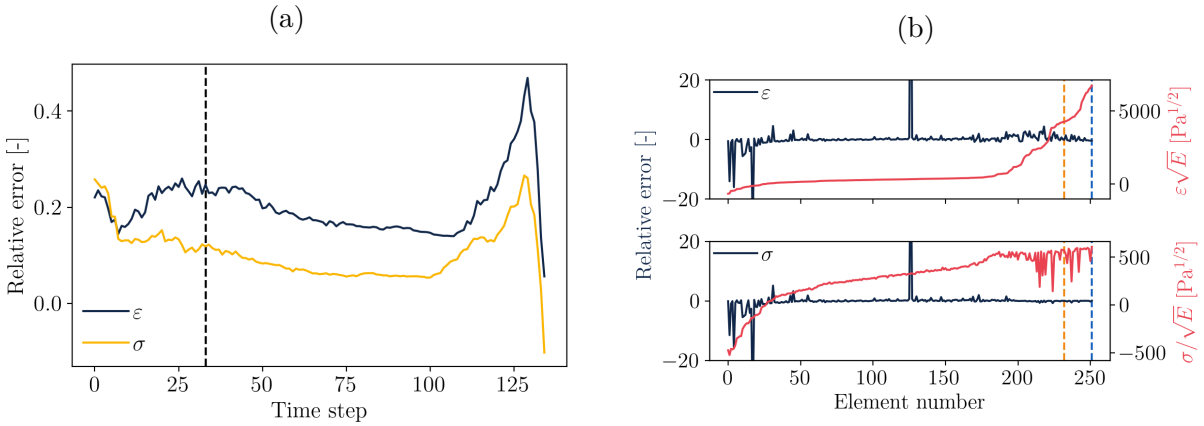

Figure VIII.7: (a) Median relative errors between DDCM and projected reference mechanical states. (b) Relative errors at time step 33 (black dotted line on plot (a)) between DDCM and projected reference mechanical states, the orange and blue dotted lines refer to the elements highlighted on Fig. VIII.1a

Finally, the evolution of resulting force against applied displacement also exhibits the consequence of local sliding for lower strains (see Fig. VIII.8). The DDCM maximum force however is close to reference as local over- and underestimations of strains offset each other.

Even though the laws of mechanics and thermodynamics are fulfilled, respectively with the mechanical fields satisfying kinematic compatibility and equilibrium, and the material fields satisfying the condition of non-negativity of dissipation, the lack of a unique solution within local material databases combined with the sensitivity of the alternated minimisation solver to local minima leads to defective results at local and global scales. We therefore discuss in the following a possible improvement of the solver for combinatorial elastoplastic problems.

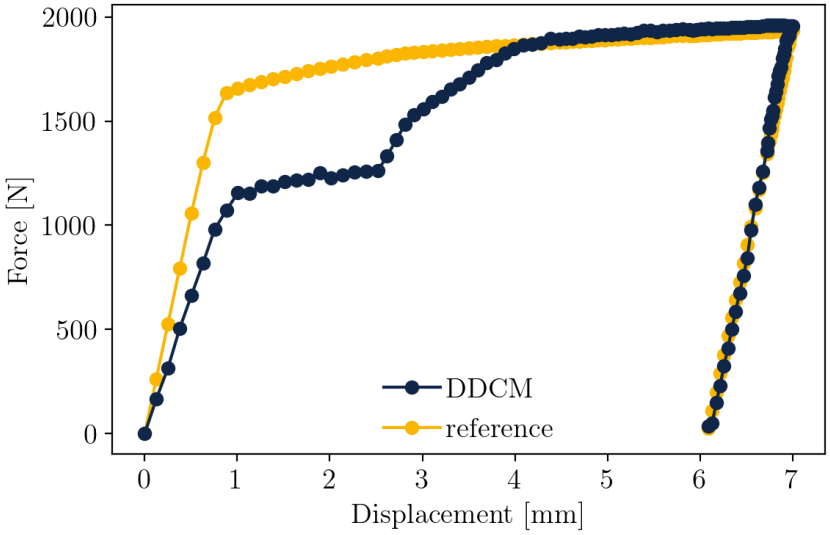

Figure VIII.8: Evolution of resulting force against displacement for the truss problem

2 Predictor-corrector algorithm

We investigated two numerical methods to improve the performance of the solver. The first one is the predictor-corrector algorithm presented in this section. An alternative based on numerical relaxation to slow down convergence and avoid remote local minima has yet proven to be ineffective. We thus relegated detailed explanations to Appendix A.

2.1 Description of the enhanced algorithmic procedure

We suggest to implement a two-step non-dissipative predictor-dissipative corrector algorithm inspired by resolution methods for constitutive models. This first requires to define two types of local databases:

- a non-dissipative prediction local database $\mathcal{D}^{\text{pred}}_{e,k+1} \subset \mathcal{D}_{e,k+1}$ that only contains states such that the dissipative cost of any path from subgraph root $y_{e,k}$ to a state of the local database is null, or equivalently, local databases only contain states belonging to the same elastic domain as the roots,
- a dissipative correction local database $\mathcal{D}^{\text{corr}}_{e,k+1} = \mathcal{D}_{e,k+1}$ obtained as defined in Chapter VI by taking the prediction's material state $y^{\text{pred}}_{e,k+1}$ as root.

Local databases $\mathcal{D}^{\text{pred}}_{e,k+1}$ and $\mathcal{D}^{\text{corr}}_{e,k+1}$ might also respect the reduction criteria based on cumu-

lated data-driven distance along path and path dissipative cost, introduced in Chapter VI. In practice, $\mathcal{D}^{\text{pred}}_{e,k+1}$ is calculated by setting the tolerance on dissipative path cost `TOL3` to zero and the tolerance on path data-driven distance `TOL2` for $\mathcal{D}^{\text{corr}}_{e,k+1}$ must be chosen such that $\mathcal{D}^{\text{pred}}_{e,k+1} \subseteq \mathcal{D}^{\text{corr}}_{e,k+1}$ to allow permanent deformation of elements.

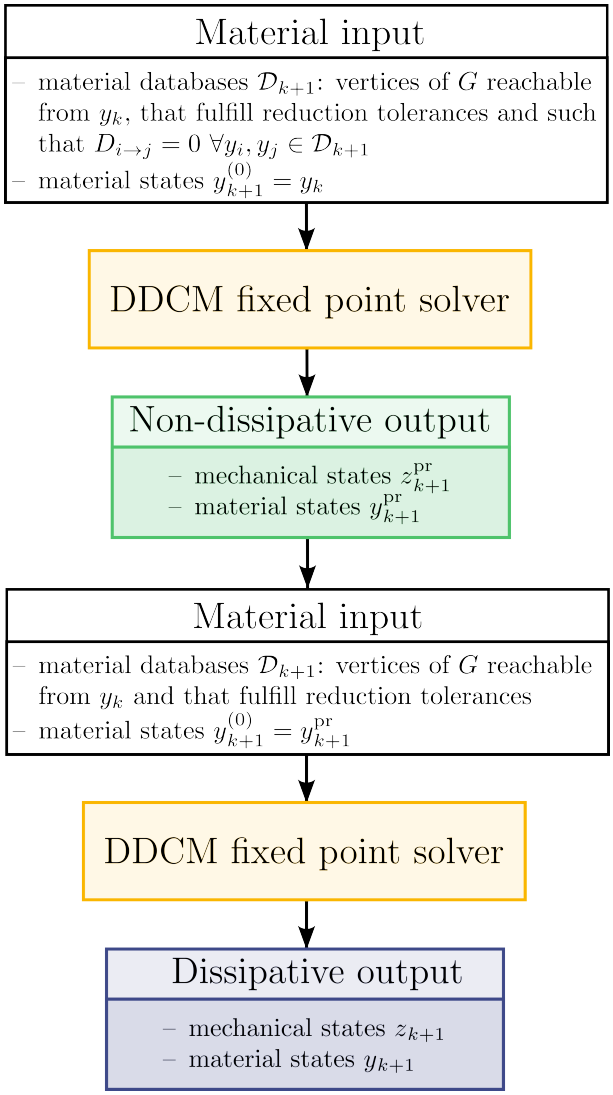

Figure VIII.9: Illustration of the predictor-corrector elastoplastic DDCM algorithm

A data-driven iteration is thus achieved in two steps as illustrated in Fig. VIII.9. First, a non-dissipative step, called predictor, where the resolution is performed using $\mathcal{D}^{\text{pred}}_{e,k+1}$ with root $y_{e,k}$ until convergence. Then a dissipative computation or correction is performed using $\mathcal{D}^{\text{corr}}_{e,k+1}$, equal to the local database defined in Chapter VI, obtained by taking the predicted material state $y^{\text{pred}}_{e,k+1}$ as root vertex. In addition, the material states

in the correction stage are initialised with the predicted material states. The corrected states are also the final solution of the loading increment. This modification of the DDCM algorithm does not involve any additional hypothesis or parameter but is solely based on physics.

2.2 Numerical results

The truss problem introduced above is now solved with the enhanced algorithm. The DDCM solution for the orange element is shown on the left graphic in Fig. VIII.10 and is mostly similar to the solution obtained in Fig. VIII.6, except in the unloading part where it is slightly overestimated. The right graphic in Fig. VIII.10 shows the states obtained for the blue element: the predicted solution improved significantly compared to Fig. VIII.6. The material response is well predicted in the reversible part, although the solver still tends to underestimate strains in the dissipative domain, leading to early unloading. This results was also observed in Section 1.2 and is thus due to the nature of the problem itself.

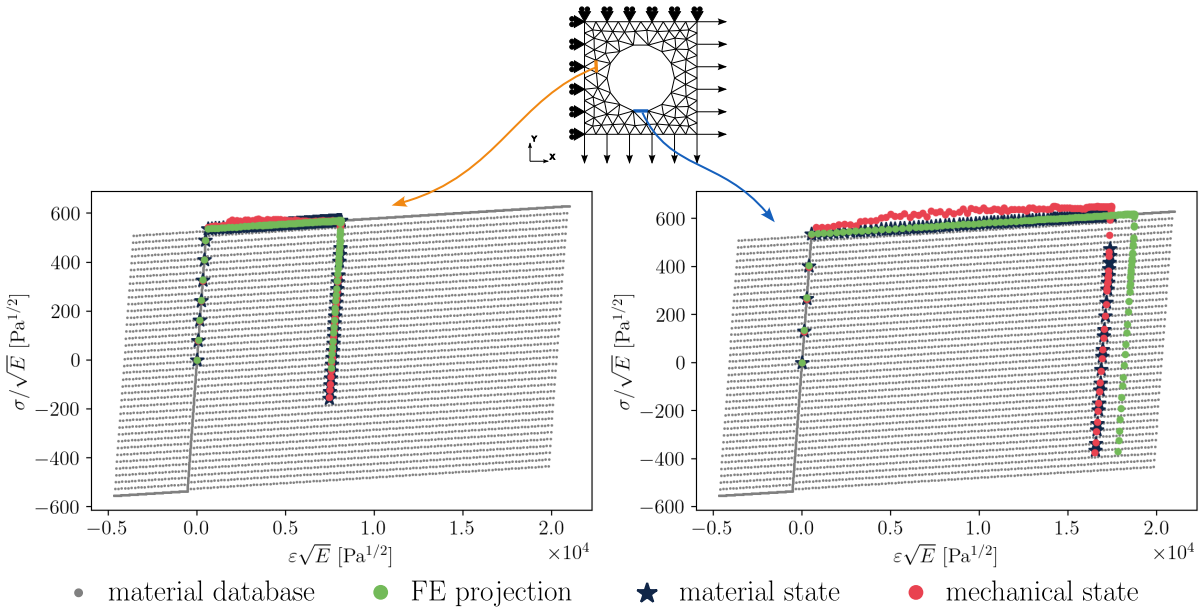

Figure VIII.10: Evolution of DDCM mechanical, material states and projected reference mechanical states for orange and blue elements with predictor-corrector algorithm

Fig. VIII.11 confirms that relative errors also improved compared to the previous simulation. The median values were reduced down to 20 % of those in the previous simulation. Additionally, at loading step 33, high relative errors mostly restrict to slightly deformed elements: only 11 % of the elements exhibit strain relative errors greater than 100 %, half of which with strain levels smaller than 500 $\mathrm{Pa}^{1/2} \approx 0.1$ %. Finally, the macroscopic response of the mesh, evaluated by the resulting force against displacement curve on Fig. VIII.12, is recovered as well.

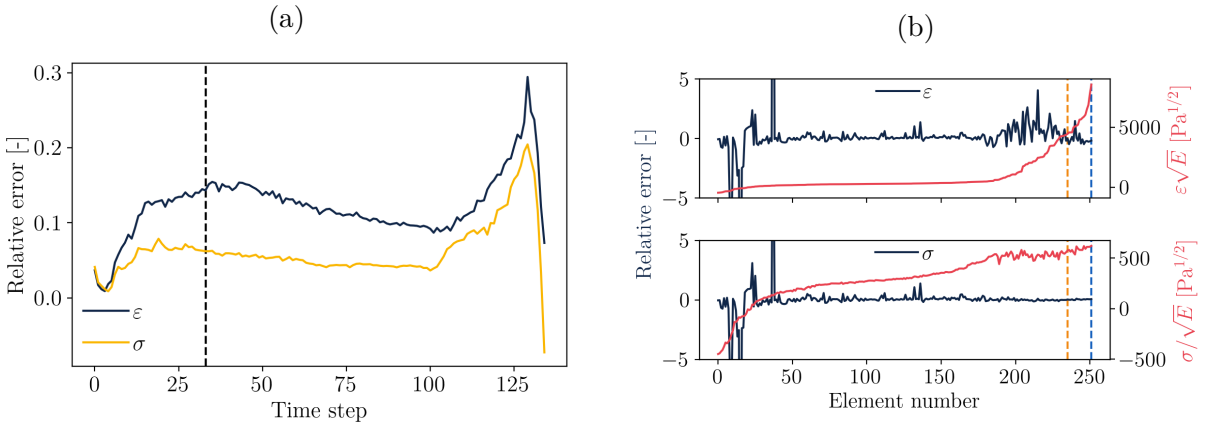

Figure VIII.11: (a) Median relative errors between DDCM and projected reference mechanical states with predictor-corrector algorithm. (b) Relative errors at time step 33 (black dotted line on plot (a)) between DDCM and projected reference mechanical states, the orange and blue dotted lines refer to the elements highlighted on Fig. VIII.1a

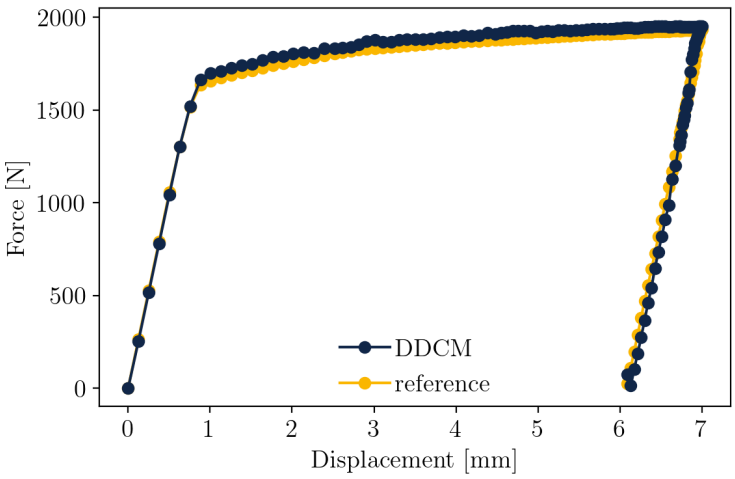

Figure VIII.12: Evolution of resulting force against displacement for the truss problem with predictor-corrector algorithm

3 Summary

The standard DDCM solver is strongly affected by the combinatorial complexity of truss problems and can reach spurious solutions. This is not specific to inelasticity, but also occurs in elasticity as demonstrated in a preliminary study. For instance, the data-driven mechanical response of an elastic truss is not necessarily reversible. In elastoplasticity, the lack of a unique solution within local material databases aggravates this phenomenon and the solver does not provide reasonable results at local nor at global scales.

Model-based computational mechanics usually circumvents such solutions by limiting the material behaviour to a tangent space and controlling loading increments. Within the DDCM framework, we take advantage of the material digraph to compute two local databases: the thermomechanically admissible database, and a smaller iso-dissipation database. The first one is called dissipative database, while the latter is non-dissipative. An enhanced two-stage solver, composed of a prediction step with the non-dissipative local database and a correction step with the dissipative database, has been developed that exhibits promising results.

All simulations were conducted with material databases computed thanks to an elastoplastic constitutive model with linear kinematic hardening. However, neither the material digraph nor the local databases used by the DDCM solver rely on any internal variable. We thus believe that the method can handle any hardening type and possibly other inelastic behaviours, although the latter may require adapting the constitutive space. Cyclic loading can be predicted as long as the constitutive space discretisation (*i.e.* the database) covers the range of strain and dissipation that needs to be studied.

Chapter IX

Material digraph construction: challenges and perspectives

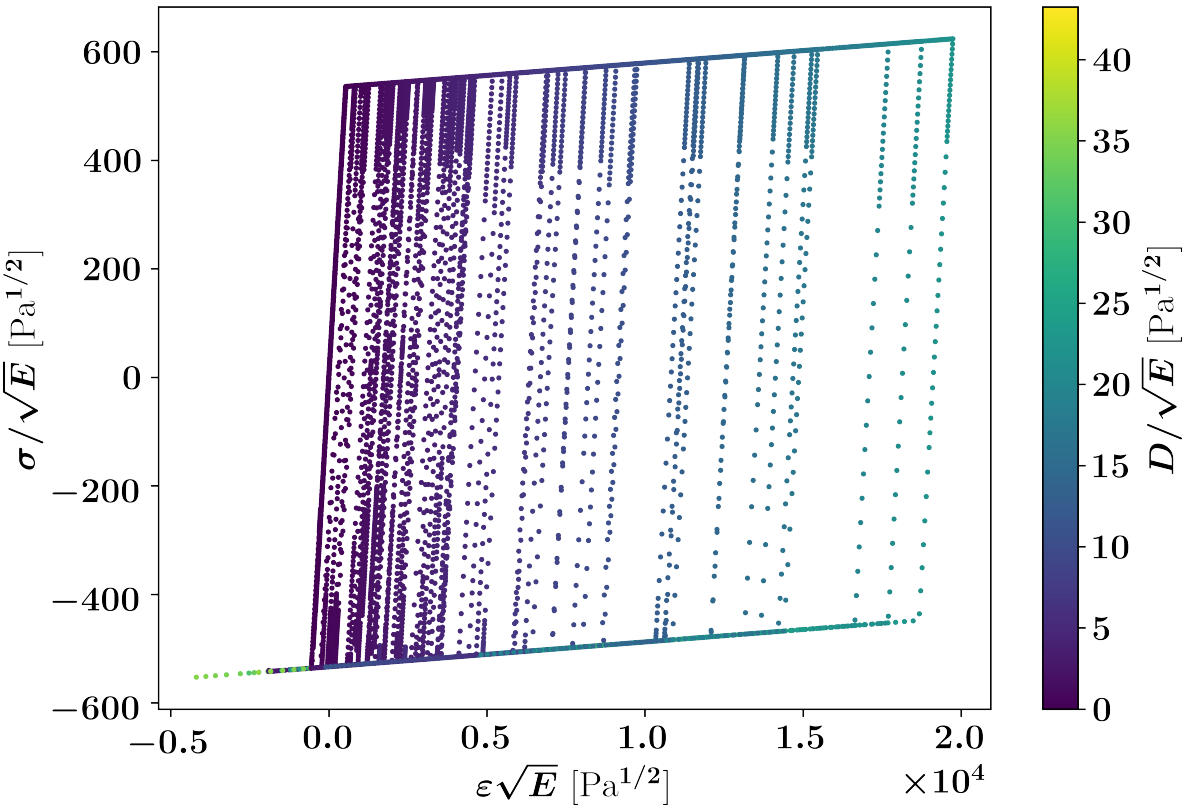

Contents

1 Material data and challenges toward digraph construction **117**
1.1 Origin of material data 117
1.2 Sparsity of adjacency matrix 118
1.3 Towards material digraph construction 118
2 Data clustering **119**
3 Concluding remarks on digraph construction **122**

In the previous chapters, numerical simulations were performed with regular material data sets that contained no redundant points. The material digraph could be built easily using internal variables, in order to get the minimum amount of arcs required to ensure connectivity and completeness of thermomechanical information. However, this method is not efficient and even impossible to apply when dealing with realistic data. The following aims to suggest and discuss possible approaches regarding the construction of the material digraph.

1 Material data and challenges toward digraph construction

1.1 Origin of material data

In practice, material data can be generated in two different ways. On the one hand, numerical simulations, for example in the context of multiscale modelling (Karapiperis *et al.*, 2021 [42], Gorgogianni *et al.*, 2023 [30]), provide comprehensive information about the material behaviour. In this case, a constitutive model provides the necessary strain, stress and dissipation fields to build the material digraph.

On the other hand, experimental tests can also be used to generate this data using a full-field strain measurement technique coupled with DDI for strains and stresses. Dissipation can be inferred from calorimetric measurements with assumptions on potential heat exchanges, as studied by (Chrysochoos *et al.*, 2010 [13], Seghir *et al.*, 2013 [70], Vinel, 2022 [74]) for example. In this latter case, internal variables are unknown, which should be taken into account when defining the construction method.

1.2 Sparsity of adjacency matrix

Furthermore, as discussed in Chapter VI and Chapter VII, the running time complexity of graph search algorithms, used to select local databases, depends on the amount of arcs and vertices in the digraph. For instance, Dijkstra's algorithm with Fibonacci heaps, used in the previous chapters, runs in time $O(|A| + |V| \times \log(|V|))$[1]. The BFS algorithm is another more efficient option with a running time complexity in $O(|A| + |V|)$. The less flexible BFS Scipy routine was not used in the current study because it did not permit a direct implementation of the reduction criteria.

Therefore, time complexity depends on the sparsity of the adjacency matrix, given by the ratio between the number of zero-valued entries (equal to $|V|^2 - |A|$) and the total number of elements (equal to $|V|^2$). The vertices of the material digraph being the strain-stress pairs (along with dissipation and potential internal variables) computed at every integration point and loading step, the number of arcs must be minimised.

1.3 Towards material digraph construction

To build the material digraph, we suggest basing on local loading histories, *i.e.* strain-stress pairs reached at an integration point at every loading step, to create histories' digraphs. This can be done easily since a loading history is an ordered sequence with dissipation levels allowing to define reversible arcs. Then, we need to connect histories together: the quality of the material digraph depends on the density of connections between different histories.

A possible method to link histories' digraphs would consist in defining adequate criteria based on proximity (data-driven distance) and thermomechanical conditions (non-negative dissipation, thermodynamic consistency). However, it is difficult to strike a balance between setting adequate tolerances for these criteria and ensuring the sparsity of the adjacency matrix. The following section thus presents another option based on k-means clustering.

1. With $|V|$ the number of vertices and $|A|$ the number of arcs in the material digraph.

2 Data clustering

k-means clustering aims to partition data into k groups with the nearest mean, the latter being the cluster centroid. We suggest clustering the material data set in space $(\varepsilon\sqrt{E}, \sigma/\sqrt{E}, D/\sqrt{E})$. The material digraph can then be built by taking cluster centroids as vertices and creating arc(s) between centroids containing data points belonging to the same loading history.

A study has been conducted on a material data set stemming from a FE simulation of the truss problem in Chapter VIII, with 252 loading histories (corresponding to each integration point) and 201 loading steps producing loading, unloading and plastic reloading (see Fig. IX.1). Different sampling rates, defined by the ratio between the number of clusters and the number of data points, have been tested.

Since the data-driven metric C is usually set equal to E, data-driven and euclidean distance are equivalent in non-dimensional space $(\varepsilon\sqrt{E}, \sigma/\sqrt{E}, D/\sqrt{E})$. Fig. IX.2 highlights cluster distribution for $r = 2$ %: largest clusters are located around the origin and in the first elastic domain, while smallest clusters contain isolated data points belonging to loading histories with high-dissipation levels and mostly situated in unloading and reloading parts.

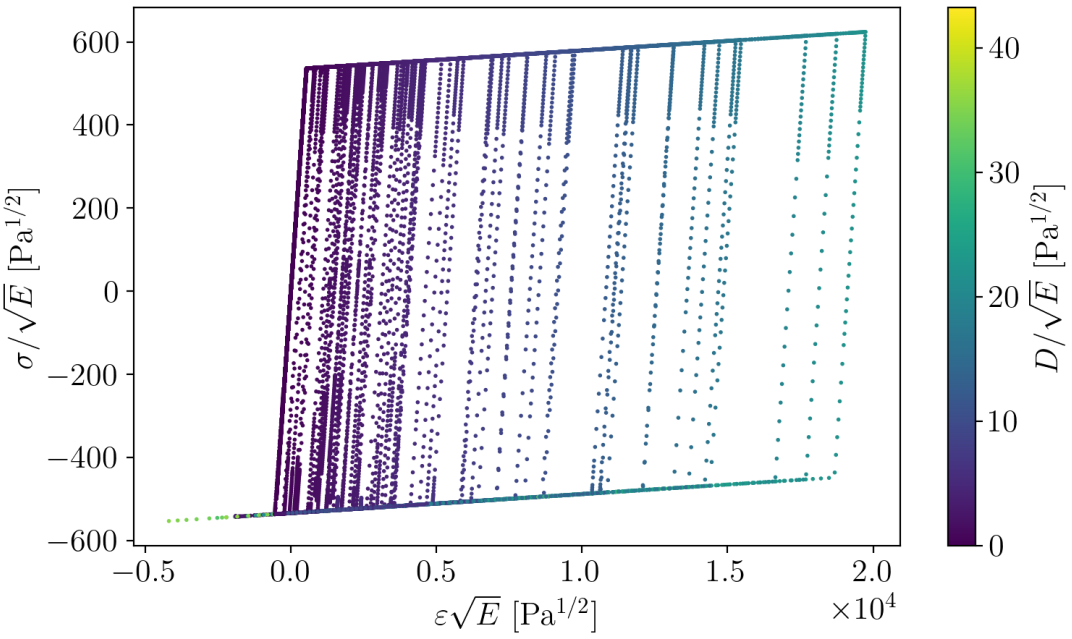

Figure IX.1: Material data set for k-means clustering obtained by FE simulation (elasto-plastic constitutive model with isotropic hardening)

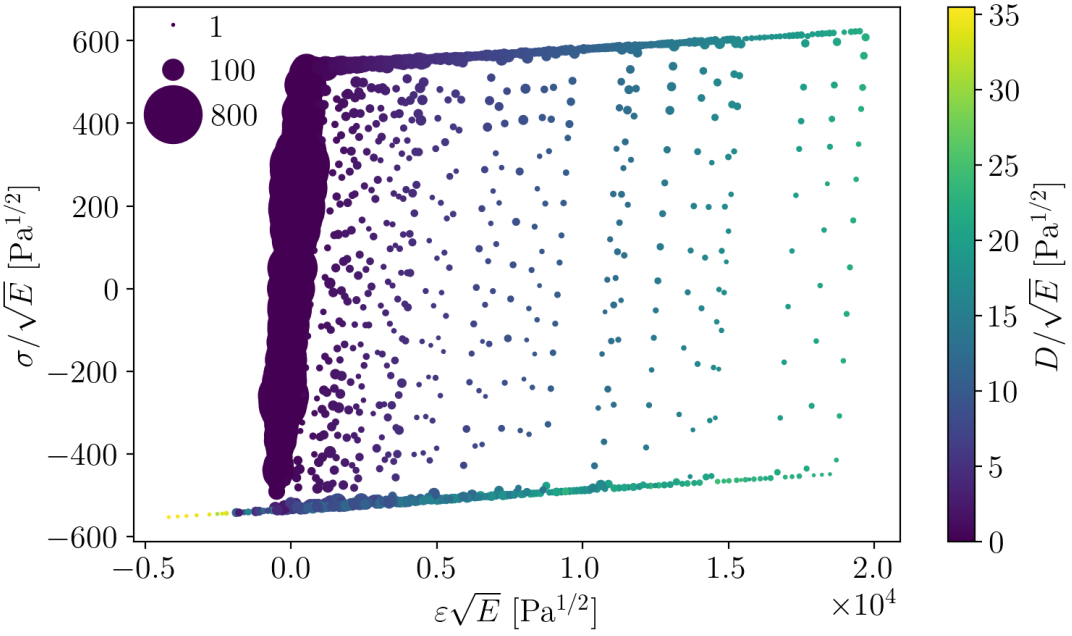

Figure IX.2: Position of clusters in space $(\varepsilon\sqrt{E}, \sigma/\sqrt{E}, D/\sqrt{E})$ for sampling rate $r = 2$ %, with marker size symbolising the number of points in a cluster

We define several indicators to evaluate clustering quality:

- proportion of large clusters,
- point-to-centroid distance per cluster size,
- count of different loading histories per cluster.

The results are illustrated in Fig. IX.3 for sampling rates $r = (2\ \%, 5\ \%, 10\ \%)$. The proportion of one-point clusters is extremely high and increases with the sampling rate, as shown by Fig. IX.3a.

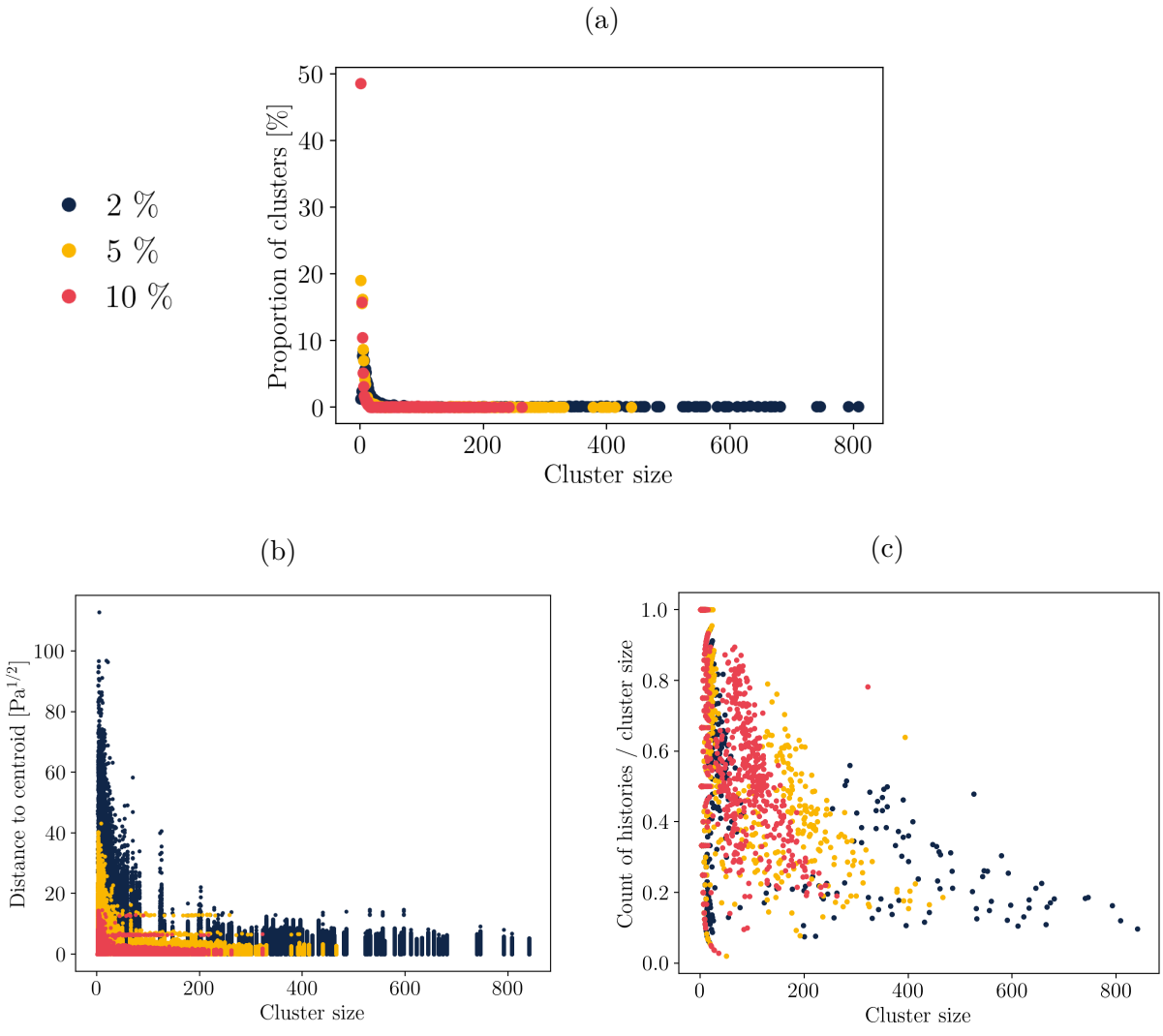

Figure IX.3: Evaluation and comparison of clustering quality for sampling rates $r = (2\ \%, 5\ \%, 10\ \%)$ in space $(\varepsilon\sqrt{E}, \sigma/\sqrt{E}, D/\sqrt{E})$

For coarse sampling ($r = 2$ %), Fig. IX.3b emphasises that point-to-centroid distance can be very high even for small clusters, which are located in sparsely discretised areas of the constitutive space. When the number of clusters increases, one-point clusters are created and maximum distance decreases.

Fig. IX.3c illustrates the ratio between the count of different loading histories represented in one cluster and the size of the cluster. When this ratio is close to 1 (for cluster size greater than 1), data clustering is able to connect different loading histories to create a valuable material digraph. For $r = 10$ %, the larger number of clusters (compared to lower sampling rates) tends to decrease their size. However, the variety of loading histories is high even in small clusters.

3 Concluding remarks on digraph construction

Data clustering is a promising tool for material digraph construction, which could not be completely accomplished during this PhD. The next stage consists in evaluating the sparsity of the adjacency matrix obtained by connecting cluster centroids, and possibly define a method for identifying and deleting insignificant arcs that could result from bad cluster assignment (for instance in the case of points belonging to adjacent elastic domains).

Furthermore, cluster centroids have no physical meaning. The clustered material digraph could yet be used as a macroscopic approximation of the "real" or "unfolded" material digraph: the material field could first be approximated by minimising the distance between mechanical states and cluster centroids, and then a more accurate solution could be computed by searching for the closest data point within the selected cluster.

This idea of a hierarchical structure of the material digraph could also be exploited in a different manner. Indeed, cliques play an important role in the graph-based representation of elastoplasticity, since they symbolise elastic domains. This could be taken advantage of to improve the solver's efficiency.

Finally, loading histories are sequences of points in chronological order. This characteristic could also be directly exploited to detect similarities. For instance, Grossi *et al.* (2020 [32]) proposed a method to retrieve similar trajectories considering both time and place. Distance between points is combined with the time at which they have been

traversed, allowing to find the topmost k trajectories having the highest similarity with respect to a specific one.

Conclusion and perspectives

Conclusion and perspectives

Structural analysis is a constantly evolving field, particularly on account of advances in numerical methods that allow for more efficient and accurate calculations, but also of the improvement of experimental methods for material characterisation, bringing about a thorough knowledge of phenomena and mechanisms involved in the mechanical response of materials.

This thesis studies the extension of model-free DDCM to inelastic behaviours, with a focus on the special case of elastoplastic behaviours. Although they have been extensively studied during the last centuries, the diversity and complexity of the phenomena involved in the latter, which brings about strongly nonlinear responses, still make them difficult to simulate. By bypassing constitutive models, DDCM offers a generic alternative for a wide range of materials.

The major contribution of this work is the mathematical background for the definitions of material digraph and local databases. The first allows to account for history to distinguish between identical states in strain-stress space, while the latter provides input data for the data-driven calculation. This formulation ensures a low increase of the dimensionality and thus guarantees the validity of the distance-minimising procedure.

Furthermore, an algorithm for solving elastoplastic truss problems has been developed. The standard DDCM solver is strongly affected by the combinatorial complexity of such problems and can reach a spurious solution. Constitutive modelling usually circumvents such solutions by limiting the material behaviour to a tangent space and controlling loading increments. Within the DDCM framework, we take advantage of the material digraph to compute two local databases: the thermomechanically admissible database, as defined above, and a smaller iso-dissipation database. The first one is called dissipative database, while the latter is non-dissipative. An enhanced two-stage solver, composed of a prediction step with the non-dissipative local database and a correction step with the dissipative database, has been developed that exhibits promising results.

The construction of the material digraph has been briefly discussed and is still an open challenge. k-means clustering seems an efficient tool to identify similar data points and create arcs. Other methods, for instance for detecting trajectories similarity, could also be tested.

The presented numerical results were obtained for material databases computed with an elastoplastic constitutive model with linear kinematic hardening. However, neither the material digraph nor the local databases used by the DDCM solver rely on any internal variable. We thus believe that the method can handle any hardening type and possibly other inelastic behaviours, although the latter may require adapting the constitutive space. Cyclic loading can be predicted as long as the constitutive space discretisation (*i.e.* the data set) covers the range of strain and dissipation that needs to be studied.

Several perspectives naturally emerge from this work:

- Fundamentally, there is *a priori* no theoretical obstacle to the extension of the method to full 3D elastoplasticity. However, the extension implies an increase of the constitutive space dimensionality and a larger number of points is required to accurately represent the material behaviour. This problem is not specific to inelastic behaviours since it even arises in elasticity, and has been addressed, e.g. with adaptive approaches. Additionally, the amount of possible dissipative paths will increase even faster than dimensionality and the material digraph will necessarily have to sample the possible transitions.
- The efficiency of the solver should be investigated, especially when considering high-dimensional problems. Because of the amount of data and possible transitions, an efficient description of the material digraph becomes necessary. Graph theory provides a wide range of tools and algorithms that have not yet been explored in detail. In particular, a hierarchical representation of the digraph based on cliques, that play an important role in the approach, could be of use.
- A deeper analysis of the expected attributes of the material digraph should be conducted to identify the constitutive space coverage and arcs density required to solve data-driven problems. In particular, the following questions arise: what makes a "good" material digraph? How can we enrich a material digraph, either with another material digraph or with data points generated on-the-fly?
- These problems should be addressed to allow for the use of experimental data, *e.g.* obtained by DDI, which would require coupling thermal and mechanical measurements to identify strain, stress and dissipation values. The quality of the obtained material digraph should then be assessed. Also, one of the major outlets of model-free data-driven mechanics is multiscale modelling. The implementation of the graph-based approach within any adaptive approach should be developed.

Appendices

Appendix A

Numerical relaxation for truss problems

Discussions in Chapter VIII highlighted the need for an efficient algorithm to counteract the alternating minimisation solver's sensitivity to local minima. An attempt has been made to implement numerical relaxation to slow down or speed up convergence and prevent the solver from falling into distant, respectively close, local minima. This appendix presents numerical results obtained for the truss problem presented in Chapter VIII.

1 DDCM algorithm with numerical relaxation

We re-write the data-driven fixed-point iteration in the following way to include numerical relaxation to the computation of mechanical states:

$$z^{(i+1)} = z^{(i)} + \alpha(\tilde{z} - z^{(i)}), \tag{A.1}$$

with z a mechanical state, i the iteration number, $0 < \alpha < 2$ the relaxation parameter and $\tilde{z} = P_{\mathcal{E}_{k+1}} y_{k+1}^{(i)}$. The updated solver is provided in Fig. A.1.

2 Sparse material data

We then decided to investigate the mechanical response in a worst-case scenario where the constitutive space sampling is sparser than the one in Chapter VIII. A new material database is generated with the same material parameters ($E = 217.5$ GPa, H $= 1$ GPa, $\sigma_{\mathrm{y}} = 250$ MPa) and constitutive space discretisation in the non-hardened elastic domain and first dissipative part ($\Delta\varepsilon = 0.001$ %), but with $\Delta\varepsilon^{\mathrm{p}} = 0.2$ % and $\Delta\varepsilon^{\mathrm{e}} = 0.01$ % for

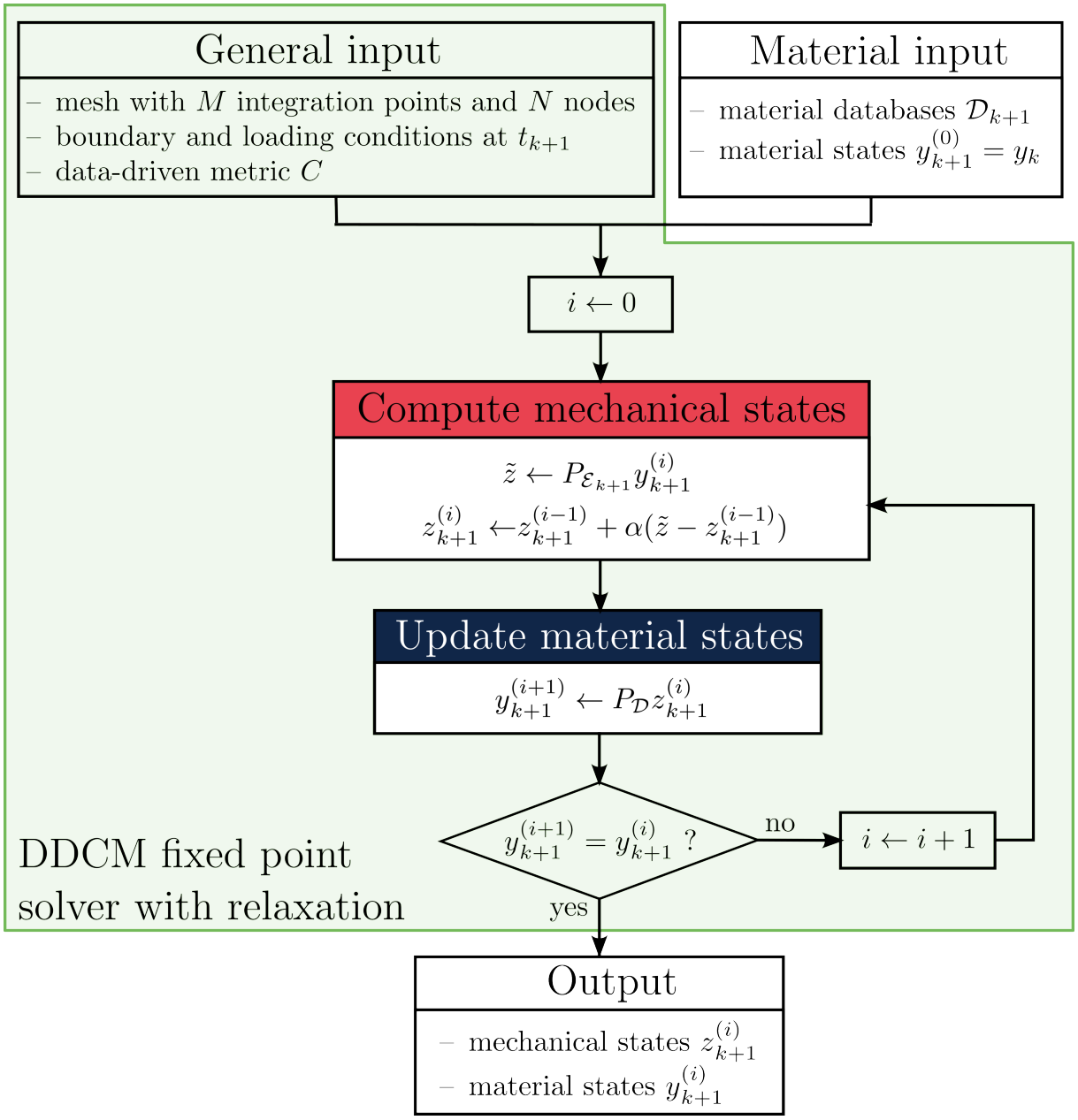

Figure A.1: Data-driven fixed-point solver with numerical relaxation

unloading paths sampling. We set all parameters to the same values chosen previously: $C = E, \texttt{TOL2} = 5 \times 10^3 \times C, \texttt{TOL3} = \times 10^{-5} \times C$.

In combination with the predictor-corrector algorithm, we choose $\alpha = 0.5$ for the non-dissipative prediction to slow down convergence and $\alpha = 1.1$ for the dissipative corrector to accelerate it, since the solver usually tends to underestimate strains in this part.

Median relative errors (defined by Eq. VIII.1) between DDCM and projected reference mechanical states are provided in Fig. A.2 for the truss problem with predictor-corrector, with and without numerical relaxation. Similar results are observed with and without relaxation until the onset of unloading. From this point on, the new relaxed solution slightly improves compared to previous results with the predictor-corrector algorithm only, but is deteriorating again during unloading. The improvements allowed by numerical relaxation did not seem clear enough to deserve further investigation.

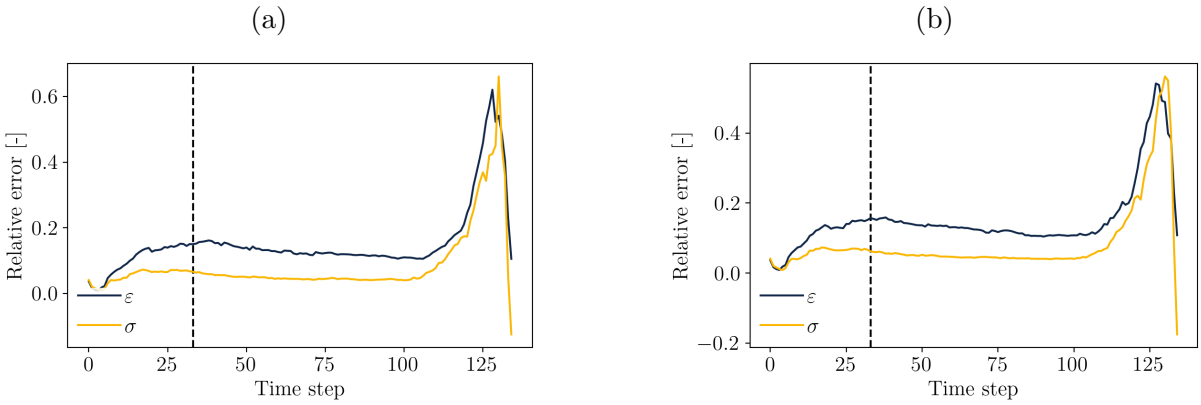

Figure A.2: Median relative errors between DDCM and projected reference mechanical states (a) without relaxation, (b) with relaxation

Moreover, since the material database is very sparse, it seemed interesting to authorise negative dissipation to recover material points normally not admissible because they belong to an elastic domain with lower dissipation level. To this end, we set the negative dissipation tolerance to $2 \times 10^{-6} \times C$. Fig. A.3a shows that, while mostly similar to previously computed results during loading, strain errors increase starting from the onset of unloading. This is also highlighted by the force-displacement response in Fig. A.3b, where strains are visually underestimated in a way similar to that observed in Chapter VIII (algorithm without predictor-corrector).

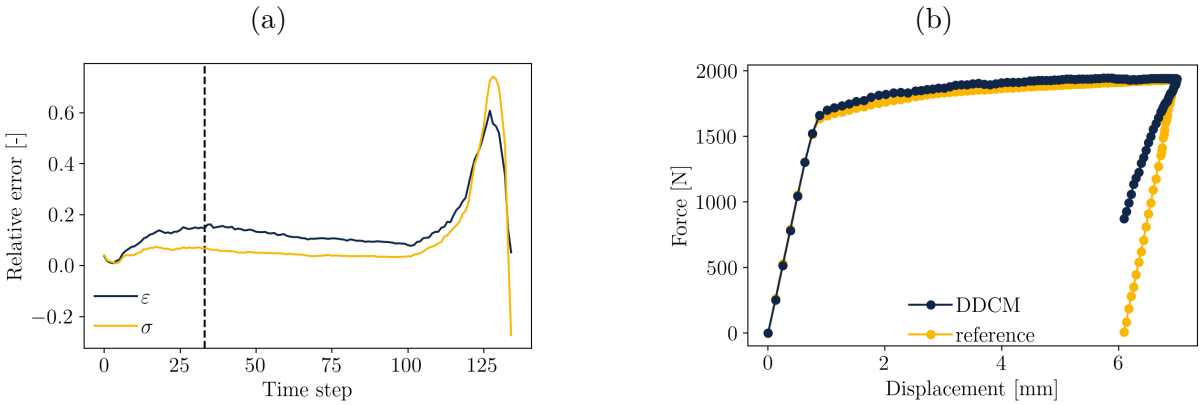

Figure A.3: Numerical relaxation and negative dissipation tolerance: (a) median relative errors between DDCM and projected reference mechanical states (b) resulting force against displacement

Annexe B

Résumé étendu en français

Cette annexe répond à la demande de l'Ecole Doctorale Sciences de l'Ingénierie et des Systèmes de fournir un résumé substantiel en français lorsque le manuscrit est rédigé en anglais. Dans le but de faciliter la compréhension et les liens avec le reste du manuscrit, cette partie respecte le même plan.

1 Principes fondamentaux de la thermomécanique des solides

En mécanique des milieux continus, la transformation d'un corps solide soumis à des sollicitations extérieures est régie par un ensemble d'équations qui déterminent l'état thermomécanique du système. Les principes de base sont la compatibilité des déformations, l'équilibre des efforts et les lois de la thermodynamique que sont la loi de conservation de l'énergie et l'irréversibilité de la production d'entropie. Ces deux derniers principes peuvent être combinés pour former l'équation de Clausius-Duhem, qui définit la condition de non-négativité de la dissipation au cours de la transformation.

D'autre part, l'état d'un système déformé dépend du comportement du matériau étudié. Les différents types de matériaux peuvent être classés en 4 catégories, selon l'allure de leur réponse mécanique. On distingue donc les comportements :

- élastiques, ou réversibles,
- viscoélastiques, dont la réponse dépend du temps,
- plastiques, pour lesquels des déformations permanentes subsistent après l'arrêt de la sollicitation,
- viscoplastiques, qui présentent des caractéristiques plastiques et visqueuses.

Le problème aux conditions aux limites à résoudre pour prédire la réponse mécanique d'un système est composé des équations thermomécaniques. En mécanique classique, le

problème est fermé en postulant un modèle de comportement, c'est-à-dire une relation mathématique entre déformations et contraintes.

Dans le cadre des petites déformations, les équations mécaniques sont linéaires. En revanche, et à l'exception de l'élasticité linéaire, le comportement du matériau est non linéaire. La définition de modèles de comportement adaptés nécessite alors un certain nombre de variables additionnelles et de multiples paramètres, et la résolution du problème aux conditions aux limites requiert des algorithmes complexes.

2 Elastoplasticité et élastoplasticité computationnelle

La plasticité est un phénomène complexe impliqué dans le comportement mécanique d'un grand nombre de matériaux d'ingénierie. La modélisation constitutive de l'élastoplasté a été principalement développée pour les métaux, mais en raison des divers mécanismes physiques à l'origine de la déformation plastique, de nombreuses hypothèses peuvent ne pas s'appliquer à d'autres matériaux. Nous limitons notre étude à la plasticité classique dans le cadre des petites déformations.

Outre la décomposition additive du tenseur de déformation en une partie élastique et une partie plastique, les trois principaux ingrédients des modèles constitutifs élastoplastiques sont le critère de plasticité, la loi d'écoulement plastique et la loi d'écrouissage. Le premier établit les conditions de l'entrée en plasticité, tandis que les deux dernières régissent l'évolution de la surface de plasticité.

Certains modèles classiques ont été présentés, qui sont encore trop restrictifs pour de nombreuses applications. Par exemple, la plasticité cyclique implique des effets supplémentaires tels que l'anisotropie et le « ratcheting » qui ne peuvent pas être prédits par ces modèles. La recherche en cours vise toujours à les améliorer pour mieux refléter les essais expérimentaux, ce qui entraîne une plus grande complexité mathématique.

Enfin, l'algorithme de retour radial a été détaillé pour résoudre les problèmes incrémentaux dans un cadre unidimensionnel. Il consiste à calculer une prédiction élastique, qui peut ensuite être corrigée, si elle excède la surface de plasticité, par projection sur la surface de plasticité.

3 Approches data-driven en mécanique numérique

Les avancées récentes en sciences des données ont conduit à des progrès majeurs en mécanique numérique. Grâce aux méthodes de *machine learning*, des simulations peuvent être réalisées à partir de modèles complexes, ce qui nécessite une capacité de calcul importante. Dans ce contexte, les outils basés sur les réseaux de neurones sont particulièrement répandus pour l'apprentissage de modèles constitutifs, la diversité des approches développées reflétant leur popularité.

En parallèle, des approches sans modèle ont émergé, introduites par Kirchdoerfer et al. (2016 [43]), qui visent à remplacer les modèles constitutifs par une « base de données matériau » discrète. Deux méthodes sont actuellement développées : la DDI pour l'identification et la DDCM pour le calcul de structure, qui est le sujet de cette thèse.

4 Mécanique numérique pilotée par les données

La mécanique numérique pilotée les données, ou *data-driven* rassemble des approches dérivées de l'approche DDCM introduite par Kirchdoerfer et al. (2016 [43]). Contrairement aux approches basées sur les modèles de comportement, le principe fondamental de ce nouveau paradigme est une représentation discrète du comportement du matériau, ce qui évite les biais induits par l'interpolation et/ou l'extrapolation. Le solveur data-driven cherche à minimiser la *distance* entre une base de données matériau discrète et les contraintes mécaniques continues que sont la compatibilité cinématique et l'équilibre. La solution du problème aux conditions aux limites est double :

- un *champ d'états matériau*, appartenant à la base de données matériau,
- un *champ d'états mécaniques* qui vérifie les contraintes mécaniques.

La méthode, initialement développée en élasticité, a depuis été étendue à diverses classes de comportements. De plus, des améliorations du *solveur de minimisation alternée* ont été proposées, par exemple pour accélérer la convergence ou traiter les données bruitées.

En ce qui concerne l'inélasticité, Eggersmann et al. (2019 [25]) ont posé les bases pour une résolution incrémentale du problème. Le cadre mathématique transforme la définition de la base de données matériau locale pour inclure le concept d'histoire.

5 Formulation incrémentale pour la résolution de problèmes anélastiques

Les comportements anélastiques dépendent de l'histoire de chargement et sont fortement non linéaires. Ces caractéristiques les rendent difficiles à modéliser ; les méthodes data-driven apparaissent donc comme des alternatives prometteuses.

Le cadre mathématique de la DDCM en anélasticité, développé par Eggersmann et al. (2019 [25]), transforme le problème data-driven en un problème incrémental qui repose sur la définition de bases de données locales. Ces dernières, calculées en chaque point d'intégration et à chaque pas de chargement, sont soumises à l'histoire locale, généralement encodée par des représentations différentielles ou des variables internes/d'histoire.

La DDCM repose sur un algorithme de minimisation de distance. Il est donc d'une importance cruciale que la définition de la distance data-driven reste valable dans n'importe quel contexte, c'est-à-dire indépendamment de la classe de comportement de matériau et de la dimensionnalité de l'espace. Cependant, les comportements anélastiques impliquent une augmentation substantielle de la dimensionnalité de l'espace constitutif, notamment en 2D et 3D, conditionnée par le paradigme choisi de représentation de l'histoire et le nombre de variables supplémentaires qu'il requiert.

Dans ce travail, nous suggérons d'augmenter la base de données matériau avec une structure sous-jacente, un graphe orienté encodant des informations thermodynamiques permettant de différencier les transitions réversibles et irréversibles entre deux états. En pratique, les points matériau sont les nœuds du graphe, tandis que les arcs orientés représentent les relations thermodynamiques. L'histoire est ainsi utilisée pour déterminer les bases de données locales en tant que futurs admissibles d'un état, et le problème anélastique incrémental est résolu comme un problème pseudo-élastique.

6 Représentation de la base de données matériau avec un graphe : cadre mathématique

Au cours de ce travail, un cadre mathématique a été développé pour une représentation data-driven de données matériau dépendant de l'histoire, par l'intermédiaire d'un graphe

matériau $G = (V(G), A(G))$.

Les points matériau de la base de données correspondent aux sommets du graphe, stockés dans le sous-ensemble $V(G)$. Les relations thermodynamiques entre ces points, déterminées par la non-négativité des incréments de dissipation, sont symbolisées par des arcs dirigés dans le sens de l'écoulement et stockées dans $A(G)$. Les transitions réversibles, ou non dissipatives, sont encodées par deux arcs de directions opposées ; deux sommets liés par un seul arc sont liés par des transitions irréversibles, ou dissipatives. Cette définition du graphe matériau garantit que des points identiques dans l'espace déformation-contrainte puissent être effectivement distingués.

Les bases de données locales sont les sommets d'un arbre, construit en parcourant le graphe matériau à partir d'un nœud racine. Ainsi, en partant d'un état matériel $y_{e,k}$ pris comme racine, nous suivons un arc après l'autre et stockons les sommets parcourus dans $\mathcal{D}_{e,k}$. En fonction de l'histoire matériau, stockée ici dans la racine de l'arbre, les bases de données locales peuvent être extrêmement grandes. Par exemple, au premier pas de temps, $\mathcal{D}_{e,k} = V(G)$. Nous avons donc en outre introduit des critères de réduction, dont le rôle est d'éliminer les solutions très improbables en raison de leur « distance » par rapport à la racine, le terme « distance » faisant référence à la distance data-driven d'un chemin issu de la racine à n'importe quel nœud de la base de données locale, et/ou au coût dissipatif due ce chemin.

Le graphe matériau est calculé dans une étape hors ligne et encodé sous la forme d'une matrice d'adjacence, une représentation numérique compacte qui permet l'utilisation efficace d'algorithmes de graphes. Par la suite, de nouvelles bases de données locales sont sélectionnées à chaque pas de temps avec un outil de parcours de graphe, et le problème incrémental est finalement résolu comme un problème pseudo-élastique.

7 Implémentation numérique et étude d'un problème à un seul élément

Une simulation numérique a permis d'illustrer la nouvelle représentation matériau basée sur le graphe et d'évaluer la précision de la procédure associée. Un problème simple consistant en un système élément-ressort, et ne présentant donc pas de problèmes combinatoires, a été étudié pour identifier les éventuels difficultés.

Une étude préliminaire du problème aux conditions aux limites (BVP) en élasticité a souligné les limites du solveur de minimisation alternée lorsque les données matériau présentent de forts changements de pente, comme c'est le cas en élastoplasticité.

De plus, l'effet des critères de réduction pour le calcul des bases de données locales, qui ont été introduits dans le chapitre précédent, est illustré pour une base de données matériau élastoplastique régulière. Les critères les plus appropriés, basés sur la distance data-driven et le niveau de dissipation du chemin de la racine vers n'importe quel sommet de la base de données locale, sont appliqués à la simulation data-driven.

Le problème élastoplastique est résolu en charge, décharge et recharge plastique. Les résultats sont comparés à un indicateur nouvellement introduit, calculé en projetant la solution éléments finis de référence sur la base de données matériau, puis de nouveau sur l'équilibre. Le champ mécanique de référence obtenu par projection est utilisé pour la comparaison et l'évaluation de la prédiction de la DDCM.

Le solveur est capable de prédire avec une grande précision la réponse mécanique de la structure même au début de la phase de décharge, où l'espace constitutif est échantillonné de manière éparse et ne contient aucun point ayant le niveau de dissipation nécessaire pour obtenir la solution exacte.

8 Essais numériques sur un problème de treillis

Le solveur DDCM standard est fortement affecté par la complexité combinatoire des problèmes de treillis et peut atteindre une solution fallacieuse. Ce phénomène n'est pas spécifique à l'anélasticité, mais se produit également en élasticité. Par exemple, la réponse mécanique d'un treillis élastique n'est pas nécessairement réversible. En élastoplasticité, l'absence d'unicité de la solution dans les bases de données matériau locales aggrave ce phénomène et le solveur ne peut fournir de résultats pertinents aux échelles locale et globale.

La mécanique numérique basée sur les modèles évite généralement de telles solutions en limitant le comportement admissible du matériau à un espace tangent et en contrôlant les incréments de chargement. Dans le cadre de la DDCM, nous tirons parti du graphe matériau pour calculer deux bases de données locales : la base de données thermomécaniquement admissible et une base de données plus petite, iso-dissipative. La première est

appelée base de données dissipative, tandis que la seconde est non dissipative. Un solveur amélioré en deux étapes, composé d'une étape de prédiction avec la base de données locale non dissipative, suivie d'une étape de correction avec la base de données dissipative, a été développé et présente des résultats prometteurs.

Toutes les simulations ont été réalisées avec des bases de données matériau calculées à l'aide d'un modèle constitutif élastoplastique avec écrouissage cinématique linéaire. Cependant, ni le graphe matériau ni les bases de données locales utilisées par le solveur DDCM ne reposent sur des variables internes. On suppose donc que la méthode peut gérer n'importe quel type d'écrouissage et éventuellement d'autres comportements anélastiques, bien que ces derniers puissent nécessiter une adaptation de l'espace constitutif. Les chargements cycliques peuvent être prédits tant que la discrétisation de l'espace constitutif (c'est-à-dire la base de données) couvre la plage de déformation et de dissipation à étudier.

9 Construction du graphe matériau : défis et perspectives

La construction du graphe matériau reste un défi à relever pour la mise en œuvre les méthodes développées dans ce mémoire. En effet, pour assurer le bon fonctionnement de l'algorithme de parcours utilisé pour sélectionner les bases de données locales, le graphe doit contenir suffisamment d'arcs. D'autre part, l'efficacité de ce même algorithme est inversement proportionnelle au nombre d'arcs du graphe. Un compromis est donc nécessaire entre perte d'information et augmentation du temps de calcul.

Une étude préliminaire a été menée pour identifier des points « proches » ou « similaires » de la base de données par clustering. Cette méthode permet notamment de relier des points appartenant à des histoires de chargement différentes (c'est-à-dire calculés en des points d'intégration différents). Cette caractéristique est primordiale, puisque la construction du graphe matériau pour une histoire de chargement est triviale, mais que le traitement d'une base de données entière est beaucoup plus complexe.

D'autres approches paraissent intéressantes, comme par exemple les algorithmes de reconnaissance de trajectoires. Enfin, une représentation hiérarchique du graphe matériau basée sur les cliques, qui jouent un rôle important puisqu'elles symbolisent des domaines élastiques, pourrait sensiblement améliorer l'efficacité des algorithmes présentés.

References

[1] J. Ayensa-Jiménez, M. H. Doweidar, J. A. Sanz-Herrera and M. Doblaré, 'A new reliability-based data-driven approach for noisy experimental data with physical constraints', *Computer Methods in Applied Mechanics and Engineering*, vol. 328, pp. 752–774, 2018. DOI: 10.1016/j.cma.2017.08.027.
Cited on page 51.

[2] B. Bahmani and W. Sun, 'Distance-preserving manifold denoising for data-driven mechanics', *Computer Methods in Applied Mechanics and Engineering*, vol. 405, p. 115 857, 2023. DOI: 10.1016/j.cma.2022.115857.
Cited on page 51.

[3] F. Barlat, J. C. Brem, J. W. Yoon, K. Chung, R. E. Dick, D. J. Lege *et al.*, 'Plane stress yield function for aluminum alloy sheets — part 1: Theory', *International Journal of Plasticity*, vol. 19, *9*, pp. 1297–1319, 2003. DOI: 10.1016/S0749-6419(02)00019-0.
Cited on page 29.

[4] T. Bartel, M. Harnisch, B. Schweizer and A. Menzel, 'A data-driven approach for plasticity using history surrogates: Theory and application in the context of truss structures', *Computer Methods in Applied Mechanics and Engineering*, vol. 414, p. 116 138, 2023. DOI: 10.1016/j.cma.2023.116138.
Cited on pages 49, 53, 62.

[5] J. Bauschinger, 'Über die Veränderung der Elastizitätsgrenze und die Festigkeit des Eisens und Stahls durch Strecken und Quetschen, durch Erwärmen und Abkühlen und durch oftmals wiederholte Beanspruchungen', vol. 13, 1886, Mittheilungen aus dem Mechanisch-Technischen Laboratorium der K. technischen Hochschule, München.
Cited on page 27.

[6] F. E. Bock, R. C. Aydin, C. J. Cyron, N. Huber, S. R. Kalidindi and B. Klusemann, 'A Review of the Application of Machine Learning and Data Mining Approaches in Continuum Materials Mechanics', *Frontiers in Materials*, vol. 6, p. 110, 2019. DOI: 10.3389/fmats.2019.00110.
Cited on page 36.

[7] A. Bondy and U. Murty, *Graph Theory* (Graduate Texts in Mathematics). London: Springer-Verlag, 2008, vol. 244.
Cited on page 69.

[8] J. Bulin, J. Hamaekers, M. P. Ariza and M. Ortiz, 'Interatomic-Potential-Free, Data-Driven Molecular Dynamics', *Computer Methods in Applied Mechanics and Engineering*, vol. 415, p. 116 224, 2023. DOI: 10.1016/j.cma.2023.116224.
Cited on page 53.

[9] P. Carrara, L. De Lorenzis, L. Stainier and M. Ortiz, 'Data-driven fracture mechanics', *Computer Methods in Applied Mechanics and Engineering*, vol. 372, p. 113 390, 2020. DOI: 10.1016/j.cma.2020.113390.
Cited on page 53.

[10] P. Carrara, M. Ortiz and L. De Lorenzis, 'Data-driven rate-dependent fracture mechanics', *Journal of the Mechanics and Physics of Solids*, vol. 155, p. 104 559, 2021. DOI: 10.1016/j.jmps.2021.104559.
Cited on page 53.

[11] J. L. Chaboche, 'A review of some plasticity and viscoplasticity constitutive theories', *International Journal of Plasticity*, Special Issue in Honor of Jean-Louis Chaboche, vol. 24, *10*, pp. 1642–1693, 2008. DOI: 10.1016/j.ijplas.2008.03.009.
Cited on page 29.

[12] I. Charon and O. Hudry, *Introduction à l'optimisation continue et discrète : avec exercices et problèmes corrigés* (Collection IRIS (Paris. 2000)). Paris: Lavoisier-Hermes, 2019.
Cited on page 69.

[13] A. Chrysochoos, V. Huon, F. Jourdan, J.-M. Muracciole, R. Peyroux and B. Wattrisse, 'Use of Full-Field Digital Image Correlation and Infrared Thermography Measurements for the Thermomechanical Analysis of Material Behaviour', *Strain*, vol. 46, *1*, pp. 117–130, 2010. DOI: 10.1111/j.1475-1305.2009.00635.x.
Cited on page 117.

[14] K. Ciftci and K. Hackl, 'Model-free data-driven simulation of inelastic materials using structured data sets, tangent space information and transition rules', *Computational Mechanics*, vol. 70, *2*, pp. 425–435, 2022. DOI: 10.1007/s00466-022-02174-x.
Cited on pages 49, 53.

[15] K. Ciftci and K. Hackl, 'Model-free data-driven inelasticity in Haigh–Westergaard space — A study how to obtain data points from measurements', *Computer Methods in Applied Mechanics and Engineering*, vol. 416, p. 116 352, 2023. DOI: 10.1016/j.cma.2023.116352.
Cited on pages 49, 53.

[16] S. Conti, S. Müller and M. Ortiz, 'Data-Driven Problems in Elasticity', *Archive for Rational Mechanics and Analysis*, vol. 229, *1*, pp. 79–123, 2018. DOI: 10.1007/s00205-017-1214-0.
Cited on page 43.

[17] S. Conti, S. Müller and M. Ortiz, 'Data-Driven Finite Elasticity', *Archive for Rational Mechanics and Analysis*, vol. 237, *1*, pp. 1–33, 2020. DOI: 10.1007/s00205-020-01490-x.
Cited on page 53.

[18] S. Conti, F. Hoffmann and M. Ortiz, 'Model-Free and Prior-Free Data-Driven Inference in Mechanics', *Archive for Rational Mechanics and Analysis*, vol. 247, *1*, p. 7, 2023. DOI: 10.1007/s00205-022-01836-7.
Cited on page 53.

[19] L. Costecalde, 'Data-Driven Model Identification for hyperelasticity: Mapping the strain energy throughout multiaxial experiments', Ph.D. dissertation, Ecole Centrale de Nantes, 2023.
Cited on page 38.

[20] M. Dalémat, M. Coret, A. Leygue and E. Verron, 'Measuring stress field without constitutive equation', *Mechanics of Materials*, vol. 136, p. 103 087, 2019. DOI: 10.1016/j.mechmat.2019.103087.
Cited on page 37.

[21] E. A. De Souza Neto, D. Peri and D. R. J. Owen, *Computational Methods for Plasticity*. Chichester, UK: John Wiley & Sons, Ltd, 2008. DOI: 10.1002/9780470694626.
Cited on pages 10, 19, 20, 30.

[22] J. Delon. 'The curse of dimensionality'. Lecture notes, Université Paris Descartes. (2017), [Online]. Available: https://mathematical-coffees.github.io/slides/mc08-delon.pdf (visited on 30/11/2023).
Cited on page 63.

[23] E. W. Dijkstra, 'A note on two problems in connexion with graphs', *Numerische Mathematik*, vol. 1, pp. 269–271, 1959. DOI: 10.1007/BF01386390.
Cited on page 72.

[24] J. Dornheim, L. Morand, H. J. Nallani and D. Helm, 'Neural Networks for Constitutive Modeling: From Universal Function Approximators to Advanced Models and the Integration of Physics', *Archives of Computational Methods in Engineering*, 2023. DOI: 10.1007/s11831-023-10009-y.
Cited on page 36.

[25] R. Eggersmann, T. Kirchdoerfer, S. Reese, L. Stainier and M. Ortiz, 'Model-Free Data-Driven inelasticity', *Computer Methods in Applied Mechanics and Engineering*, vol. 350, pp. 81–99, 2019. DOI: 10.1016/j.cma.2019.02.016.
Cited on pages 47, 48, 49, 53, 54, 61, 62, 66, 79, 137, 138.

[26] R. Eggersmann, L. Stainier, M. Ortiz and S. Reese, 'Efficient data structures for model-free data-driven computational mechanics', *Computer Methods in Applied Mechanics and Engineering*, vol. 382, p. 113 855, 2021. DOI: 10.1016/j.cma.2021.113855.
Cited on page 52.

[27] R. Eggersmann, L. Stainier, M. Ortiz and S. Reese, 'Model-free data-driven computational mechanics enhanced by tensor voting', *Computer Methods in Applied Mechanics and Engineering*, vol. 373, p. 113 499, 2021. DOI: 10.1016/j.cma.2020.113499.
Cited on pages 49, 51.

[28] C. Frederick and P. Armstrong, 'A mathematical representation of the multiaxial Bauschinger effect', *Materials at High Temperatures*, vol. 24, *1*, pp. 1–26, 2007. DOI: 10.3184/096034007X207589.
Cited on page 29.

[29] A. Galetzka, D. Loukrezis and H. De Gersem, 'Three-dimensional data-driven magnetostatic field computation using real-world measurement data', *COMPEL - The international journal for computation and mathematics in electrical and electronic engineering*, vol. 41, *2*, pp. 615–627, 2021, Publisher: Emerald Publishing Limited. DOI: 10.1108/COMPEL-06-2021-0219.
Cited on page 53.

[30] A. Gorgogianni, K. Karapiperis, L. Stainier, M. Ortiz and J. E. Andrade, 'Adaptive goal-oriented data sampling in Data-Driven Computational Mechanics', *Computer Methods in Applied Mechanics and Engineering*, vol. 409, p. 115 949, 2023. DOI: 10.1016/j.cma.2023.115949.
Cited on pages 38, 53, 117.

[31] M. Grédiac and F. Hild, *Full-Field Measurements and Identification in Solid Mechanics*. John Wiley & Sons, 2012.
Cited on page 37.

[32] R. Grossi, A. Marino and S. Moghtasedi, 'Finding Structurally and Temporally Similar Trajectories in Graphs', vol. 160, 2020, p. 1. DOI: 10.4230/LIPIcs.SEA.2020.24.
Cited on page 122.

[33] X. Guo, Z. Du, C. Liu and S. Tang, 'A New Uncertainty Analysis-Based Framework for Data-Driven Computational Mechanics', *Journal of Applied Mechanics*, vol. 88, *11*, 2021. DOI: 10.1115/1.4051594.
Cited on page 51.

[34] F. Harary, R. Z. Norman and D. Cartwright, *Structural models: an introduction to the theory of directed graphs*. New York, Wiley, 1965, vol. IX.
Cited on pages 64, 69.

[35] Q. He and J.-S. Chen, 'A physics-constrained data-driven approach based on locally convex reconstruction for noisy database', *Computer Methods in Applied Mechanics and Engineering*, vol. 363, p. 112 791, 2020. DOI: 10.1016/j.cma.2019.112791.
Cited on page 51.

[36] R. Hill, 'A theory of the yielding and plastic flow of anisotropic metals', *Proceedings of the Royal Society of London. Series A. Mathematical and Physical Sciences*, vol. 193, *1033*, pp. 281–297, 1948, Publisher: Royal Society. DOI: 10.1098/rspa.1948.0045.
Cited on page 29.

[37] M. Huang, C. Liu, Z. Du, S. Tang and X. Guo, 'A sequential linear programming (SLP) approach for uncertainty analysis-based data-driven computational mechanics', *Computational Mechanics*, 2023. DOI: 10.1007/s00466-023-02395-8.
Cited on page 52.

[38] H. Hübel, 'Basic conditions for material and structural ratcheting', *Nuclear Engineering and Design*, vol. 162, *1*, pp. 55–65, 1996. DOI: 10.1016/0029-5493(95)01136-6.
Cited on page 29.

[39] V. Kamasamudram and L. Stainier, 'A strain based Lipschitz regularization for materials undergoing damage', *Comptes Rendus. Mécanique*, vol. 351, *G1*, pp. 125–149, 2023. DOI: 10.5802/crmeca.176.
Cited on page 53.

[40] Y. Kanno, 'Simple Heuristic for Data-Driven Computational Elasticity with Material Data Involving Noise and Outliers: A Local Robust Regression Approach', *Japan Journal of Industrial and Applied Mathematics*, vol. 35, *3*, pp. 1085–1101, 2018. DOI: 10.1007/s13160-018-0323-y.
Cited on page 51.

[41] Y. Kanno, 'Mixed-integer programming formulation of a data-driven solver in computational elasticity', *Optimization Letters*, vol. 13, *7*, pp. 1505–1514, 2019. DOI: 10.1007/s11590-019-01409-w.
Cited on page 50.

[42] K. Karapiperis, L. Stainier, M. Ortiz and J. E. Andrade, 'Data-Driven multiscale modeling in mechanics', *Journal of the Mechanics and Physics of Solids*, vol. 147, p. 104 239, 2021. DOI: 10.1016/j.jmps.2020.104239.
Cited on pages 38, 53, 117.

[43] T. Kirchdoerfer and M. Ortiz, 'Data-driven computational mechanics', *Computer Methods in Applied Mechanics and Engineering*, vol. 304, pp. 81–101, 2016. DOI: 10.1016/j.cma.2016.02.001.
Cited on pages 3, 37, 39, 43, 47, 50, 52, 54, 137.

[44] T. Kirchdoerfer and M. Ortiz, 'Data Driven Computing with noisy material data sets', *Computer Methods in Applied Mechanics and Engineering*, vol. 326, pp. 622–641, 2017. DOI: 10.1016/j.cma.2017.07.039.
Cited on pages 51, 77.

[45] T. Kirchdoerfer and M. Ortiz, 'Data-driven computing in dynamics', *International Journal for Numerical Methods in Engineering*, vol. 113, *11*, pp. 1697–1710, 2018. DOI: 10.1002/nme.5716.
Cited on page 53.

[46] T. F. Korzeniowski and K. Weinberg, 'A comparison of stochastic and data-driven FEM approaches to problems with insufficient material data', *Computer Methods in Applied Mechanics and Engineering*, vol. 350, pp. 554–570, 2019. DOI: 10.1016/j.cma.2019.03.009.
Cited on page 51.

[47] T. F. Korzeniowski and K. Weinberg, 'A multi-level method for data-driven finite element computations', *Computer Methods in Applied Mechanics and Engineering*, vol. 379, p. 113 740, 2021. DOI: 10.1016/j.cma.2021.113740.
Cited on page 52.

[48] T. F. Korzeniowski and K. Weinberg, 'Data-driven finite element computation of open-cell foam structures', *Computer Methods in Applied Mechanics and Engineering*, vol. 400, p. 115 487, 2022. DOI: 10.1016/j.cma.2022.115487.
Cited on page 53.

[49] R. Langlois, 'Non-parametric evaluation of stress fields for history-dependent materials : Formulation, Validation and Applications', Ph.D. dissertation, Ecole Centrale de Nantes, 2023.
Cited on page 50.

[50] R. Langlois, M. Coret and J. Réthoré, 'Non-parametric stress field estimation for history-dependent materials: Application to ductile material exhibiting Piobert–Lüders localization bands', *Strain*, e12410, 2022. DOI: 10.1111/str.12410.
Cited on page 62.

[51] J. Lemaitre, J.-L. Chaboche, A. Benallal and R. Desmorat, *Mécanique des matériaux solides*, 3e éd. Dunod, 2009.
Cited on pages 10, 12, 13, 14, 15.

[52] A. Leygue, M. Coret, J. Réthoré, L. Stainier and E. Verron, 'Data-based derivation of material response', *Computer Methods in Applied Mechanics and Engineering*, vol. 331, pp. 184–196, 2018. DOI: 10.1016/j.cma.2017.11.013.
Cited on page 37.

[53] C. Lienstromberg, S. Schiffer and R. Schubert, 'A Data-Driven Approach to Viscous Fluid Mechanics: The Stationary Case', *Archive for Rational Mechanics and Analysis*, vol. 247, *2*, p. 30, 2023. DOI: 10.1007/s00205-023-01849-w.
Cited on page 53.

[54] J. Lubliner, *Plasticity Theory*. Dover edition, 2008.
Cited on pages 19, 21.

[55] M. Mahan, Y. Dafalias, M. Taiebat, Y. Heo and S. Kunnath, 'SANISTEEL: Simple anisotropic steel plasticity model', *Journal of Structural Engineering*, vol. 137, *2*, pp. 185–194, 2011. DOI: 10.1061/(ASCE)ST.1943-541X.0000297.
Cited on page 29.

[56] R. von Mises, 'Mechanik der festen Körper im plastisch-deformablen Zustand', *Nachrichten von der Gesellschaft der Wissenschaften zu Göttingen, Mathematisch-Physikalische Klasse*, vol. 1913, pp. 582–592, 1913.
Cited on page 25.

[57] Z. Mróz, 'On the description of anisotropic workhardening', *Journal of the Mechanics and Physics of Solids*, vol. 15, *3*, pp. 163–175, 1967. DOI: 10.1016/0022-5096(67)90030-0.
Cited on page 29.

[58] L. T. K. Nguyen and M.-A. Keip, 'A data-driven approach to nonlinear elasticity', *Computers & Structures*, vol. 194, pp. 97–115, 2018. DOI: 10.1016/j.compstruc.2017.07.031.
Cited on page 53.

[59] L. T. K. Nguyen, M. Rambausek and M.-A. Keip, 'Variational framework for distance-minimizing method in data-driven computational mechanics', *Computer Methods in Applied Mechanics and Engineering*, vol. 365, p. 112 898, 2020. DOI: 10.1016/j.cma.2020.112898.
Cited on page 49.

[60] H. M. Paranjape, A. P. Stebner and K. Bhattacharya, 'A macroscopic strain-space model of anisotropic, cyclic plasticity with hardening', *International Journal of Mechanical Sciences*, vol. 149, pp. 365–372, 2018. DOI: 10.1016/j.ijmecsci.2018.01.012.
Cited on page 29.

[61] D. K. N. Pham, N. Blal and A. Gravouil, 'Tangent space Data Driven framework for elasto-plastic material behaviors', *Finite Elements in Analysis and Design*, vol. 216, p. 103 895, 2023. DOI: 10.1016/j.finel.2022.103895.
Cited on pages 49, 53, 90.

[62] A. Platzer, 'Finite strain data-driven computational mechanics. From tailored data to adaptive solvers for multiscale simulations', Ph.D. dissertation, École Centrale de Nantes, 2020.
Cited on pages 10, 38, 45, 50, 53.

[63] A. Platzer, A. Leygue, L. Stainier and M. Ortiz, 'Finite element solver for data-driven finite strain elasticity', *Computer Methods in Applied Mechanics and Engineering*, vol. 379, p. 113 756, 2021. DOI: 10.1016/j.cma.2021.113756.
Cited on page 53.

[64] K. Poelstra, T. Bartel and B. Schweizer, 'A data-driven framework for evolutionary problems in solid mechanics', *ZAMM - Journal of Applied Mathematics and Mechanics / Zeitschrift für Angewandte Mathematik und Mechanik*, vol. 103, e202100538, 2022. DOI: 10.1002/zamm.202100538.
Cited on pages 50, 53.

[65] W. Prager, 'The Theory of Plasticity: A Survey of Recent Achievements', *Proceedings of the Institution of Mechanical Engineers*, vol. 169, *1*, pp. 41–57, 1955. DOI: 10.1243/PIME_PROC_1955_169_015_02.
Cited on page 27.

[66] E. Prume, S. Reese and M. Ortiz, 'Model-free Data-Driven inference in computational mechanics', *Computer Methods in Applied Mechanics and Engineering*, vol. 403, p. 115 704, 2023. DOI: 10.1016/j.cma.2022.115704.
Cited on page 53.

[67] M. Rigo, *Advanced Graph Theory and Combinatorics*. John Wiley & Sons, 2016.
Cited on page 69.

[68] A. B. de Saint-Venant, 'Mémoire sur l'établissement des équations différentielles des mouvements intérieurs opérés dans les corps solides ductiles au delà des limites où l'élasticité pourrait les ramener à leur premier état.', *Journal de Mathématiques Pures et Appliquées*, vol. 16, pp. 308–316, 1871.
Cited on page 14.

[69] H. Salahshoor and M. Ortiz, 'Model-free Data-Driven viscoelasticity in the frequency domain', *Computer Methods in Applied Mechanics and Engineering*, vol. 403, p. 115 657, 2023. DOI: 10.1016/j.cma.2022.115657.
Cited on page 53.

[70] R. Seghir, J.-F. Witz, L. Bodelot, E. Charkaluk and P. Dufrénoy, 'An improved lagrangian thermography procedure for the quantification of the temperature fields within polycrystals', *Quantitative InfraRed Thermography Journal*, vol. 10, *1*, pp. 74–95, 2013. DOI: 10.1080/17686733.2013.785207.
Cited on page 117.

[71] J. C. Simo and T. J. R. Hughes, *Computational Inelasticity* (Interdisciplinary Applied Mathematics). NY: Springer New York, 1998, vol. 7. DOI: https://doi.org/10.1007/b98904.
Cited on pages 10, 32.

[72] L. Stainier, A. Leygue and M. Ortiz, 'Model-free data-driven methods in mechanics: Material data identification and solvers', *Computational Mechanics*, vol. 64, *2*, pp. 381–393, 2019, Publisher: Springer Nature. DOI: 10.1007/s00466-019-01731-1.
Cited on page 38.

[73] J. Ulloa, A. Gorgogianni, K. Karapiperis, M. Ortiz and J. E. Andrade, 'Data-driven breakage mechanics: Predicting the evolution of particle-size distribution in granular media', *Journal of the Mechanics and Physics of Solids*, vol. 178, p. 105 328, 2023. DOI: 10.1016/j.jmps.2023.105328.
Cited on page 53.

[74] A. Vinel, 'Characterization of the thermomechanical behaviour of metals for high strain-rates, using ultra-high speed imaging cameras', Ph.D. dissertation, Ecole Centrale de Nantes, 2022.
Cited on page 117.

[75] P. Virtanen, R. Gommers, T. E. Oliphant, M. Haberland, T. Reddy, D. Cournapeau *et al.*, 'SciPy 1.0: Fundamental algorithms for scientific computing in Python', *Nature Methods*, vol. 17, *3*, pp. 261–272, 2020. DOI: 10.1038/s41592-019-0686-2.
Cited on page 72.

[76] K. Weinberg, L. Stainier, S. Conti and M. Ortiz, 'Data-Driven Games in Computational Mechanics', *Computer Methods in Applied Mechanics and Engineering*, vol. 417, p. 116 399, 2023. DOI: 10.1016/j.cma.2023.116399.
Cited on pages 52, 89.

[77] Z. Zheng, Z. Zhang, H. Ye, H. Zhang and Y. Zheng, 'Distance minimizing based data-driven computational method for the finite deformation of hyperelastic materials', *International Journal for Numerical Methods in Engineering*, vol. 124, *10*, pp. 1–26, 2023. DOI: 10.1002/nme.7212.
Cited on page 53.

[78] S. Zschocke, F. Leichsenring, W. Graf and M. Kaliske, 'A concept for data-driven computational mechanics in the presence of polymorphic uncertain properties', *Engineering Structures*, vol. 267, p. 114 672, 2022. DOI: 10.1016/j.engstruct.2022.114672.
Cited on page 53.

COLLEGE SCIENCES
DOCTORAL DE L'INGENIERIE
PAYS DE LA LOIRE ET DES SYSTEMES

CENTRALE NANTES

Titre : Une approche basée sur les graphes pour le calcul piloté par les données en anélasticité. Application à l'élastoplasticité

Mot clés : Mécanique numérique, data-driven, anélasticité, élastoplasticité, théorie des graphes

Résumé : En calcul de structures, la réponse mécanique d'un matériau est généralement approximée par un modèle de comportement, c'est-à-dire une loi mathématique reliant déformations et contraintes. Cette représentation entraîne de nombreux biais, dûs non seulement au choix du modèle lui-même, mais aussi à la perte d'information qu'elle implique.
L'essor de la science des données et l'amélioration des techniques expérimentales au cours des dernières décennies ont conduit à d'importants changements dans le domaine de la mécanique numérique. En particulier, l'approche dite « pilotée par les données » introduite par Kirchdoerfer et Ortiz en 2016 utilise une représentation discrète de la réponse du matériau. Le problème mécanique se transforme alors en problème de minimisation de la distance entre deux champs, l'un étant mécaniquement admissible et l'autre issu de la base de données matériau.
Les présents travaux se concentrent sur l'extension de cette méthode, développée à l'origine en élasticité, aux comportements anélastiques. Ces derniers sont caractérisés par leur irréversibilité et nécessitent de tenir compte de l'histoire locale. A cette fin, la base de données matériau discrète est augmentée par une information thermodynamique sur les transitions entre états, de manière à construire un graphe orienté ; le problème incrémental est alors ramené à une série de problèmes pseudo-élastiques. L'algorithme qui en découle est appliqué à des treillis en élastoplasticité.

Title: A graph-based model-free data-driven computing approach for inelasticity. Application to elastoplasticity

Keywords: Computational mechanics, data-driven, inelasticity, elastoplasticity, graph theory

Abstract: In structural analysis, the mechanical response of a material is usually approximated with a constitutive model, *i.e.* a mathematical relation between strains and stresses. This representation introduces biases, arising not only from the choice of the model itself but also from the loss of information it involves.
Recent advances in data science and experimental techniques have brought about significant changes in the field of computational mechanics. In particular, the Data-Driven Computational Mechanics approach, introduced by Kirchdoerfer and Ortiz in 2016, is based on a discrete representation of the material response. The mechanical problem then transforms into a minimisation problem involving the distance between two fields — one being mechanically admissible and the other derived from the material database.
This work focuses on extending this method, originally developed in elasticity, to inelastic behaviours, the latter being characterised by their irreversibility. To take local history into account, the discrete material database is augmented with thermodynamic information on state transitions, building a directed graph. The incremental problem thus reduces to a series of pseudo-elastic problems. The resulting algorithm is applied to rate-independent elastoplastic trusses.